PB82-101 932

MODELING OF S02 OXIDATION IN SMOG (FINAL REPORT)

D. F. Miller

Battelle Columbus Laboratories
Columbus, OH

JUN 81

?

U.S. Department of Commerce
National Technical Information Service
NTIS

TECHNICAL REPORT DATA
(Please read Instructions on the reverse before completing)

1. REPORT NO. EPA-600/3-81-040	2. ORD Report	3. RECIPIENT'S ACCESSION NO. PB82 101932
4. TITLE AND SUBTITLE MODELING OF SO_2 OXIDATION IN SMOG		5. REPORT DATE June 1981
		6. PERFORMING ORGANIZATION CODE
7. AUTHOR(S) David F. Miller		8. PERFORMING ORGANIZATION REPORT NO.
9. PERFORMING ORGANIZATION NAME AND ADDRESS Battelle-Columbus Laboratories 505 King Avenue Columbus, Ohio 43201		10. PROGRAM ELEMENT NO. 1NE832B EA-050 (FY-79)
		11. CONTRACT/GRANT NO. R-805335
12. SPONSORING AGENCY NAME AND ADDRESS Environmental Sciences Research Laboratory-RTP, NC Office of Research and Development U.S. Environmental Protection Agency Research Triangle Park, North Carolina 27711		13. TYPE OF REPORT AND PERIOD COVERED Final
		14. SPONSORING AGENCY CODE EPA/600/09
15. SUPPLEMENTARY NOTES		

16. ABSTRACT

Smog chamber experiments were conducted to investigate the (1) kinetics of free radical reactions of SO_2 in smog and (2) SO_2 transformation to sulfate for atmospheric simulations. Rate constants were derived for the following reactions: $SO_2+HO+M \rightarrow$ sulfate (60), $SO_2+HO_2 \rightarrow$ sulfate (61), $SO_2+CH_3O_2 \rightarrow$ sulfate (64); $k_{60} = 1600$ $k_{61} < 0.2$, $k_{64} < 0.8$ $ppm^{-1} min^{-1}$. Oxidation of SO_2 by HO led exclusively to particulate sulfate. Even under favorable NO_x conditions, particulate nitrate was not a product. Hydrocarbon mixtures typical of urban environments promoted SO_2 oxidation faster than hydrocarbons selected to represent rural conditions. Maximum rates of SO_2 oxidation occurred during periods of peak NO_2 formation. SO_2 oxidation rates for aged smog were 25-35% of the maximum values. Model calculations indicated that reaction 60 dominates sulfate production from SO_2 in polluted air. Models that adequately estimate [HO] in smog should suffice to approximate the conversion rates. The model used in this study indicated that SO_2 oxidation depends strongly on solar radiation intensity and pollutant conditions. For clear-sky and a variety of HC-NO_x conditions, maximum SO_2 conversion rates ranged from 3.7-7.4%/hr. Models used to simulate reactions in power plant plumes showed that SO_2 oxidation is strongly dependent on plume dispersion rates coupled to the same parameters governing SO_2 oxidation in ambient air. Generally the rates of SO_2 oxidation in plumes are bound by the ambient rates, although exceptions will occur for certain HC-NO_x conditions.

17. KEY WORDS AND DOCUMENT ANALYSIS

a. DESCRIPTORS	b. IDENTIFIERS/OPEN ENDED TERMS	c. COSATI Field/Group

18. DISTRIBUTION STATEMENT RELEASE TO PUBLIC	19. SECURITY CLASS *(This Report)* UNCLASSIFIED	21. NO. OF PAGES 146
	20. SECURITY CLASS *(This page)* UNCLASSIFIED	22. PRICE

EPA Form 2220-1 (Rev. 4-77) PREVIOUS EDITION IS OBSOLETE

EPA-600/3-81-040
June 1981

PB82-101932

MODELING OF SO_2 OXIDATION IN SMOG

BY

David F. Miller
Battelle Columbus Laboratories
Columbus, Ohio

Grant No. R805335

Project Officer

Joseph J. Bufalini
Atmospheric Chemistry and Physics Division
Environmental Sciences Research Laboratory
Research Triangle Park, NC 27711

ENVIRONMENTAL SCIENCES RESEARCH LABORATORY
OFFICE OF RESEARCH AND DEVELOPMENT
U. S. ENVIRONMENTAL PROTECTION AGENCY
RESEARCH TRIANGLE, PARK, NC 27711

REPRODUCED BY
NATIONAL TECHNICAL
INFORMATION SERVICE
U.S. DEPARTMENT OF COMMERCE
SPRINGFIELD, VA 22161

DISCLAIMER

This report has been reviewed by the Environmental Sciences Research Laboratory, U.S. Environmental Protection Agency, and approved for publication. Approval does not signify that the contents necessarily reflect the views and policies of the U. S. Environmental Protection Agency, nor does mention of trade names or commercial products constitute endorsement or recommendation for use.

ABSTRACT

Smog chamber experiments were conducted to investigate the kinetics of the free radical reactions of SO_2 in smog and to investigate SO_2 transformation to sulfate for atmospheric simulations. Rate constants were derived for the following reactions: $SO_2 + HO + M \rightarrow SULFATE$ (60), $SO_2 + HO_2 \rightarrow SULFATE$ (61), $SO_2 + CH_3O_2 \rightarrow SULFATE$ (64); $k_{60} = 1600$, $k_{61} < 0.2$, $k_{64} < 0.8$ $ppm^{-1}min^{-1}$. Oxidation of SO_2 by HO led exclusively to particulate sulfate. Even under favorable NO_x conditions, particulate nitrate was not a product. Hydrocarbon mixtures typical of urban environments promoted SO_2 oxidation faster than hydrocarbons selected to represent rural conditions. Maximum rates of SO_2 oxidation occurred during periods of peak NO_2 formation. SO_2 oxidation rates for aged smog were 25-35% of the maximum rates.

Model calculations indicated that reaction 60 dominates sulfate production from SO_2 in polluted air. Models that adequately estimate [HO] in smog should suffice to approximate the gas phase conversion rates. The model used in this study indicated that SO_2 oxidation depends strongly on solar radiation intensity and pollutant conditions. For clear-sky and a variety of HC-NO_x conditions, maximum SO_2 conversion rates ranged from 3.7 - 7.4%/hr. Models used to simulate reactions in power plant plumes showed that SO_2 oxidation is strongly dependent on plume dispersion rates coupled to the same parameters governing SO_2 oxidation in ambient air. Generally the rates of SO_2 oxidation in plumes are bound by the ambient rates, although exceptions to the rule will occur for certain HC-NO_x conditions.

This report was submitted in fulfillment of Grant No. R805335 by Battelle Columbus Laboratories under the sponsorship of the U.S. Environmental Protection Agency. This report covers the period September 15, 1977 to December 15, 1979, and work was completed as of January 30, 1980.

CONTENTS

Abstract. iii

Figures and Tables. vii

Acknowledgement ix

1. Introduction 1

2. Summary and Conclusions. 3

3. Experimental Methods 8
    - A. Smog chamber facility 8
    - B. Background conditions and contamination 8
    - C. Surface effects and wall losses 9
    - D. Analytical methods - Gas phase. 10
    - E. Analytical methods - Condensed phase. 12

4. Results and Discussion 16
    - A. Experimental approach for kinetic data. 16
    - B. Inorganic system ($HNO_2/NO_x/CO/SO_2$). 20
        - (1) Preliminary experiments 20
        - (2) Experiments to investigate HNO_2 reactions and NO_x Losses 21
        - (3) SO_2 Oxidation by HO radicals. 28
        - (4) SO_2 Oxidation by HO_2 radicals 42
    - C. Organic Systems ($HNO_2/NO_x/CH_4/SO_2$ and CH_3NNCH_3/SO_2) . . . 48
        - (1) Experiments with Methane as Methylperoxy Source . . . 48
        - (2) Azomethane and Methylperoxy source. 54
    - D. Role of NO_x in SO_2 Oxidation via HO radicals. 58
    - E. Summary of kinetics studies 61
        - (1) $O_3 + HNO_2 \rightarrow HNO_3 + O_2$ 61
        - (2) $N_2O_5 + H_2O \rightarrow 2\ HNO_3$ 61
        - (3) $SO_2 + HO\ (M) \rightarrow$SULFATE 62
        - (4) $SO_2 + HO_2 \rightarrow$SULFATE. 62
        - (5) $SO_2 + CH_3O_2 \rightarrow$SULFATE. 63
        - (6) $SO_2 + HNO_2 \rightarrow$Products. 64

F. SO_2 Oxidation in Simulations of Urban and Rural Atmospheres. 64
  (1) Experimental Data 65
  (2) Discussion. 80
  (3) Kinetic Model Applied to Smog Chamber Experiments . 82
    a. Scope of Model. 82
    b. Hydrocarbon Reactivity. 83
    c. Model Results 84
    d. Limitations of Model. 87
    e. Analysis of SO_2 Conversion. 89
  (4) Model Applications to Field Data. 91
    a. Model Equations 91
    b. Solar Radiation 92
    c. Plume Dispersion. 93
    d. Computational Description 94
    e. Simulation Results. 95
    f. Comparison of Model Predictions with Project MISTT Field Data. 96
    g. Hydrocarbon and Nitrogen Oxides Effects 98
References. 101

Appendices

A. Smog Profiles 106
B. Hydrocarbon and PAN Data. 123

FIGURES

Number		Page
1	Particulate Sulfate Size Distribution	13a
2	Relationship Between Particulate Sulfate Concentrations Determined by EAA and FPD	13b
3	Relationship Between Particulate Sulfate Concentrations Determined by IC and FPD	15a
4	Rates of SO_2 Conversion to Sulfate	55a
5	SO_2 Oxidation Rates Simulated by Kinetic Modeling . . .	95a
6	SO_2 Oxidation Rates Composited from 9 Sampling Missions of the Labadie Power Plant	97a

TABLES

Number		Page
1	Literature on SO_2 Oxidation	17
2	Description of Kinetic Model	18
3	Preliminary Experiment - Initial Conditions	17
4	Experiment and Modeling Results; 6-2-78	23
5	Experiment and Modeling Results; 4-25-79 - Dark	23
6	Experiment and Modeling Results; 4-25-79 - Light	27
7	Initial Conditions for SO_2 + HO Experiments	30
8	Experimental and Modeling Results; 6-5-78	31
9	Experimental and Modeling Results; 6-6-78	32
10	Experimental and Modeling Results; 11-10-77	34
11	Experimental and Modeling Results; 1-9-78	35
12	Experimental and Modeling Results; 6-14-78	37
13	Experimental and Modeling Results; 6-8-78	38
14	Experimental and Modeling Results; 6-15-78	39
15	Experimental and Modeling Results; 6-16-78	41
16	Initial Conditions for HO_2 + SO_2	43

Number Page

17 Experimental and Modeling Results; 12-13-77 43

18 Experimental and Modeling Results; 12-14-77 45

19 Experimental and Modeling Results; 6-23-78 47

20 Initial Conditions for $CH_3O_2 + SO_2$ with CH_4 48

21 Experimental and Modeling Results; 1-11-78 50

22 Experimental and Modeling Results; 1-10-78 51

23 Relative Contribution of HO, HO_2, RO_2 to SO_2 Oxidation - CH_4 System 52

24 Modeling Results with Azomethane 56

25-36 Urban/Rural Experiment Results 67-78

37 Summary of Results 79

38 Experimental and Modeling Results - Experiment 3 . . . 85

39 Experimental and Modeling Results - Experiment 11 . . . 85

40 HC-NO_X Effects for Plumes 100

ACKNOWLEDGEMENT

The author is very grateful for the assistance of his colleagues at Battelle: Richard Easter, Darrell Joseph, G. William Keigley, John Koetz, Chester Spicer, George Sverdrup and Jerry Ward.

SECTION 1.

INTRODUCTION

The widespread distribution of sulfate aerosols and their associated effects on visibility and precipitation pH are serious environmental concerns in the United States. Evidence has been presented in numerous studies that submicron-radii sulfates are predominantly $(NH_4)_X H_{2-X}SO_4$ with associated water.

Recent measurements by Pierson et al.(1) on Allegheny Mountain provide examples of the sulfate problem. Hydrogen ions were found to be the predominant aerosol cation when higher sulfate concentrations prevailed. Rainwater collected during their two-month study had a pH range from 2.7 to 4.1. And, as found in so many studies, virtually all of the variance in light scattering at their site could be empirically accounted for by the concentrations of sulfate in the submicron size fraction.

While oxidation of SO_2 in the atmosphere is considered to be the primary source of sulfate particulates, the chemical and microphysical processes involved in the gas-to-particle transformations are highly complex. In spite of numerous scientific efforts to better understand the transformation processes, many of the essential details pertaining to reaction rates and mechanisms are apparently missing. Thus it has not yet been possible to formulate either strategies to control the sulfate problem or models to predict regional sulfate levels as related to SO_2 sources.

Microphysical aspects of the formation of H_2SO_4 particles appear to be fairly well understood(2), although there is still much uncertainty in defining nucleation rates of new particles(3). Model calculations by Kiang and Middleton(4) led to the conclusion that oxidation of SO_2 in the gas phase is the rate limiting step for the formation and growth of secondary H_2SO_4

particles in the atmosphere. The rate limiting reactions are the subject of this investigation.

The kinetics and mechanisms of the elementary gas phase reactions of SO_2 in air have been reviewed in several articles(5-8). It is clear from the extensive review by Calvert et al.(7) that all known reactions involving electronically excited states of SO_2 are insignificantly slow in the troposphere. Furthermore, compeling evidence was presented in the same review to say that HO, HO_2 and RO_2 radicals are the only tropospheric species likely to be capable of oxidizing SO_2 at substantial rates.

The objective of this study was to provide a new and more comprehensive body of data useful in evaluating the kinetic and mechanistic theories pertaining to those free radical reactions with SO_2. Based on the new findings and on additional smog chamber data obtained with rural and urban hydrocarbon systems, a photochemical smog model was applied to simulate gas phase SO_2 oxidation rates for various atmospheric conditions. The results are summarized in Section 2.

SECTION 2.

SUMMARY AND CONCLUSIONS

Experiments were conducted in Battelle's 17 m^3 smog chamber to investigate the kinetics of the free radical reactions of SO_2 in smog and to provide data on SO_2 transformation to sulfate during atmospheric simulations of urban and rural conditions.

Rate constants were derived for the following reactions: $SO_2 + HO + M \rightarrow$ sulfate (60), $SO_2 + HO_2 \rightarrow$ sulfate (61), $SO_2 + CH_3O_2 \rightarrow$ sulfate (64). Psuedo second-order rate constants ($ppm^{-1}min^{-1}$)are: $k_{60}=1600$, $k_{61} < 0.2$, $k_{64} < 0.8$. The values for k_{61} and k_{64} are only upper limit estimates, and the rates pertain to the overall conversion of SO_2 to particulate sulfate. Rates of SO_2 consumption were not measured directly and may be larger than the reported values if oxidation products persisted in the gas phase. Regarding reaction 60, it appears that all of the SO_2 oxidized by this route results in the formation of sulfate particles.

The mechanisms of SO_2 conversion were not investigated although some work was done to determine if NO and/or NO_2 form stable aerosol products with the intermediates created after HO addition to SO_2. According to the analyses for particulate nitrate, they did not, in spite of relatively high concentrations of HO, SO_2 and NO_X.

In the course of the experiments with inorganic smog systems ($HNO_2/NO_X/SO_2$), additional kinetic information was obtained, particularly as it pertained to the experimental system. An upper limit rate of $3x10^{-7}ppm^{-1}min^{-1}$ was derived for the homogeneous reaction between dinitrogen pentoxide and water vapor to yield nitric acid. It was also determined that ozone and nitrous acid do not react at a significant rate to produce nitric acid. And we could not detect any heterogeneous reaction between SO_2 and nitrous acid in the presence of sulfuric acid aerosols.

Mixtures of hydrocarbons (HC) were used in smog chamber experiments to simulate SO_2 oxidation under urban and rural conditions. Although the average reactivity for the two mixtures, based on rate constants of individual hydrocarbons with HO radicals, was nearly equal, there were marked differences in several important smog parameters. With the urban HC mixture, the rates of NO oxidation and xylene disappearance and the maximum rates of SO_2 oxidation were about twice as great as for the rural HC mixture. The formation of PAN and other products of NO_2 oxidation were also greater for the experiments with urban HC.

For both hydrocarbon mixtures, the rates of SO_2 oxidation were greatest near the periods of peak NO_2 formation, and gradually diminished thereafter. After 24 hours of irradiation, the rate of SO_2 oxidation was about one-fourth as large as the maximum rate observed with the urban HC mix; for the rural HC mix, the rate of SO_2 oxidation at 24 hours was about one-third the maximum rate.

In some experiments, NO was added together with SO_2 to emulate the emission into the atmosphere of these pollutants from point sources. The addition of NO with SO_2 (at SO_2/NO ratios of 4/1) at different intervals of the irradiation period had mixed results. When added at five hours, NO had small positive effects on the rates of SO_2 oxidation, but when added at one hour, NO reduced the rates of SO_2 oxidation.

Incorporating the new rate constants for SO_2 oxidation, a very general mechanism of smog chemistry was applied to model the chamber experiments. In most cases, the predictions for SO_2 conversion to sulfate were reasonably good; within 20 percent for the inorganic smog systems and within 25 percent for the hydrocarbon-NO_x systems. The model tended to underestimate SO_2

conversion, and the worst discrepancies arose during the period of most rapid SO_2 oxidation in the hydrocarbon systems when the model estimates were only one-half the actual rates. For the smog conditions that were modeled, it was estimated that at least 75 percent and sometimes greater than 90 percent of the SO_2 oxidation was initiated by reactions of SO_2 with HO radicals.

The kinetic model was used to simulate SO_2 oxidation for ambient conditions. Effects of variable solar radiation were simulated by using time dependent photodissociation rates for NO_2, HNO_2, H_2O_2 and aldehydes. According to the modeling results, the production of HO and the oxidation of SO_2 depend strongly on solar radiation intensity. Reduced radiation resulted in disproportionately lower rates of SO_2 oxidation. For reduced radiation conditions, the maximum rates of SO_2 oxidation were predicted to occur near mid-afternoon, while for clear sky conditions, the maximum oxidation rates occurred between 11:00 and noon. The rates of SO_2 oxidation were shown to depend on ambient HC and NO_x conditions. For the range of conditions modeled, the maximum rate of SO_2 oxidation (clear sky) varied from 3.7 to 7.4 percent/hr.

The computer code was also incorporated with a model of plume dispersion to simulate the interaction of power plant emissions with polluted ambient atmospheres. Rates of SO_2 oxidation were estimated in plumes as functions of plume dispersion rates, plume emission periods, solar radiation and ambient concentrations of hydrocarbons and NO_x. Plume dispersion rates affected the induction period of NO and SO_2 oxidation. Variations in solar radiation intensity and thus the diurnal period of the power plant emissions strongly affected SO_2 oxidation rates. For well-dispersed plumes and clear sky conditions, maximum SO_2 oxidation rates (ranging from 2.7 to 6.9 percent/hr.) were estimated to occur during the noon to early afternoon periods. The patterns of SO_2 oxidation predicted by the model agreed well with the data for the Labadie plume as reported in the MISTT project (Midwest Interstate Sulfur Transport and Transformation.)

For relatively low HC/NO_X ratios for ambient air, SO_2 oxidation rates computed for plumes were bound by the ambient rates of SO_2 oxidation. At high HC/NO_X ratios, the rates of SO_2 oxidation in plumes were predicted to exceed the rates in ambient air. Under such conditions, the model also predicted an excess (or bulge) in the plume O_3 concentrations. These features have been observed in actual plume studies.

The major conclusions regarding SO_2 conversion to sulfate in polluted atmospheres are set forth below:

- Oxidation of SO_2 is dominated by the reaction with hydroxyl radicals. This initial reaction is the rate-limiting step in the conversion of SO_2 to sulfate.
- It follows that relatively simple kinetic models that adequately describe the variations in atmospheric [HO] should suffice to estimate gas phase SO_2 transformation rates.
- Experimental and theoretical simulations of urban and rural atmospheres show that the rates of SO_2 oxidation are strongly coupled to solar radiation intensity and pollution conditions. Although high concentrations of NO generally suppress or delay HO production and SO_2 oxidation, NO is a key element in regenerating HO from peroxy radicals. NO_2,on the other hand, inhibits SO_2 oxidation by scavenging HO. CO, aldehydes, and possibly some

hydrocarbons tend to inhibit SO_2 oxidation by converting HO into products which are less efficient in oxidizing SO_2. In general, reactive hydrocarbons serve to promote SO_2 oxidation, and the stochiometry or net flux of HO affected by hydrocarbon degradation appears to be key to the acceleration of SO_2 oxidation in polluted air.

- SO_2 oxidation rates in moderately polluted air or in well-aged air that was once polluted are expected to be 60-80 percent lower than the rates in freshly polluted air.
- Modeling results indicate the SO_2 oxidation rates in power plant plumes are highly dependent on plume dispersion rates and are coupled to the same parameters governing SO_2 oxidation in the ambient air. For well-dispersed plumes, most rapid SO_2 conversion is predicted to occur from noon through early afternoon. The accompaniment of NO in plumes generally suppresses [HO] and the rate of SO_2 oxidation. However, under certain circumstances where high concentrations of reactive HC have been mixed into a rapidly-dispersing plume, the rate of SO_2 oxidation is expected to exceed the oxidation rate in ambient air. Under such conditions, an excess of O_3 is also predicted in the plume.

SECTION 3

EXPERIMENTAL METHODS

A. Smog Chamber Facility

Experiments were conducted in Battelle Columbus' 17.4 m^3 smog chamber having a surface/volume ratio of 0.8 m^{-1}; the surface is polished aluminum (∿80%) and FEP Teflon (∿20%). The series of experiments with rural and urban hydrocarbon mixtures was conducted with the chamber completely lined with 5-mil Teflon film. Irradiation was provided by a bank of 95 fluorescent blacklamps and 15 fluorescent sunlamps. Combined intensity of the lamps yielded a NO_2 photo-dissociation rate of 0.14 ± .01 min^{-1}. Replacement of the lamps for the experiments with Teflon lining gave a NO_2 photo-dissociation rate of 0.17 min^{-1}. These rates were about one-half that for previous studies in the chamber and must be taken into consideration if data are extrapolated to atmospheric conditions where the solar intensity is larger and variable.

B. Background Conditions and Contamination

Background air for the chamber was passed through a purification system which included a dehumidification unit, permanganate pellets, a charcoal filter system designed to remove acidic and basic gases, and an absolute filter. Background CCN were < 100 cm^{-3}. SO_2 and NO_2 were generally below the detection levels of 1 and 2 ppb, respectively. Background NO concentrations ranged from 1-12 ppb.

Background THC ranged between 1.9 and 2.5 ppmC, of which nearly 2 ppm was CH_4. On days when higher THC concentrations were present, no experiment was conducted. Numerous gas chromatographic (G.C.) analyses of background air when NMHC was 0.1-0.3 ppmC showed no detectable olefins or aromatics in the C_2-C_9 range. Traces of high molecular weight hydrocarbons sometimes appeared when NMHC was 0.4-0.5 ppmC. When relatively small concentrations of nitrous acid (a source of HO radicals and NO_x)were added to the background air under these contamination conditions, irradiation resulted in peak O_3 concentrations in the 8-12 ppb range. In theory, the reactivity (in terms of O_3 production) of this amount of hydrocarbon contamination corresponds to the reactivity of about 4-6 ppm CO. Therefore, the intentional addition of 4.5 ppmC hydrocarbons and/or large quantities of CH_4 and CO clearly overwhelmed any effects due to background HC contaminants. Also, the intentional introduction of nitrous acid into the air for most of the experiments was believed to have overcome any spurious surface contaminant effects which might have led to the generation of free radicals at the outset of irradiation.

C. Surface Effects and Wall Losses

During the summer that preceded this study, it was discovered that some deterioration of the smog chamber's aluminum surfaces had occurred due to prolonged exposures to high nitric acid concentrations. The surface had become dull and rough. The chamber walls were therefore cleaned and repolished, and some preliminary experiments were conducted to assess the "condition" of the chamber. Loss rates for NO_2, PAN, HNO_2 and O_3 were found to be satisfactorily small. However, SO_2 loss rates were unacceptable (∿5%/hr. above the dilution rate), and HNO_3 losses were so large that it was difficult to measure the rate. Repeated exposure of the chamber surfaces to H_2SO_4 aerosols and other products of smog finally appeared to have passivated the surfaces. More detailed investigations after the chamber stabilized showed no discernible wall loss for SO_2. HNO_3 losses were still a problem and varied depending on humidity conditions. At 50% rh and under irradiation conditions, the loss rate was approximately $2\times10^{-2}\text{min}^{-1}$. This is about twice the theoretical rate based on diffusive transport alone. Eddies due to temperature gradients were presumably responsible for the additional contact frequency.

In the computer models used to analyze the chamber data, the wall loss rate for HNO_3 was ascribed to other reactive or acid species; e.g. N_2O_5, HO_2, HO_2NO_2, NO_3, RO_2NO_2, and HO_2.

The loss of O_3 under irradiation conditions was $1.2\times10^{-3}min^{-1}$, and H_2SO_4 aerosol losses consistently averaged $2.5\times10^{-3}min^{-1}$. These rates were also incorporated into the modeling program along with dilution losses for all species.

D. Analytical Methods - Gas Phase

PAN was analyzed by EC-GC at 35C using a 2-ft. glass column, 1/8 in ID, Carbowax 400, and argon-methane carrier.

C_1-C_4 hydrocarbons were analyzed by FID-GC at room temperature using a 16 ft. x 1/8 in. aluminum column, phenylisocyanate on Durapak Porosil-C. C_5-C_9 hydrocarbons were chromatographed using a 300 ft. stainless steel capillary column with DC-200 support and cryogenic programming from -100C to +135C.

CO was analyzed by nondispersive IR, total aldehydes by bisulfite titration, and formaldehyde by the chromotropic acid method. O_3 was monitored with a REM model 612-B chemiluminescence analyzer. Attempts to measure H_2O_2 by the method of Kok et al.(9) were unsuccessful; large negative interferences due to SO_2 were discovered.

Nitrous acid, generated by the method of Chan et al.(10) was determined by a Mast Acid Analyzer, a Thermo Electron (TECO) model 14-D chemiluminescence analyzer and a Beckman K-76 Acralyzer that is a continuous Saltzman analyzer. Saltzman solution responsed equally to HNO_2 and NO_2, as did the TECO in the NO_X channel. The Mast acid instrument had a ten-fold greater response to HNO_2

than to NO_2. NO was determined specifically by chemiluminescence. HNO_3 was determined using nylon in conjunction with the TECO analyzer. It was determined that N_2O_5 does not interfere with the nylon method for HNO_3, and thus it was recorded ambiguously in the NO_x channel together with PAN, NO_2 and HNO_2. A Bendix-NO_x analyzer that did not convert N_2O_5 to NO was also used in some experiments. In those cases, the difference between the TECO-NO_x and Bendix-NO_x channels was interpreted as N_2O_5.

SO_2 was measured at the beginning of an experiment with a Meloy 285 flame photometer. Upon irradiation, the instrument was used to monitor sulfate aerosol. The photometer was intermittently operated in the total sulfur mode (SO_2 plus sulfate) to check on the SO_2 concentration.

Gas calibrations were performed routinely. The chemiluminescence analyzer used to monitor NO, HNO_2 and NO_2 were spanned before nearly every experiment with an NO source referenced to a NBS standard. In situ O_3 titrations were conducted in the chamber to check on the span of the O_3 analyzer and the efficiency of the NO_x converters. After an experiment (lamps off), excess NO was injected into the chamber to more than titrate the remaining O_3. Excellent correspondence between NO_2 production and O_3 loss was always observed. This also indicated that no other strong oxidants existed in the air or on the chamber walls.

The SO_2 analyzer was calibrated by Meloy Laboratories and the calibration agreed with injections of known SO_2 volumes in the smog chamber.

Instruments for hydrocarbon analyses were calibrated with a NBS source of propane.

E. Analytical Methods - Condensed Phase

Because calculations of SO_2 oxidation rates rely on experimental data for the SO_2/sulfate distribution, the most important measurement in this study was for sulfate aerosol. During the early portion of the study, our approach for sulfate determinations consisted of sequential aerosol collections (and subsequent analyses for $SO_4^=$ and NO_3^- by ion chromatography) during discrete periods of the smog experiments. However, the amount of air in the chamber imposed a serious limitation on the available sample volume. The sampler we employed sampled at 2 ℓ/min through 47-mm Fluoropore (Teflon) membranes. Preliminary work showed that sampling for 15 min. was too short to observe sulfate levels above the filter blanks (5 ± 1 μg for sulfate and 3 ± 1 μg for nitrate). For three subsequent experiments, 30 min. collections were obtained on Fluoropore. In these cases the sulfate data were reasonable, but the precision was still not satisfactory.

To improve the situation, particulate collections during another experiment were made on acid-treated quartz which had no detectable blank for sulfate. In this case, parallel collections for 30 minutes yielded sulfate concentrations of 33 $\mu g/m^3$ and 34 $\mu g/m^3$ which compared well with a sulfate concentration estimated by an electrical aerosol analyzer.

In spite of improvement in the reliability of the sulfate determinations offered by the treated quartz filters, it was concluded that the best available filter-extraction-analysis procedure for sulfate was still not satisfactory for the degree of resolution required by this study. Shorter sampling periods at higher flow rates would have improved on the temporal structure of the sulfate data, but at considerable sacrafice to the analyses of the overall smog experiments. As discussed later in this section, the primary method adopted for monitoring sulfate was based on continuous sampling by a flame photometric detector (FPD). To provide checks on that method, large volume ($\sim 10\ m^3$) collections on 4 in. diameter quartz filters (acid treated) were made at the conclusion of several experiments, and the sulfate concentrations so obtained were compared to those determined by FPD. Those results are also presented later in this section.

During many of the earlier experiments an electrical aerosol analyzer (EAA) was used to monitor the evolution of sulfate aerosols as a function of irradiation time. An example of the volumetric size distribution is shown in Figure 1. Typically, all of the sulfate particles were within the size range of the EAA, and the volume or mass mean diameter of the particles was near 0.1 μm at the end of the growth period. Presumably the total volume concentration, obtained by integrating the size distribution function, equates with the sulfate mass concentration, assuming certain chemical properties for the sulfate particles. In previous smog chamber studies, mass concentrations computed from EAA data correlated well with concentrations obtained by filter analyses. However, for unknown reasons our experience in this study was different. Comparisons between aerosol volume concentrations (derived from the EAA) and particulate sulfur concentrations determined by the FPD method are shown in Figure 2. The results are highly irregular. From the limited data it was not possible to determine the source(s) of the discrepancies. For some time, it was suspected that variable concentrations of nitrate or combined sulfate-nitrate aerosols might be the cause, but this was not borne out by chemical analyses for nitrate. Humidity also seemed to be a factor but theoretical arguments could not account for the large discrepancies.

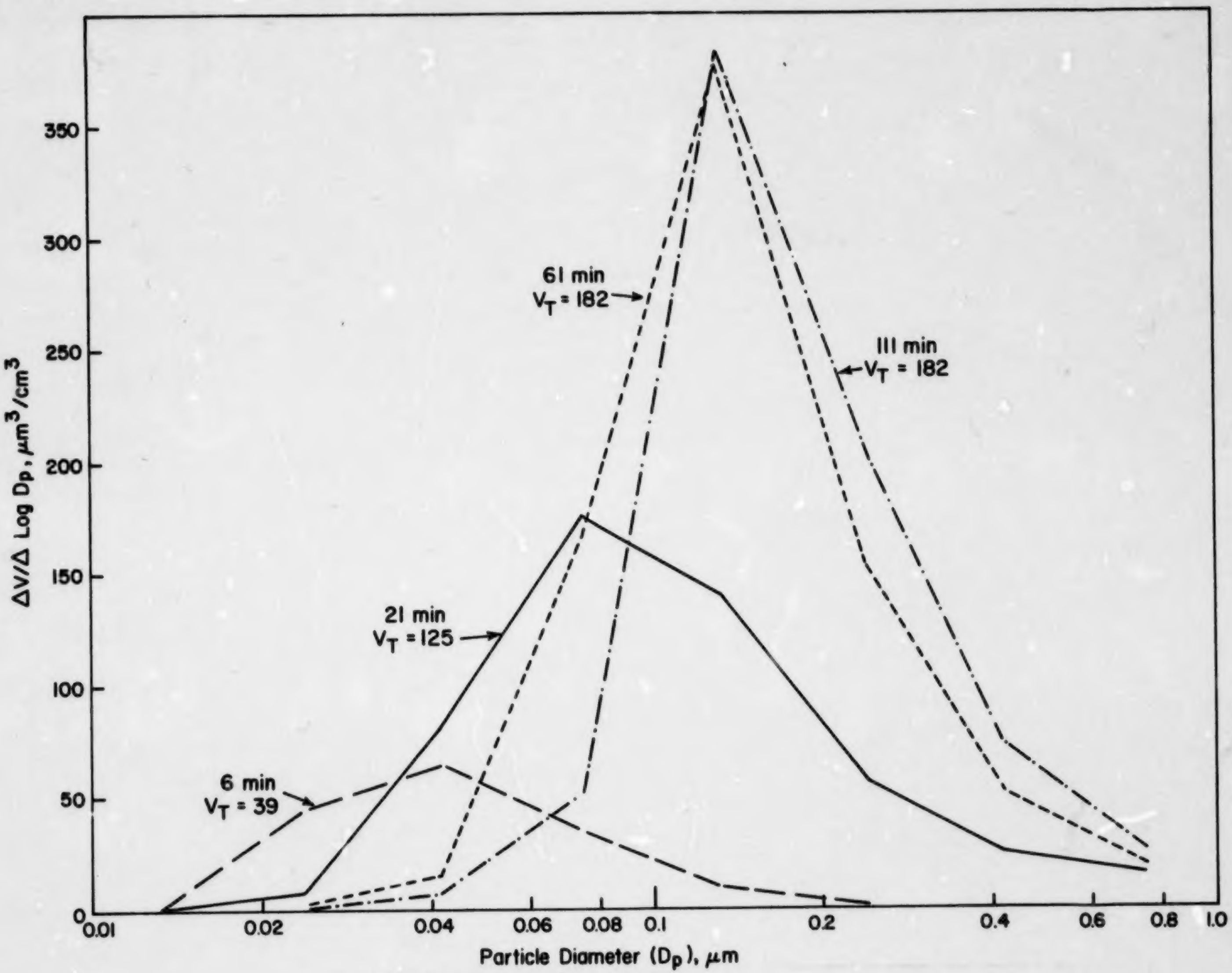

Figure 1. Particulate Sulfate Size Distribution Showing Growth in Particulate Size and Volume Concentration During SO_2 Oxidation in the $HNO_2/NO_X/SO_2$ Smog System.

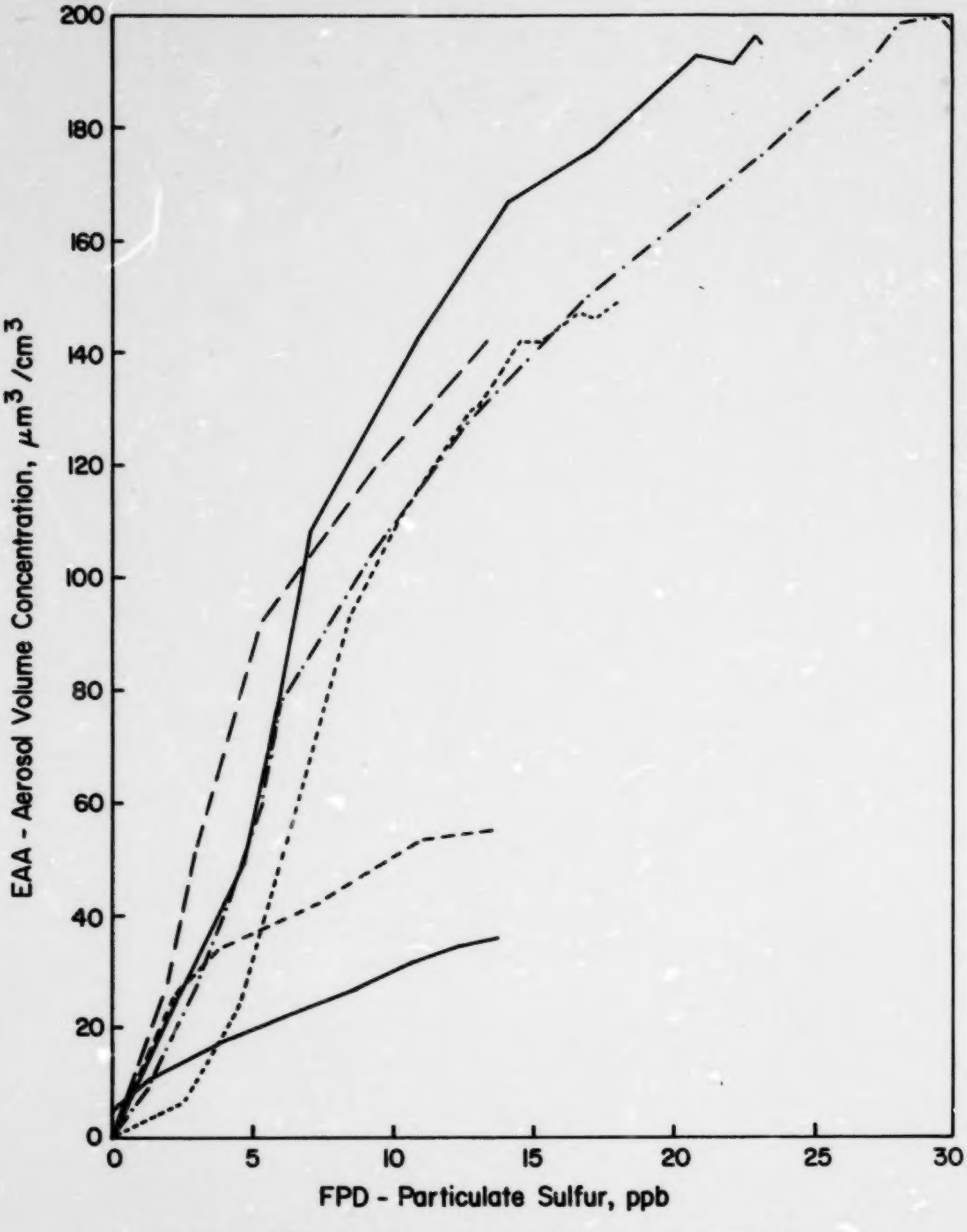

Figure 2. Relationships Between Particulate Sulfate Concentrations Determined by an Electrical Aerosol Analyzer (EAA) and a Flame Photometric Detector (FPD) for Several Experiments of SO_2 Oxidation.

Since very reproducible results were obtained with the FPD method, and since it could be more easily standardized, it was used as the principal analyzer for sulfate.

Use of the FPD method for sulfate measurements has been described by Durham et al.(11). By taking advantage of the tremendous difference in diffusivity between SO_2 ($D = 1.4 \times 10^{-1}$ cm^2 sec^{-1}) and H_2SO_4 aerosols ($D = 7 \times 10^{-6}$ cm^2 sec^{-1} for 0.1 μm diameter aerosols), a diffusion-denuder tube was designed to remove virtually all of the SO_2 in the air sample entering the FPD, while allowing most of the particulate sulfur to pass to the detector. Optimization between maximum SO_2 removal and minimum H_2SO_4 loss was determined experimentally by generating independently known concentrations of SO_2 and H_2SO_4 aerosol in the smog chamber. This procedure also permitted direct calibration of the Meloy for H_2SO_4. The end result of the optimization work was a sample flow of 200 ml/min. through a 35-cm lead acetate diffusion tube, with >99.5 percent removal of SO_2 and 35 percent loss of H_2SO_4 aerosol.

An example of the calibration procedure follows. An aqueous solution containing 1.47×10^{-3}g H_2SO_4 was evaporated and allowed to recondense in the smog chamber. Subsequent aerosol collections and analyses for $SO_4^=$ by IC confirmed a theoretical concentration of 22 ppbS in the chamber.

Direct sampling by the Meloy FPD yielded a concentration of 17 ppbS. This represented a 23 percent loss of sulfate in the plumbing or a slightly reduced response to H_2SO_4. Exposing the sample to NH_3 upstream of the detector did not change the response. When the SO_2 denuder was incorporated in the sample line the response diminished to 11 ppbS, indicating a 35 percent loss in the diffusion tube. In this configuration, the FPD response to sulfate aerosol was 50 percent theoretical. These losses were considerably greater than those reported by Durham et al. (11)

In addition to calibrations with pure H_2SO_4, FPD results were compared to sulfate analyses of aerosol collections made after several smog chamber experiments with hydrocarbon-NO_X-SO_2 mixtures. The results are shown in Figure 3. There appears to be good correspondence between four of the six determinations -- there was no apparent reason for the divergence of the other two points. In these cases, sulfate concentrations determined by the aerosol filtration-IC method were about 15 percent lower than those determined by FPD.

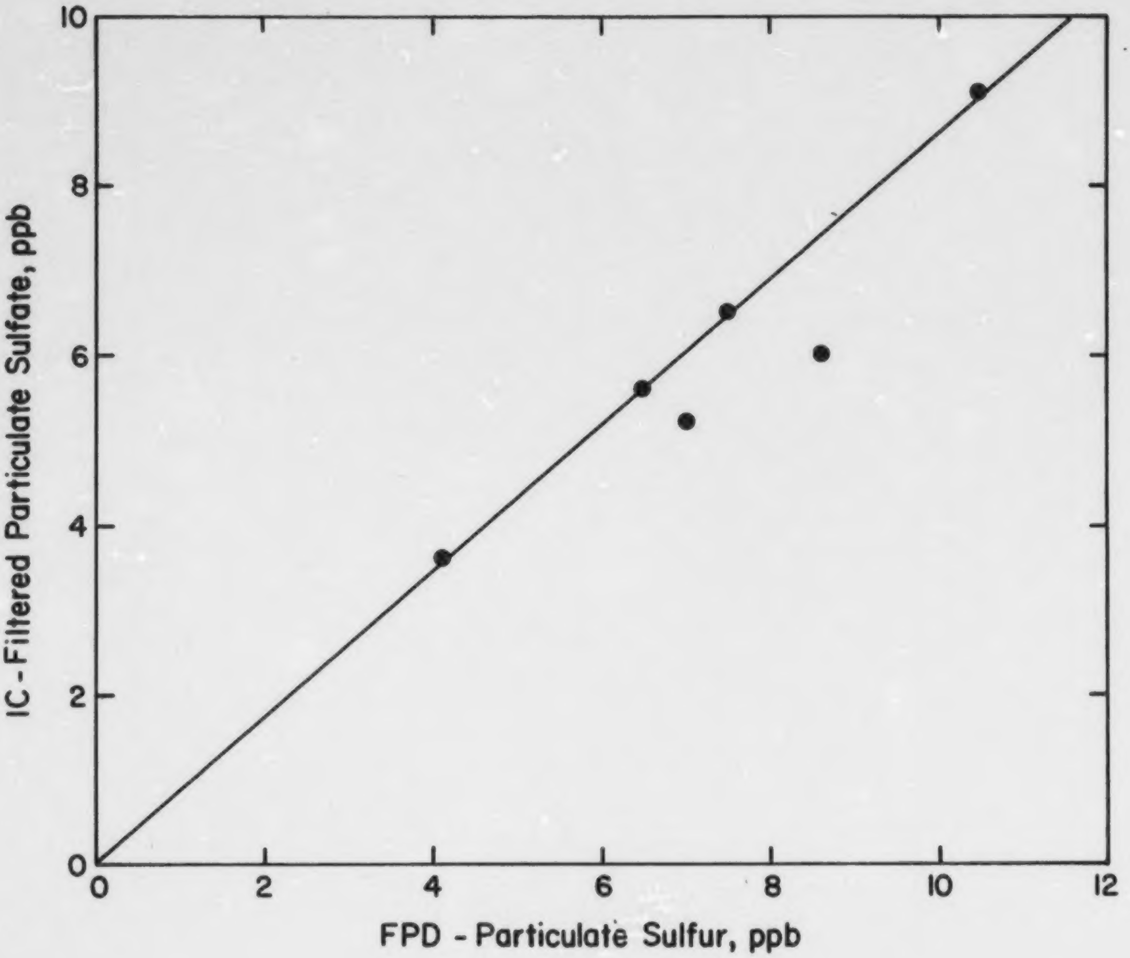

Figure 3. Relationships Between Particulate Sulfate Concentrations Determined by Ion Chromatographic (IC) Analyses of Filter Collections and a Flame Photometric Detector (FPD).

SECTION 4.

RESULTS AND DISCUSSION

A. Experimental Approach for Kinetic Data

The objective of this part of the project was to investigate the kinetics (and mechanisms where feasible) of SO_2 oxidation by free radicals; namely, HO, HO_2, CH_3O_2. Current evaluations of the rate constants for these reactions are shown in Table 1. Data from the literature together with data obtained in this study are discussed at the conclusion of this section.

Our approach for studying these reactions was to generate a variety of distributions between HO, HO_2 and CH_3O_2 in a smog chamber containing SO_2. The starting point for this work was a series of smog chamber experiments with an inorganiz smog system ($HNO_2/NO_x/CO/SO_2$). By selecting the initial concentrations of system components, it was possible to affect a range of HO/HO_2 ratios and thereby observe the relative rates of SO_2 oxidation attributable to the respective radicals. For example, in experiments where the NO/NO_2 ratio was large, the HO_2 concentration was suppressed relative to HO. On the other hand, when large concentrations of CO were incorporated, HO was suppressed relative to HO_2 radicals.

To obtain estimates of the free radical concentrations, and hence to calculate absolute rate constants, it was necessary to "fit" the experimental data with a chemical kinetics model. Throughout this project numerous adjustments in reaction mechanisms and rate constants were made as new information became available in the literature and to reflect our experimental findings. For consistency, only those results obtained with the code appearing in Table 2 are reported here, together with comments on the effects of some changes in rate constants or mechanisms. To some extent, the code in Table 2 represents a

TABLE 1

Literature Values for the Free Radical Reactions with SO_2

Reaction No.(1)	Reaction	Rate Constant (ref) $ppm^{-1}min^{-1}$
60	$HO+SO_2+M \rightarrow$ products	1.6×10^3 (Calvert, et al.)
61	$HO_2+SO_2 \rightarrow$ products	1.3 (Payne, et al.) $< 1.5 \times 10^{-3}$ (Graham, et al.)
64	$CH_3O_2+SO_2 \rightarrow$ products	12 (Sanhuega, et al.) 7.8 (Kan, et al.)

---

(1) Reaction Nos. are keyed to the kinetic model appearing in Table 2.

TABLE 3

Initial Conditions of Preliminary Experiments with the Inorganic Smog Systems

Experimental Date	Initial Reactant Concentrations (ppb) NO	NO_2	HNO_2	$CO(\times 10^3)$	SO_2
11-7-77(1)	262	35	153	102	0
11-9-77(1)	218	38	179	57	470
11-10-77	268	42	165	< 5	490
11-11-77(1)	197	17	201	160	490

---

(1) CO contamination suspected

TABLE 2. DESCRIPTION OF KINETIC MODEL

No.	Reaction	Rate Constant(1)	Units(2)
	Inorganic System		
1	$NO_2 = NO + O_3$	.17E + 00(3)	min^{-1}
5	$HONO = NO + HO$	.34E - 01	min^{-1}
6	$HONO + HO = NO_2 + H_2O$	.90E + 04	
8	$NO + O_3 = NO_2$	.25E + 02	
9	$NO + HO = HONO$	.90E + 04	
10	$NO + HO_2 = NO_2 + HO$	.12E + 05	
12	$NO_2 + HO = HONO_2$	.15E + 05	
13	$NO_2 + HO_2 = HO_2NO_2$	.16E + 04	
14	$HO_2NO_2 = NO_2 + HO_2$	.76E + 01(4)	min^{-1}
15	$NO_2 + O_3 = NO_3$	.55E - 01	
16	$NO_3 = NO_2 + O_3$	.21E + 01(3)	
17	$NO_3 + NO = 2NO_2$	.28E + 05	
18	$NO_3 + NO_2 = NO + NO_2$	.63E + 00	
19	$NO_3 + NO_2 = N_2O_5$	.67E + 04	
20	$N_2O_5 = NO_2 + NO_3$	.50E + 01(4)	min^{-1}
21	$N_2O_5 + H_2O = 2HONO_2$	.30E - 06	
22	$O_3 + HO = HO_2$	.82E + 02	
23	$O_3 + HO_2 = HO$	.16E + 01	
30	$HO_2 + HO = H_2O$	.44E + 05	
31	$HO_2 + HO_2 = H_2O_2$	.37E + 04	
32	$H_2O_2 = 2HO$	.84E - 03	min^{-1}
33	$H_2O_2 + HO = HO_2 + H_2O$	.13E + 04	
34	$HO + HO = H_2O_2$	.65E + 05	
	NMHC System		
41	$NMHC + HO = RO_2$	.10E + 05(3)	
42	$ALD = 0.75\ HO_2 + 0.25\ RO_2 + CO$	.30E - 02(3)	min^{-1}
43	$ALD + HO = 0.50\ HO_2 + 0.50\ RCO_3 + 0.50\ CO$	.22E + 05(3)	
44	$RO_2 + NO = RO + NO_2$	.12E + 05	
45	$RO_2 + NO_2 = RO_2NO_2$	.16E + 04	
46	$RO_2NO_2 = RO_2 + NO_2$	.50E + 00(4)	min^{-1}
47	$RCO_3 + NO = RO_2$	.12E + 05	
48	$RCO_3 + NO_2 = PAN$	.12E + 05	
49	$PAN = RCO_3 + NO_2$	.55E - 01(4)	
50	$RO = ALD + HO_2$	.88E + 03	
51	$RO_2 + RO_2 = RO + 0.50\ ALD + 0.50\ ALC$	.54E + 03(3)	
52	$RO_2 + HO_2 = RO_2H$	.22E + 03	
	Methane System		
70	$CH_4 + HO = CH_3O_2$	.12E + 02	
71	$CH_3O_2 + CH_3O_2 = CH_3OH + CH_2O$	.45E + 03	
72	$CH_3O_2 + CH_3O_2 = 2CH_3O$	.22E + 03	
73	$CH_3O_2 + HO_2 = CH_3O_2H$	.15E + 04	
74	$CH_3O_2H + HO = CH_3O_2$	.12E + 04	
75	$CH_3O_2H = CH_3O + HO$	.46E - 03	min^{-1}
76	$CH_3O = CH_2O + HO_2$	.88E + 03	
77	$CH_2O + HO = CO + HO_2$	.22E + 05(3)	
78	$CH_2O = CO + 2HO_2$	.13E - 02	min^{-1}
79	$CH_3O_2 + NO = CH_3O + NO_2$	.12E + 05	

Table 2 - CONTINUED

TABLE 2. DESCRIPTION OF KINETIC MODEL

No.	Reaction	Rate Constant(1)	Units(2)
	Azomethane Surface Reactions - 200 Liter Chamber		
90	AZOME = CH_3O_2	.10E - 02(3)	min^{-1}
91	CH_3O_2H =	.50E + 00(5)	min^{-1}
92	CH_2O =	.60E + 00(5)	min^{-1}
93	CH_3O_2 =	.50E + 00(5)	min^{-1}
94	HO_2 =	.60E + 00(5)	min^{-1}
	SO_2 Reactions		
60	SO_2 + HO = SULFATE + HO_2	.16E + 04(3)	
61	SO_2 + HO_2 = SULFATE + HO	.20E + 00(3)	
62	SO_2 + RO_2 = SULFATE + RO	.80E + 00(3)	
64	SO_2 + CH_3O_2 = SULFATE + CH_3O	.80E + 00(3)	
	Surface Reactions - 17 m^3 Chamber		
80	O_3 =	.12E - 02(5)	min^{-1}
81	SULFATE = SWALL	.25E - 02(5)	min^{-1}
82	N_2O_5 = 2NWALL	.20E - 01(5)	min^{-1}
83	NO_3 = NWALL	.20E - 01(5)	min^{-1}
84	$HONO_2$ = NWALL	.20E - 01(5)	min^{-1}
85	HO_2NO_2 = NWALL	.20E - 01(5)	min^{-1}
86	RO_2NO_2 = NWALL	.20E - 01(5)	min^{-1}
87	$CH_3O_2NO_2$ = NWALL	.20E - 01(5)	min^{-1}

(1) hν, M and O_2 assumed

(2) Units are $ppm^{-1}min^{-1}$ unless noted

(3) Surrogate reaction; rate constant represents rate-limiting step

(4) Thermal decomposition

(5) Heterogeneous reaction on chamber surface

compromise among alternatives, and it does not fit all of the data well, as discussed in the report. For the most part, rate constants for the selected reactions are consistent with the data published by the National Bureau of Standards(12).

It should be emphasized that throughout this study the SO_2 oxidation rates related to the subject radicals were determined solely in terms of sulfate aerosol product. Any sulfur products remaining in the gas phase were not determined. As such, the rate constants obtained represent rate limiting kinetics for conversion of SO_2 to sulfate and not the upper limit rates for SO_2 removal. In general, good material balances were observed between gas-phase and condensed-phase sulfur, but once the reactions began it was not certain that the gas-phase sulfur was exclusively SO_2.

B. Inorganic System ($HNO_2/NO_x/CO/SO_2$)

(1) Preliminary Experiments

A series of preliminary experiments were conducted early in the project during which time analytical procedures were being developed and evaluated. Initial reactant concentrations for the experiments are summarized in Table 3. Smog profiles (plots of reactant and product concentrations versus irradiation time) of these and other experiments are presented in Appendix A.

With the exception of the experiment on 11-10-77, which will be discussed later, the results of these initial experiments will be disregarded due to suspected contamination and analytical difficulties. For example, some problems were encountered with the O_3 monitor. And, based on large negative interferences to the FPD when CO was introduced to the chamber, it was thought that the CO source might have been contaminated with an inpurity such as iron carbonyl. These experiments were repeated later using a new bottle of CO in an aluminum container.

(2) Experiments to Investigate HNO_2 Reactions and NO_x Losses

In the inorganic smog system, nitrogen oxides govern the free radical concentrations of interest because their reaction rates with the radicals are typically orders of magnitude larger than those of the corresponding reactions with SO_2.

Thus before attempting to interpret experimental data pertaining to SO_2 oxidation, it was necessary to understand the nitrogen oxides chemistry as it occurred in the smog chamber.

Since substantial concentrations of HNO_2 were used as a radical source in many of the experiments, it was important to determine the reaction rates for HNO_2 under experimental conditions. It was also necessary to account for the large NO_x losses observed in most experiments. The experimental results discussed next focus on these subjects.

Experiment 6-2-78

In this experiment, HNO_2 was simply injected into the chamber and irradiated. As usual, small quantities of NO and NO_2 were inadvertently added together with HNO_2 such that the initial concentrations were NO = 110 ppb, NO_2 = 79 ppb and HNO_2 = 261 ppb. As the irradiation proceeded, it was difficult to accurately determine HNO_2 from NO_2 and we have generally combined their concentrations when profiling the experiments (Appendix A).

The main interest in this experiment was to determine the HNO_2 photolysis rate. This was not entirely straightforward since the reaction products, HO and NO, rapidly recombine (at a somewhat uncertain rate) and trace levels of contamination cause NO to be oxidized to NO_2. The rapid reaction between HO and NO_2 to give HNO_3 and subsequent wall losses of this product further complicate the picture.

In Table 4, the concentrations of pertinent species are shown as a function of the irradiation time. Theoretical data (i.e., kinetic simulation results) are presented directly below the respective experimental data.

As indicated in Table 4, N^{5+} is meant to represent the nitrogen oxide loss (or unaccounted NO_X) that occurs as the reactions proceed. In this report, NO_X represents HNO_2 as well as NO and NO_2. Thus NO_X loss, or N^{5+}, represents undetermined products of NO_2 oxidation, such as HNO_3, HO_2NO_2, NO_3 and N_2O_5. In some cases, HNO_3 was successfully measured; in many cases it was not.

Our experience indicated that the majority of the N^{5+} products were lost due to absorption on the chamber surfaces. The possibilities for incorporation into the condensed (particulate) phase were investigated, and those results are discussed later in the section.

In this particular experiment, 9 ppb of O_3 was produced after a 90 min. irradiation period. As discussed in the previous section on analytical methods, O_3 production following the initial irradiation period is largely attributed to organic contaminants in the air, such as CO and traces of hydrocarbons. In attempting to model the formation of O_3 observed experimentally, an appropriate concentration of CO is included in the model to represent the contamination effect. For this experiment, model [CO] = 8 ppm.

The NO concentration throughout the experiment is largely a function of the photolysis rate for $HNO_2(k_5)$ and the HO+NO recombination rate (k_g). The modeling results shown in Table 4 were obtained with a k_1/k_5 ratio of 5, and $k_g = 9x10^3 ppm^{-1} min^{-1}$. Use of $k_g = 1.5x10^4 ppm^{-1} min^{-1}$ as recommended by Cox, et al(13) resulted in poorer fits with the experimental data.

Material balances between the model and experimental data in Table 4 are reasonably good, although the model slightly underestimates the NO_X losses.

---

[*] Throughout the report, tabulated data obtained by kinetic modeling will be presented in script to offset it from the experimental data.

TABLE 4

Experimental and Modeling Results for Experiment 6-2-78

Irradiation Time, min.	Specie Concentrations (exp/*model*), ppb O_3	NO	$NO_2 + HNO_2$	N^{5+} (1)
0	0	110	338	0
	0	*110*	*338*	*0*
30	7	120	248	69
	7.7	*116*	*264*	*57*
60	8	118	207	102
	8.6	*113*	*223*	*90*
90	9	113	187	117
	9.0	*110*	*199*	*106*

---

(1) N^{5+} represents, in theory, the sum of N_2O_5, HNO_3, HO_2NO_2 and the wall losses of the same species. In the actual smog chamber experiment, N^{5+} represents total NO_x loss corrected for dilution.

TABLE 5

Experimental and Modeling Results for Experiment 4-25-79, Dark

Irradiation Time	Specie Concentrations (exp/*model*), ppb O_3	HNO_2	NO_2	N_2O_5	NO_3	HNO_3	N WALL (1)
0	970	340	130	0	0	0	0
	970	*340*	*130*	*0*	*0*	*0*	*0*
23	880	(350)		(75)		0	36
	872	*334*	*14*	*74*	*2*	*5*	*32*

---

(1) In this experiment where HNO_3 and N_2O_5 were monitored, NWALL is a term to represent the N^{5+} species presumably absorbed on the chamber surfaces.

Experiment 4-25-79 Dark

The next two experiments were conducted to further investigate the smog chamber reactions involving HNO_2 and the formation of HNO_3 and N_2O_5. In the subject experiment, HNO_2 was introduced into the chamber followed by a rapid injection of excess O_3. The subsequent thermal reactions were monitored in the dark. In this case, N_2O_5 concentrations were inferred from the difference between NO_X channels of two chemiluminescence analyzers; one reduced N_2O_5 and the other did not.

Initial experimental concentrations (ppb) were: HNO_2 = 340, NO_2 = 130, O_3 = 970 and H_2O = $1.4x10^4$ ppm, and the dilution rate was 4%/hr. Under these circumstances there are two routes for HNO_3 formation in the gas phase:

$$HNO_2 + O_3 \rightarrow HNO_3 + O_2. \qquad (i)$$

and

$$NO_2 + O_3 \rightarrow NO_3 + O_2 \qquad (15)$$

$$NO_3 + NO_2 \rightarrow N_2O_5 \qquad (19)$$

$$N_2O_5 + H_2O \rightarrow 2HNO_3 \qquad (21)$$

After a 23 min. reaction period, the reading for HNO_3 was nearly zero (certainly < 5 ppb considering sensitivity limitations). The instrument monitoring total nitrogen indicated a 45 ppb loss of NO_X over the 23 min. period which we assumed was a 9 ppb dilution loss and a 36 ppb wall loss. Other gaseous concentrations (ppb) at this point were: O_3 = 880, HNO_2 + NO_2 = 350, and N_2O_5 = 75 ppbN*.

Roughly speaking, the experimental results suggested that appreciable amounts of HNO_3 were not formed by either route outlined above.

To obtain more precise estimates of reaction rates and to further evaluate the experimental results, the chamber data were modeled as in the previous case. Here reactions nos. 8, 15, 17-21, 80 and 82-84 were used.

Gas-phase concentrations predicted by the model at 23 min. are shown in Table 5 together with the experimental data.

Overall, the model predictions are in good agreement with the experimental results. If the model, in fact, adequately represents the experimental chemistry, arguments can be stated about the results.

(i) First, the actual wall losses of NO_x products appear to be accounted for by the model.

(ii) The reaction rate for the homogeneous formation of HNO_3 from N_2O_5 and water vapor (reaction No. 21) must be $< 3\times10^{-7}ppm^{-1}$. This is an upper limit value based on the detection limitations for HNO_3(5 ppb). For example, when $k_{21} = 1\times10^{-6}ppm^{-1}min^{-1}$ was incorporated in the model, the theoretical concentration for HNO_3 was 19 ppb, in large excess of the measured value.

(iii) The rate for the reaction of O_3 with HNO_2 to yield HNO_3 must be $<1\times10^{-3}ppm^{-1}min^{-1}$. This is also an upper limit based on our negative observations for HNO_3.

---

*N_2O_5, having two N atoms per molecule, gives twice the chemiluminescence response as monatomic-N compounds. For convenience of maintaining a N material balance, 1 ppb (vol) N_2O_5 is 2 ppbN.

It is also noted that under the experimental conditions described above, about 10 percent of the initial O_3 was "catalytically" destroyed by the sequence of reactions No. 15, 18 and 8.

Experiment 4-25-79 Light

To further investigate the NO_x behavior in the smog chamber, and particularly to further investigate the photolysis of HNO_2, the preceeding experiment was continued under irradiation conditions.

As indicated previously one of the complications in determining the photolysis rate for HNO_2 in the smog chamber is the rapid recombination of HO and NO. The presence of excess O_3 in this experiment was designed to eliminate the reverse reaction by converting nearly all of the NO to NO_2.

Experimental results are presented in Table 6 together with the corresponding results predicted by kinetic modeling.

The model data and the experimental data agree fairly well for O_3, total nitrogen oxides (N_T), and thus for wall losses (NWALL). Under irradiation conditions, the loss of O_3 reflects mainly the influx of NO due to HNO_2 photolysis - the parameter of principal interest here. Thus the parallel data for O_3 suggested that the HNO_2 photolysis rate used in the model was suitable. However, major discrepancies (between experiment and model) are found when comparing the distributions for HNO_3, N_2O_5 and $NO_2 + HNO_2$. Since each of these determinations is made by subtraction, any single error would affect the outcome of all three. For example, absorption problems with HNO_3 were frequently experienced in sampling lines, and that might have resulted in smaller than actual values during the early part of the irradiation period.

TABLE 6

Experimental and Modeling Results for Experiment 4-25-79, Light

Irradiation Time, min.	Specie Concentrations (exp/*model*), ppb					
	O_3	N_T (1)	$NO_2 + HNO_2$	N_2O_5	HNO_3	NWALL
0	880	425	350	75	0	0
	880	*425*	*350*	*75*	*0*	*0*
10	790	393	295	79	19	29
	800	*405*	*329*	*47*	*29*	*12*
20	726	365	260	74	31	54
	737	*384*	*276*	*55*	*53*	*30*
30	692	340	230	71	39	76
	688	*350*	*228*	*54*	*68*	*59*
40	660	320	215	58	47	94
	656	*327*	*203*	*51*	*73*	*84*
50	640	303	200	49	54	108
	631	*302*	*183*	*46*	*73*	*107*
60	620	280	190	35	55	128
	610	*277*	*107*	*42*	*68*	*127*

---

(1) N_T is the sum of NO_2, HNO_2, N_2O_5 and HNO_3.

Alternatively, good agreement (between model and experiment) in HNO_3 profiles was obtained when the HNO_2 photolysis rate was reduced from 0.034 to 0.017 min^{-1}, but then the model's O_3 concentrations went much too high.

In summary, this experiment alone did not provide conclusive data for the HNO_2 photolysis rate in the smog chamber. Nonetheless, the choice of $k_5 = 0.28 \times 10^{-1} min^{-1}$ seemed to fit this and other experimental data as well as alternative values.

(3) SO_2 Oxidation by HO Radicals

To study the conversion of SO_2 to sulfate via hydroxyl radicals, SO_2 was added to air mixtures of HNO_2 and NO_X in the smog chamber. Under these conditions, sulfate aerosol formation was observed immediately after the lamps were turned on. The rate of sulfate formation was generally found to maximize early in the irradiation period and then diminish with time. An example of the evolution of the stable condensed phase was shown in Figure 1. The physical characteristics of the aerosol size spectrum are consistent with those obtained in earlier studies of secondary sulfate formation.

The experiments were simulated by kinetic modeling in order to estimate the HO profiles and assess the overall conversion rate for SO_2, as initiated by HO radicals.

As discussed further on in this section, the mechanisms by which SO_2 transforms to particulate sulfate after the initial encounter of SO_2 with HO are unknown. It has been suggested that nitrogen oxides may have various roles in the transformation process and may even become incorporated in the condensed phase as the reactions approach completion.(7)

In an attempt to investigate those possibilities, various amounts of NO or NO_2 were intentionally added to some of the experimental mixtures, in addition to the amounts produced while charging HNO_2 to the chamber.

Initial concentrations for the experiments in this series are given in Table 7. The results of each experiment, as interpreted by kinetic modeling, are discussed below. Results pertaining to the reaction mechanisms and the role of NO_X are discussed later.

Experiment 6-5-78

The results of this experiment are presented in Table 8. For the nitrogen chemistry, agreement between the model and experimental data is considered to be quite good, although the model slightly underestimated NO_X losses during the latter half of the experiment. Comparing the sulfate data, correspondence between the model and experimental data is also good. Here too the model underestimated sulfate production near the latter part of the experiment. Since NO_X losses (due mainly to HNO_3 formation) and sulfate formation are both linked to HO concentrations, it appears that the model slightly underestimated the HO levels during the last 60 minutes. Overall, the model fits the experimental data very well, which implies that a rate constant of $1.6x10^3 ppm^{-1} min^{-1}$ for the reaction of $SO_2 + HO =$ products is appropriate as the rate limiting step for conversion to sulfate.

Experiment 6-6-78

This experiment was nearly identical to the previous one except that the initial SO_2 concentration was higher here. The experimental and modeling results are shown in Table 9.

Compared to the previous case, the model fits the data rather poorly. NO oxidation and subsequent NO_X losses (N^{5+} formation) were apparently faster than predicted by the model. Unaccounted NO_X losses amounted to 12 percent of total NO_X by the end of the 2-hr. reaction period.

TABLE 7

Initial Conditions for the Experiments Designed to Test the Rate of SO_2 Conversion by HO Radicals

Experiment No.	Initial Concentrations NO ppb	 NO_2 ppb	 HNO_2 ppb	 SO_2 ppb
11-10-77	268	42	165	490
1-09-78	310	60	175	530
6-05-78	120	97	248	342
6-06-78	120	120	205	480
6-08-78	730	124	186	390
6-14-78	293	74	216	405
6-15-78	80	153	257	400
6-16-78	120	583	257	385

TABLE - 8

Experimental and Modeling Results for Experiment 6-5-78

Irradiation Time, min.	Specie Concentrations (exp/*model*), ppb				
	O_3	NO	NO_2+HNO_2(1)	N^{5+}	SULFATE
0	0 *0*	120 *120*	345 *345*	0 *0*	0 *0*
30	6 *5.9*	150 *145*	238 *252*	68 *65*	15 *15*
60	6 *6.0*	150 *147*	193 *207*	101 *86*	21 *19*
90	6 *6.0*	143 *146*	175 *182*	115 *101*	24 *21*
120	6.0	135 *143*	165 *169*	122 *107*	26 *21*

---

(1) Initial [NO_2] = 97 ppb; [HNO_2] = 248 ppb

TABLE - 9

Experimental and Modeling Results for Experiment 6-6-78

Irradiation Time, min.	Specie Concentrations (exp/*model*), ppb				
	O_3	NO	NO_2+HNO_2(1)	N^{5+}	SULFATE
0	0	120	325	0	0
	0	*120*	*325*	*0*	*0*
30	7	133	225	75	20
	6.6	*136*	*245*	*50*	*17*
60	7	128	180	114	29
	6.8	*135*	*207*	*80*	*24*
90	7	118	157	136	33
	6.8	*133*	*185*	*93*	*25*
120	7	108	145	148	35
	6.8	*130*	*172*	*99*	*25*

---

(1) Initial [NO_2] = 120 ppb; [HNO_2] = 205 ppb

Analyses for sulfate indicated that SO_2 conversion was also greater than predicted by the model. Thus, it seemed that actual HO concentrations were larger than those estimated by the model and that might account for the discrepancy in N^{5+}.

Experiment 11-10-77

The next four experiments, including this one, were conducted with NO added initially to moderate the depletion rate of NO and conserve NO_x.

Results for experiment 11-10-77 are shown in Table 10. This was one of the earliest experiments where low concentrations of O_3 were not accurately measured. In this case, about 200 ppb of additional NO was added prior to irradiation.

As indicated in Table 10, the fit of the model data to the distribution of nitrogen oxides was good except for the discrepancy in N^{5+} early in the experiment. Conversion of SO_2 to sulfate was less than that predicted by the model, but in this case, the sulfate concentration was inferred from aerosol size distribution data obtained with an EAA.

Experiment 1-9-78

This experiment is similar to the previous one except that the flame photometric technique was used here for monitoring sulfate. The results of the experiment are given in Table 11. The experimental and modeling results for sulfate agree well. There is also good agreement for the nitrogen oxides distributions.

TABLE - 10

Experimental and Modeling Results for Experiment 11-10-77

Irradiation Time, min.	Specie Concentrations (exp/*model*), ppb				
	O_3	NO	NO_2+HNO_2(1)	N^{5+}	SULFATE
0	0	268	207	0	0
	0	*268*	*207*	*0*	*0*
20	< 5	253	187	26	10
	2	*253*	*195*	*15*	*12*
40	< 5	240	174	45	15
	2.4	*244*	*182*	*32*	*19*
60	< 5	230	162	59	17
	2.8	*236*	*169*	*44*	*22*
80	< 5	222	155	66	19
	3.0	*230*	*159*	*53*	*24*
100	< 5	215	147	74	19
	3.1	*224*	*150*	*60*	*26*

---

(1) Initial $[NO_2]$ = 42 ppb; $[HNO_2]$ = 165 ppb

TABLE - 11

Experimental and Modeling Results for Experiment 1-9-78

Irradiation Time, min.	Specie Concentrations (exp/*model*), ppb				
	O_3	NO	NO_2+HNO_2 (1)	N^{5+}	SULFATE
0	0	310	235	0	0
	0	*310*	*235*	*0*	*0*
20	< 5	305	216	18	12
	1.9	*299*	*216*	*18*	*11.5*
50	< 5	295	200	32	20
	2.2	*291*	*198*	*35*	*19.5*
60	< 5	288	190	39	25
	2.5	*284*	*185*	*49*	*23.5*
90	< 5	275	182	48	28
	2.7	*274*	*169*	*64*	*26.5*
120	< 5	262	174	56	30
	2.8	*266*	*156*	*69*	*27*

---

(1) Initial [NO_2] = 60 ppb; [HNO_2] = 175 ppb

Experiment 6-14-78

This experiment, also containing about 300 ppb of NO, was conducted some five months later when more accurate O_3 determinations were made. The results are recorded in Table 12.

In comparison with the two similar tests described previously, the fit of the model to these data is poorer. The model appeared to underestimate the conversion of NO to NO_2 and the corresponding losses of NO_2 as N^{5+}. The model predictions for sulfate were reasonably good.

Experiment 6-8-78

The final experiment of this group was conducted with an initial NO concentration in excess of 700 ppb. The results are given in Table 13.

Given a large excess of NO, the model more severely underestimated HO levels, as evidenced by the low predictions for sulfate and N^{5+}. Those results might possibly be related to an inadequacy of the model to accurately replicate the NO oxidation rate under these experimental conditions.

Experiment 6-15-78

In this experiment and the one to follow, NO_2 rather than NO was added to the initial reaction mixtures. NO_2 had the effect of intensifying the competition between HNO_3 and sulfate formation via the HO radical. The results of experiment 6-15-78 are given in Table 14.

TABLE - 12

Experimental and Modeling Results for Experiment 6-14-78

Irradiation Time, min.	Specie Concentrations (exp/*model*), ppb				
	O_3	NO	NO_2+HNO_2(1)	N^{5+}	SULFATE
0	0	293	280	0	0
	0	*293*	*280*	*0*	*0*
30	2	279	248	42	13
	2.6	*285*	*246*	*36*	*13*
60	3	270	200	85	20
	3.0	*276*	*214*	*63*	*19*
90	3	261	183	97	24
	3.3	*268*	*192*	*79*	*22*
120	3	247	170	110	27
	3.3	*260*	*178*	*88*	*22*

---

(1) Initial $[NO_2]$ = 74 ppb; $[HNO_2]$ = 216 ppb

TABLE - 13

Experiment and Modeling Results for Experiment 6-8-78

Irradiation Time, min.	Specie Concentrations (exp/*model*), ppb				
	O_3	NO	NO_2+HNO_2(1)	N^{5+}	SULFATE
0	0 *0*	730 *730*	310 *310*	0 *0*	0 *0*
30	< 2 *1.1*	690 *715*	280 *272*	44 *25*	8.7 *7.3*
60	< 2 *1.2*	650 *699*	270 *243*	68 *45*	13.3 *11.5*
90	< 2 *1.3*	620 *681*	260 *221*	83 *58*	17.1 *13.6*
120	< 2 *1.3*	590 *665*	250 *205*	99 *68*	20 *14.7*

---

(1) Initial [NO_2] = 124 ppb; [HNO_2] = 186 ppb

TABLE - 14

Experimental and Modeling Results for Experiment 6-15-78

Irradiation Time, min.	Specie Concentrations (exp/*model*), ppb				
	O_3	NO	NO_2+HNO_2 (1)	N^{5+}	SULFATE
0	0	80	410	0	0
	0	*80*	*410*	*0*	*0*
30	10	123	267	87	16
	9.5	*114*	*298*	*70*	*16*
60	9	124	226	115	23
	9.4	*117*	*237*	*104*	*21*
90	9	121	204	129	26
	9.3	*117*	*216*	*121*	*22*
120	9	112	183	147	27
	9.2	*114*	*202*	*125*	*22*

---

(1) Initial $[NO_2]$ = 153 ppb; $[HNO_2]$ = 257 ppb

The quality of fit of the model to the experimental data is very good for O_3 and NO, and only somewhat less satisfactory for NO_X, N^{5+} and sulfate. Formation of N^{5+} and sulfate are slightly faster than the model predicted.

Experiment 6-16-78

A much higher dose of NO_2 was used in this experiment compared to the last. Results are summarized in Table 15.

The overall fit of the model to the experimental data was poor. Upon irradiation, the O_3 concentration immediately reached a peak of 20 ppb and thereafter diminished gradually to 4 ppb. The model also predicted an early O_3 maximum of 20 ppb, but a final value that was twice the size of the experimental concentration. Throughout the experiment the model seriously underestimated NO_X losses (presumably HNO_3 formation) and it underestimated sulfate formation during the last 60 minutes of irradiation. It is possible that under such conditions there is a substantial NO_2 sink that is not adequately represented by the model, and that would account, in part, for the discrepancy in O_3, as well as that for N^{5+}.

To summarize this series of experiments, the model gave satisfactory fits to the experimental data with the exception of experiment 6-16-78. In general, the model tended to underestimate NO_2 conversion (N^{5+} concentrations) and sulfate aerosol concentrations, particularly during the latter half of the experimental periods. This could be interpreted as underestimates of the HO concentrations which, in turn, could be related to many subtle inadequacies in the model. With few exceptions, the discrepancies did not exceed 20 percent of the experimental values.

The data overall support a rate constant of 1.6×10^3 $ppm^{-1}min^{-1}$ for the conversion of SO_2 to sulfate aerosol, as initiated by the HO radical (reaction 60). This assumes, of course, that the kinetic model predicts the correct

TABLE - 15

Experimental and Modeling Results for Experiment 6-16-78

Irradiation Time, min.	Specie Concentrations (exp/*model*), ppb				
	O_3	NO	NO_2+HNO_2 (1)	N^{5+}	SULFATE
0	0	120	840	0	0
	0	*120*	*840*	*0*	*0*
30	8	255	530	150	7
	12	*230*	*607*	*98*	*7*
60	5	295	415	202	11
	9.5	*264*	*505*	*142*	*10*
90	4	300	355	234	14
	8.5	*276*	*452*	*161*	*11*
120	4	300	315	252	16
	8.1	*278*	*419*	*168*	*11*

---

(1) Initial [NO_2] = 583 ppb; [HNO_2] = 257 ppb

HO concentrations. Circumstantial evidence indicates that the model underestimates OH so the actual rate constant for reaction 60 might be somewhat larger than $1.6 \times 10^3 ppm^{-1} min^{-1}$.

(4) SO_2 Oxidation by HO_2 Radicals

As indicated earlier, there is considerable uncertainty about the kinetics of SO_2 oxidation by hydroperoxy radicals. To investigate the reaction in our smog chamber, relatively large concentrations of CO were added to mixtures of $NO_X/HNO_2/SO_2$. CO has the effect of converting HO to HO_2,

$$CO + HO \rightarrow CO_2 + H$$

$$H + O_2 + M \rightarrow HO_2 + M.$$

The net equation, $CO + HO\ (O_2, M) = CO_2 + HO_2$, is included in the kinetic model as reaction 40.

In some preliminary experiments with CO, contamination due to iron carbonyl was suspected. In the experiments reported here, precautions were taken to avoid contamination.

CO was found to give a negative interference to the analyses of SO_2 and sulfate aerosols with the flame photometric detector. For example, 100 ppm CO reduced a true SO_2 reading of 400 ppb to 370 ppb. This unfortunate interference severaly limited the range of useful CO concentrations in this work.

Initial reactant concentrations for the experiments with added CO are summarized in Table 16. In the first experiment to be discussed, CO was irradiated with a HNO_2-NO_X mixture without SO_2. SO_2 was included in the other two experiments of this group.

Experiment 12-13-77

This experiment was conducted with 196 ppm CO. To observe its effect on HO_2 production additional amounts of NO were also added. The results are summarized in Table 17.

TABLE - 16

Initial Conditions for the Experiments Designed to Test the Rate of SO_2 Conversion by HO_2 Radicals

	Initial Concentrations				
Experiment No.	NO ppb	NO_2 ppb	HNO_2 ppm	CO ppm	SO_2 ppb
12-13-77	275	60	170	196	0
12-14-77	305	40	215	190	490
6-23-78	305	85	260	215	390

TABLE - 17

Experimental and Modeling Results for Experiment 12-13-77

	Specie Concentrations (exp/*model*), ppb				
Irradiation Time, min.	O_3	NO	NO_2+HNO_2(1)	N^{5+}	SULFATE
0	0	275 *275*	230 *230*	0 *0*	-
20	241 *229*	< 10 *5*	425 *421*	61 *69*	-
40	397 *408*	0 *2.6*	362 *339*	118 *146*	-
60	438 *496*	0 *1.9*	313 *277*	160 *198*	-
90	460 *549*	0 *1.5*	260 *213*	203 *252*	-

---

(1) Initial $[NO_2]$ = 60 ppb; $[HNO_2]$ = 170 ppb

As indicated in Table 17, the addition of CO resulted in very rapid oxidation of NO and high ozone yields. The model seemed to do a reasonably good job in matching these data considering that the O_3 levels are extremely sensitive to small variations in NO under these conditions.

Unlike the experiments without added CO, here the model overestimated NO_X losses (N^{5+} formation) after the first 30 min. This was thought to result from the high levels of CO which effect the distribution of N^{5+} products. In the previous cases where CO was low, virtually all of the N^{5+} was HNO_3. With high CO concentrations, the concentrations of N_2O_5 and HO_2NO_2 became very substantial due to elevated levels of O_3, NO_2 and HO_2. For example, in this particular experiment, the model estimated a HO_2NO_2 peak of 20 ppb early in the run and a peak of 60 ppb N_2O_5 near the end of the reaction period.

Because the nylon filter does not absorb N_2O_5, it is suspected that some N_2O_5, and possibly some HO_2NO_2, was recorded in the NO_X channel together with HNO_2 and NO_2. This interference would yield excessive concentrations for the HNO_2 + NO_2 sum and deficiencies for the N^{5+} category.

With those considerations in mind, similar experiments with added SO_2 are discussed next.

Experiment 12-14-77

The results of this experiment with 490 ppb SO_2 are presented in Table 18. As in the previous experiment, the model overestimated the O_3 concentrations by some 20 percent, and the distributions between NO_X and N^{5+} are somewhat skewed.

Experimentally, the addition of CO resulted in a marked reduction in SO_2 oxidation. In an effort to match these data, the experiment was modeled using various rate constants for the oxidation of SO_2 by HO_2 (k_{61}). Results of two simulations with k_{61} = 1.2 and 0.12 $ppm^{-1}min^{-1}$ are shown in Table 18. While the sulfate concentrations obtained with k_{61} = 0.12 $ppm^{-1}min^{-1}$ provided

TABLE - 18

Experimental and Modeling Results for Experiment 12-14-77

Irradiation Time, min.	Specie Concentrations (exp/*model*), ppb				
	O_3	NO	NO_2+HNO_2 (1)	N^{5+}	SULFATE (2)
0	0	305	255	0	0
	0	*305*	*255*	*0*	*0/0*
20	234	15	450	85	6
	266	*4.4*	*453*	*91*	*8.4/6.3*
40	382	<5	378	151	7.5
	442	*2.4*	*361*	*175*	*14.3/9.0*
60	430	0	315	207	8
	530	*1.8*	*291*	*236*	*18.2/10.6*
90	440	0	250	258	8.2
	584	*1.3*	*219*	*298*	*21.4/11.0*

---

(1) Initial $[NO_2] = 40$ ppb; $[HNO_2] = 215$ ppb

(2) The two values for SULFATE represent results using two rate constants for the reaction of HO_2 with SO_2; $k_{61} = 1.2$ and 0.12 $ppm^{-1}min^{-1}$, respectively.

the better fit to the experimental data, one sees that the total production of sulfate is not very sensitive to k_{61} in this case.

It is clear, however, that k_{61} must be substantially less than 1.2 $ppm^{-1}min^{-1}$ since that rate overestimated sulfate production by a factor of 2 or more.

Experiment 6-23-78

This experiment is similar to the one just discussed but with a slightly higher CO concentration. The results are given in Table 19, and the modeling data reflect the theoretical effects of k_{61} = 1.2, 0.12 and 0.0 $ppm^{-1}min^{-1}$.

Here the sensitivity to the model value for k_{61} is more pronounced than in the previous case. Still, HO radicals apparently dominated SO_2 oxidation. According to the modeling results, SO_2 conversion in this experiment could be attributed entirely to oxidation by HO.

Some additional experiments conducted with intermediate CO concentrations were likewise inconclusive because of the dominance of HO. Extremely high concentrations of CO were not used to improve the HO_2/HO ratio because oxidation would be very slow under such conditions and sulfate measurements would have been severely compromised by CO interference.

Based on the data from this group of experiments, the selection of an upper limit for the reaction between SO_2 and HO_2 becomes arbitrary. For subsequent modeling purposes, we selected 0.2 $ppm^{-1}min^{-1}$ as a certain upper limit, although the true rate is likely to be much lower.

TABLE - 19

Experimental and Modeling Results for Experiment 6-23-78

Irradiation Time, min.	Specie Concentrations (exp/*model*), ppb				
	O_3	NO	NO_2+HNO_2 (1)	N^{5+}	SULFATE (2)
0	0	305	345	0	0
	0	*305*	*345*	*0*	*0/0/0*
30	430	< 10	465	158	3.2
	426	*3*	*450*	*176*	*10/6.5/6.0*
60	570	0	365	252	4.8
	597	*2*	*314*	*301*	*16.3/8.2/7.6*
90	560	0	291	311	5.0
	654	*1*	*230*	*372*	*19.5/8.8/7.9*
120	540	0	260	327	5.2
	663	*1*	*171*	*412*	*20.7/8.8/7.8*

---

(1) Initial [NO_2] = 85 ppb; [HNO_2] = 260 ppb

(2) The three model values for SULFATE represent results using three rate constants for the reaction of HO_2 with SO_2; k_{61} = 1.2, 0.12 and 0.0 $ppm^{-1}min^{-1}$, respectively.

C. Organic Systems ($HNO_2/NO_X/CH_4/SO_2$ and CH_3NNCH_3/SO_2)

(1) Experiments with Methane as Methylperoxy Source

Until very recently, no kinetic data were available on the oxidation of SO_2 by methylperoxy radicals, although the general class of alkylperoxy radicals has long been thought to play a significant role in SO_2 oxidation in polluted air. Two recent measurements of the subject rate constant, referenced in Table 1, are in good agreement.

Our investigation of the methylperoxy-SO_2 reaction began with the same approach used to investigate the HO_2-SO_2 kinetics. The approach consisted of irradiating high concentrations of CH_4 with controlled $HNO_2/NO_X/SO_2$ mixtures in the smog chamber.

The hydroxyl radicals produced from HNO_2 photolysis abstract a hydrogen atom from CH_4, and the resulting methyl radical presumably adds an oxygen molecule. Subsequent reactions involving CH_3O_2 and related species are listed in Table 2. The reaction of principal concern is

$$CH_3O_2 + SO_2 \rightarrow CH_3O + \text{SULFATE} \qquad (64)$$

It is highly uncertain whether or not reaction 64 proceeds as written; it may, for example, yield $CH_3O_2SO_2$ initially and require a third body. Our objective was to determine the overall rate of the reaction 64 based on sulfate aerosol formation in an atmosphere of moderate humidity. The initial experimental conditions are listed in Table 20.

TABLE 20

Initial Conditions for the Experiments Designed to Test the Rate of SO_2 Conversion by CH_3O_2 Radicals

	Initial Concentrations				
Experiment No.	NO ppb	NO_2 ppb	HNO_2 ppb	CH_4 ppm	SO_2 ppb
1-10-78	65	65	190	520	530
1-11-78	340	80	230	930	530

Experiment 1-11-78

This experiment was conducted with 930 ppm CH_4. NO was also added. Methane gave roughly the same degree of interference to the FPD as CO did.

Experimental and modeling results are presented in Table 21. The overall quality of the model fit to the O_3 and nitrogen oxides data was very good. An exception was more rapid conversion of NO during the first 30 minutes of irradiation than predicted by the model.

With regard to SO_2 oxidation, it is clear from the modeling results in Table 21 that sulfate formation was almost exclusively due to HO radicals. Insensitivity to changes in k_{64} reflects that fact. In this experiment, substantial NO concentrations kept CH_3O_2 suppressed via reaction 79, and it was not possible to estimate a rate for reaction 64.

Experiment 1-10-78

In this experiment, 530 ppm CH_4 was present initially and no NO was added except for that which resulted while generating HNO_2.

The results are summarized in Table 22. The temporal distributions between NO_X and N^{5+} are fit well by the model, although the predictions for O_3 are too low until the latter part of the experiment.

The model sulfate data in Table 22 represents results using k_{64} = 8.0 and 1.6 $ppm^{-1}min^{-1}$. Compared to the previous experiment, total sulfate formation here is a bit more sensitive to the value for k_{64}. As indicated in Table 22, reduction of k_{64} from 8.0 to 1.6 improved the model fit to the sulfate data, but the overwhelming influence of HO makes it impossible to accurately determine k_{64} by this method.

TABLE - 21

Experimental and Modeling Results for Experiment 1-11-78

Irradiation Time, min.	Specie Concentrations (exp/*model*), ppb				
	O_3	NO	NO_2+HNO_2(1)	N^{5+}	SULFATE
0	0	340	310	0	0 (2)
	0	*340*	*310*	*0*	*0/0*
30	30	90	450	81	9.4
	17	*109*	*461*	*62*	*13/13*
60	70	40	450	127	13.3
	51	*41*	*467*	*107*	*17.7/17.2*
90	98	25	427	150	13.4
	94	*21*	*443*	*134*	*19.2/18.4*
120	120	20	400	167	13.5
	131	*14*	*416*	*154*	*19.6/18.6*

---

(1) Initial [NO_2] =80 ppb; [HNO_2] = 230 ppb; CH_4 = 930 ppm.

(2) The two model values for SULFATE represent results using two rate constants for the reaction of CH_3O_2 with SO_2; 8.0 and 1.6 ppm^{-1}min^{-1}, respectively.

TABLE - 22

Experimental and Modeling Results for Experiment 1-10-78

Irradiation Time, min.	Specie Concentrations (exp/*model*), ppb				
	O_3	NO	NO_2+HNO_2(1)	N^{5+}	SULFATE
0	0	65	255	0	0
30	120 *70*	6 *10*	229 *236*	77 *64*	17.5 *18/17*
60	180 *137*	<5 *5.4*	198 *197*	106 *100*	22.8 *25/23*
90	195 *194*	0 *3.5*	176 *170*	120 *122*	23.2 *30/26*

---

(1) Initial $[NO_2]$ = 65 ppb; $[HNO_2]$ = 190 ppb; CH_4 = 520 ppm.

(2) The two model values for SULFATE represent results using two rate constants for the reaction of CH_3O_2 with SO_2; 8.0 and 1.6 $ppm^{-1}min^{-1}$, respectively.

To illustrate the situation more clearly, the modeled rates of SO_2 oxidation by HO, HO_2 and CH_3O_2 are shown below for the simulation that provided the better sulfate prediction; i.e., $k_{64} = 1.6\ ppm^{-1}min^{-1}$. In this case, the largest contribution to SO_2 conversion by CH_3O_2 radicals is estimated by about 10 percent of the total.

TABLE 23

Relative Contribution of HO, HO_2, and CH_3O_2 Radicals to SO_2 Oxidation as Estimated by Kinetic Model used to Simulate Experiment 1-10-78.

Irradiation Time min.	SO_2 Oxidation Rate, %/hr.			
	$R_{SO_2\text{-}HO}$	$R_{SO_2\text{-}HO_2}$	$R_{SO_2\text{-}CH_3O_2}$	$R_{SO_2\text{-}Total}$
30	4.22	.015	0.23	4.47
60	2.49	.023	0.17	2.69
90	1.72	.028	0.20	1.95

From an earlier analysis of this data, as reported in the Fourth Quarterly Progress Report, upper limit rate constants of 2 $ppm^{-1}min^{-1}$ for k_{64} and 1 $ppm^{-1}min^{-1}$ for k_{61} (oxidation by HO_2) were derived. At that time, however, the rate constants used in the model for NO oxidation by CH_3O_2 and HO_2 were a factor of 6 too small. Consequently, the peroxy radical concentrations predicted by the model were erroneously large, and we were led to believe that the sensitivity of these smog systems was adequate to establish, with reasonable accuracy, upper limits for k_{61} and k_{64}. Accepting the more recent values for the reactions of peroxy radicals with NO, it is clear that the investigative approach taken was not very satisfactory for determining k_{61} and k_{64}, if the actual values are substantially smaller than the literature values. Our results show that to be true.

It is worth noting that in the previous two experiments CH_4 oxidation resulted in an apparent loss of HO radicals. This conclusion is based on comparisons of the rates of SO_2 oxidation by HO (a measure of the relative HO concentrations) with similar experiments without CH_4. Compare, for example, Experiment 6-14-78 (Table 12) with Experiment 1-11-78 (Table 21) and Experiment 6-6-78 (Table 9) with Experiment 1-10-78 (Table 22). In the first comparison, notice that SO_2 oxidation in the presence of CH_4 nearly stopped (actually approached the dilution rate) after 60 minutes, while in the companion run without CH_4 (Table 12), SO_2 oxidation proceeded throughout the 120 minute period. Similar trends are apparent in the comparison between Experiments 6-6-78 and 1-10-78.

Actually, if the following interpretation is correct, degeneration of HO in the course of the experiments with CH_4 is the result of changes in the rates among competitive reaction routes as NO becomes oxidized to NO_2. When NO is prevalent, the most probably sequence of reactions for CH_4 is 70, 79, 76, 77 and 78 (Table 2). Assuming that every HO_2 returns HO by reacting with NO, no losses of HO are predicted by that route. However, when the NO_2/NO ratio becomes large via those reactions, the route by which CH_3O_2 converts to formaldehyde and continued HO_2 production becomes unfavorable, and the methylperoxy radicals react to form products that are less efficient in regenerating HO. Likewise, at high NO_2/NO ratios, HO_2 does not readily convert to HO except by reaction with O_3. Furthermore, we presume that in smog chambers, there are significant losses of $CH_3O_2NO_2$ and HO_2NO_2 to surfaces which contribute to the HO sink.

In similar kinds of experiments, Cox et al.(14) showed that the HO stoichiometry for propane was near unity. Their results do not appear to differ from ours for CH_4 since their estimates of [HO] were made during the initial period of propane oxidation when NO was in large excess.

(2) Azomethane as Methylperoxy Source

Because of the inconclusive results obtained with the $CH_4/HNO_2/NO_X/SO_2$ smog system, a few experiments were conducted with azomethane and SO_2 in the absence of NO_X. These experiments were conducted in Battelle's 200-liter, Teflon-lined, Pyrex smog chamber irradiated by fluorescent blacklamps.

The overall reaction of interest was again

$$CH_3O_2 + SO_2 \rightarrow CH_3O + \text{SULFATE} \qquad (64)$$

Azomethane was photolyzed in the chamber to produce methyl radicals which, in turn, were assumed to add oxygen to yield methylperoxy radicals. Photolytic decay of azomethane in the concentration range of 0.2 - 30 ppmC followed first-order behavior with a rate constant of $1.8 \times 10^{-2} \text{min}^{-1}$. In the absence of SO_2, the decay rate was slightly lower.

Rate data pertaining to reaction 64 were obtained by following the decay of SO_2 while irradiating mixtures of azomethane and SO_2 in air. The decay of azomethane and the formation of formaldehyde were also monitored to provide additional interpretive information. Ideally in this type of experiment it is desirable to follow the formation of sulfate aerosol together with the decay of SO_2, but our sulfate monitor was undergoing repairs during this period. Therefore, in these experiments, SO_2 was monitored with a Meloy 285 total sulfur analyzer equipped with a Teflon filter for removing H_2SO_4 aerosol. Although relatively dry air (rh ∿ 1% @ 30C) was used, previous work has shown that SO_3 converts immediately to H_2SO_4 under these conditions(15).

It should be emphasized that the analytical technique employed measured total sulfur in the gas phase and, as such, did not give an unambiguous measure of

SO_2 consumption. Thus, as indicated previously in this report, our measurements provided data on the conversion of SO_2 to the condensed phase and, in this case, the calculated rate (k_{64}) may have been lower than the actual oxidation rate for SO_2.

The chemistry of the azomethane/SO_2 system was also computer-modeled to aid in the interpretation of the experimental data. The mechanism utilized is listed in Table 2. The last four reactions listed in Table 2 represent wall losses in the 200-liter chamber for hydroperoxide, formaldehyde and free radicals. It was assumed that radicals were removed at surfaces with unity collision efficiency while hydroperoxide and aldehyde were removed at one-tenth that rate. It turned out that the theoretical rate of SO_2 oxidation was not very sensitive to reasonable variations of the wall-loss rates.

Kinetic modeling results for an experiment beginning with 0.95 ppm azomethane and 0.91 ppm SO_2 are shown in Table 24. The upper panel of data were obtained using k_{64} = 8.0 $ppm^{-1}min^{-1}$, while the lower data set are results using k_{64} = 0.8 $ppm^{-1}min^{-1}$. The formaldehyde concentration, obtained at the end of the 60 minute irradiation period, was 172 ppb compared to the theoretical values of 157 and 127 ppb.

The rates of SO_2 conversion calculated from the experimental data are plotted in Figure 4. A relatively constant first-order rate of $2x10^{-3}min^{-1}$, or 12%/hr., was obtained. In marked contrast, SO_2 oxidation rates ranging from 1.3 to 1.9 x $10^{-2}min^{-1}$ (78 to 114 %/hr.) were predicted by the model when k_{64} = 8 $ppm^{-1}min^{-1}$ was incorporated (Table 24, upper panel).

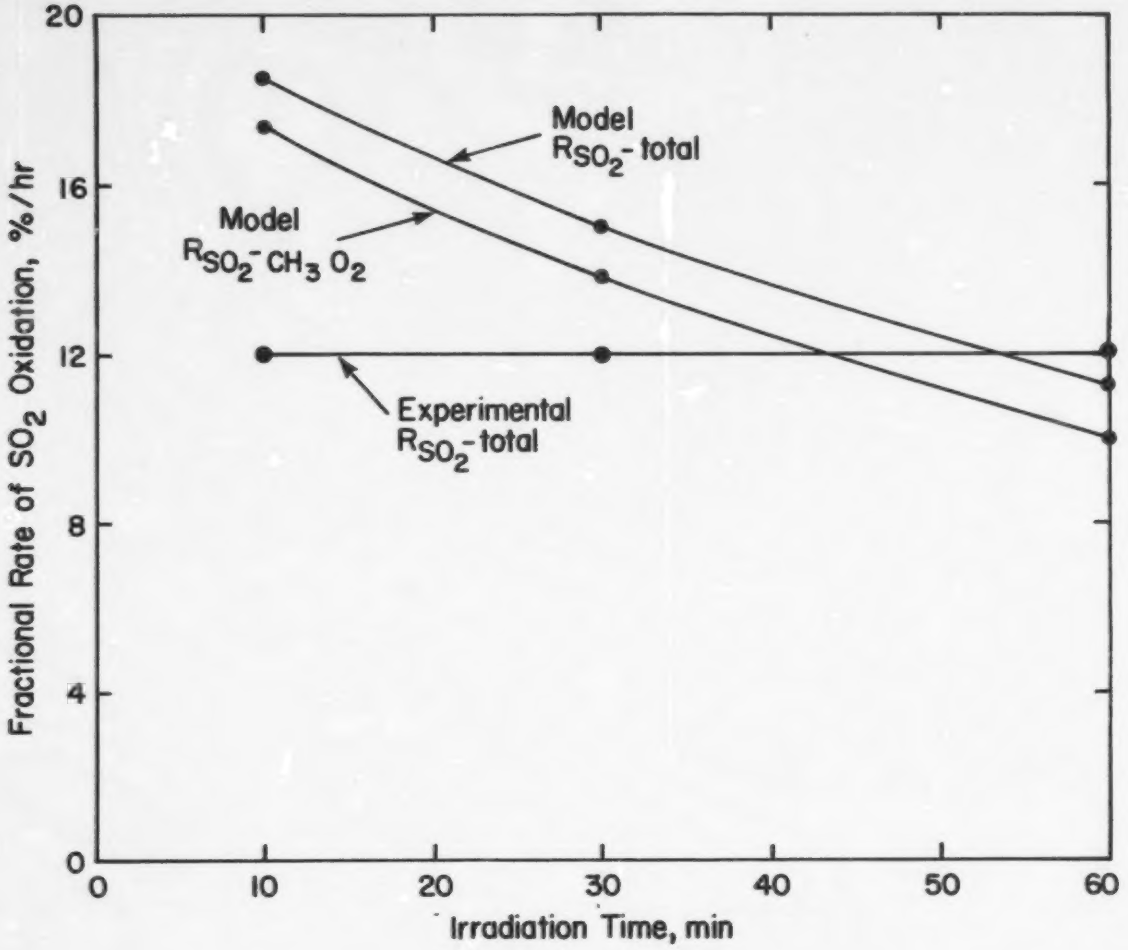

Figure 4. Rates of SO_2 Conversion to Sulfate. Experimental Rate Compared with Modeling Results when $k_{SO_2} + CH_3O_2 = 0.8\ ppm^{-1}min^{-1}$.

TABLE 24

Modeling Results for the Reaction of Methylperoxy Radicals With SO_2; Experiment 3-6-79.

Irradiation Time, min.	SO_2 ppm	CH_3NNCH_3 ppm	CH_2O ppm	$R_{SO_2-CH_3O_2}$ ppm min^{-1}	$R_{SO_2-HO_2}$ ppm min^{-1}	R_{SO_2-HO} ppm min^{-1}
[Results with k_{64} = 8.0 $ppm^{-1}min^{-1}$]						
0	.910	.950	0	0	0	0
10	.723	.761	.164	.136(-1)	.108(-3)	.592(-4)
30	.498	.515	.228	.737(-2)	.522(-4)	.455(-4)
60	.291	.267	.157	.369(-2)	.241(-4)	.461(-4)
[Results with k_{64} = 0.8 $ppm^{-1}min^{-1}$]						
0	.910	.950	0	0	0	0
10	.858	.754	.126	.249(-2)	.773(-4)	.456(-4)
30	.775	.489	.177	.179(-2)	.586(-4)	.440(-4)
60	.680	.261	.127	.111(-2)	.391)-4)	.558(-4)

When a lower value of 0.8 $ppm^{-1}min^{-1}$ was used for k_{64} the model's estimates for the SO_2 oxidation rate were within the right order of magnitude, but the agreement with the experimental data was still poor. These data are plotted in Figure 4. We cannot explain the apparently constant SO_2 oxidation rate in the experiment compared to the temporal variation in CH_3O_2 concentrations, as expected in theory.

Under these conditions, reaction 64 ($CH_3O_2 + SO_2 \rightarrow$ SULFATE) theoretically accounted for about 90 percent of the total oxidation rate while the reactions of HO_2 and HO with SO_2 accounted for 4 and 6 percent, respectively. Thus, in the experiment with azomethane, SO_2 oxidation was unquestionably dominated by CH_3O_2 radicals rather than by HO_2 and/or HO.

Another experiment at a lower azomethane concentration (0.095 ppm azomethane and 0.91 ppm SO_2) also gave disconcerting results. In that case, the observed SO_2 conversion rate was about one-half the rate obtained at the higher azomethane concentration, while the model (with $k_{64} = 0.8\ ppm^{-1}min^{-1}$) predicted about one-fourth the rate.

In summary, the experiments with azomethane were quite limited. It appeared that the overall reaction of CH_3O_2 with SO_2 to yield sulfate aerosol was much slower than the rates of SO_2 oxidation obtained by measuring CH_3O_2 disappearance (Table 1). Comparisons of our experimental findings with the literature are discussed in a later section of the report.

D. Role of NO_X in SO_2 Oxidation via HO Radicals

Speculation about the fate of the $HOSO_2$ product of reaction 60 includes the possibilities for NO_X involvement and even "nitrate" incorporation with H_2SO_4 in the condensed phase. These considerations were reviewed by Calvert, et al. (7).

According to that review, it is pretty well agreed that $HOSO_2$ first adds O_2 to yield $HOSO_2O_2$. This specie likely reacts with NO and NO_2 in a fashion that is analogous with the HO_2 reactions:

$$HOSO_2O_2 + NO \rightarrow HOSO_2O + NO_2$$

$$HOSO_2O_2 + NO_2 \rightleftarrows HOSO_2O_2NO_2.$$

The fate of the $HOSO_2O$ specie derived from the oxidation of NO is of principal interest. Apart from the possibility of abstracting a H atom to form H_2SO_4, $HOSO_2O$ may react further with NO and NO_2 to yield $HOSO_2ONO$ (nitrosylsulfuric acid) and $HOSO_2ONO_2$ (nitrylsulfuric acid), respectively. Hydrolysis of these acids might liberate HNO_2 and HNO_3 vapors, or it is imaginable that the acid products might become stabilized in the aerosol phase as nitrates.

Experimental evidence suggests that such possibilities exist, at least in laboratory studies. Schroeder and Urone(16) isolated and identified $HOSO_2ONO$, a white solid, during smog chamber experiments with SO_2 and NO_2 in dry air. They reported that the material was hydroscopic and hydrolized to give H_2SO_4 plus gaseous mixtures of NO, NO_2 and HNO_3.

In irradiation experiments with HNO_2 and SO_2, Cox(17) observed that increasing concentrations of SO_2, like CO, reduced the rate of formation of NO_X during HNO_2 photolysis. The results implied that an undetermined radical loss mechanism was operating.

With high CO levels, the sources of NO_X and radical losses in Cox's system were quite likely manifestations of N_2O_5 and HO_2NO_2 formation and subsequent termination upon the reaction vessel surfaces. We observed similar experimental results, even in a comparatively large chamber.

Cox reported that the SO_2 effect on NO_X losses was three times as great as that due to CO. In that case, unaccounted NO_X losses could possibly be linked to unknown $HOSO_2NO_X$ products. Similar effects related to SO_2 were not adequately explored in this study although unaccounted losses of NO_X seemed to rise when the initial levels of either NO_X of SO_2 were increased.

The experiments conducted with the $HNO_2/NO_X/SO_2$ smog system served to investigate the possibility for particulate nitrate formation, as outlined in the discussion above. At the conclusion of an experiment, sample air was drawn through acid washed and neutralized quartz filters and analyzed for NO_3^-, $SO_4^=$ and NH_4+. To guard against the possibility for HNO_2 or HNO_3 losses to the vapor phase after collection, filter samples were immediately halved; one-half was stored in a desiccator containing NH_3, and the other was refrigerated without treatment. It was presumed that the NH_3 would react with the acids to give ammonium salts.

The analytical results from nine experiments showed no substantial differences in either $SO_4^=$ or NO_3^- for the NH_3 treated samples versus the untreated samples. Although, in general, the ammoniated samples contained somewhat higher NH_4^+ concentrations, nearly all samples were deficient in NH_3 when compared to the expected stoichiometry for $(NH_4)_2SO_4$ and NH_4NO_3. Reasons for this were not apparent.

In every case, the particulate nitrate concentrations were very low compared to the sulfate concentrations, and ranged from about 0.4 - 1.2 ppbN. The highest particulate nitrate concentrations were recorded for the two experiments (Nos. 3 and 7) without SO_2. Thus a substantial amount of nitrate was not incorporated in the particulate phase under the conditions of these experiments. While the results do not rule out the possibility that $HOSO_2O$ interacts with NO_2 to produce H_2SO_4 and HNO_3, they do indicate that nitrate (if formed via this route) is not maintained in the aerosol phase, even under the presumably stabilizing influence of NH_3,

At this point, it must be stated that the predominant mechanistic route for sulfate aerosol formation following HO addition to SO_2 remains unclear.

In the computer simulations of our experiments, we represented the overall reaction process as

$$SO_2 + HO\ (M{+}O_2) = \text{SULFATE} + HO_2 \qquad (60)$$

HO was regenerated by reactions of HO_2 with NO, SO_2 and O_3. When intermediates such as $HOSO_2$, $HOSO_2O_2$, $HOSO_2O$, $HOSO_2ONO$ and $HOSO_2ONO_2$ and the reactions thereof were included in the model, the quality of the model fits to the experimental data (i.e., O_3, NO, NO_X, NO_X loss, $SO_4^=$ and NO_3^-) was not substantially affected. Thus, although the abbreviated mechanism gave reasonably good fits to the data, the adequacy of a mechanism was really not tested here. At best, it was conlcuded that nitrate aerosols are not likely to be generated in the atmosphere due to the formation of HSO_XNO_X intermediates.

E. Summary of Kinetic Studies

Kinetic data determined in this study are summarized here and discussed in light of other literature data.

$$(1)\ O_3 + HNO_2 \rightarrow HNO_3 + O_2.$$

The second order rate for this reaction must be $<1\times10^{-3}ppm^{-1}min^{-1}$. Based on reasonable concentrations for O_3 and HNO_2, this reaction cannot be important to atmospheric chemistry.

$$(2)\ N_2O_5 + H_2O \rightarrow 2\ HNO_3.$$

We have estimated an upper limit of $3\times10^{-7}ppm^{-1}min^{-1}$ for this reaction. Morris and Niki(18) reported an upper limit of about $2\times10^{-5}ppm^{-1}min^{-1}$; the rate reportedly being limited by heterogeneous reactions.

In general, heterogeneous complications induced by reactor surfaces are proportional to the surface to volume ratio of the reactor. S/V for the cell used by Morris and Niki was some 40 times greater than that for the Battelle chamber.

Thermal decomposition of N_2O_5 apparently limits its concentrations in the troposphere. According to the study by Connell and Johnston(19) the thermal decay rate at 27C is 7.5 min^{-1}. The slow rate we find for homogeneous conversion to HNO_3 coupled to the strong temperature dependence for N_2O_5 decomposition(19) suggest that N_2O_5 may persist for substantial periods in the colder regions of the lower atmosphere and that clouds and perhaps moist aerosols may be the dominant sink for N_2O_5.

(3) SO_2 + HO (M) → SULFATE

Experiments conducted here strongly support a rate of $1.6x10^3 ppm^{-1} min^{-1}$ for the rate limiting step in the conversion of SO_2 to sulfate aerosols. Since that agrees with the recommendation of Calvert et al.(7) for the reaction SO_2 + HO (M) → products, it appears that all of the SO_2 oxidized by HO converts to the particulate phase.

The mechanism(s) involved in the conversion were not elucidated. However, NO_X was not found to be incorporated with sulfate in the condensed phase, even under favorable conditions of high concentrations of HO, NO and NO_2. IF $HOSO_2O$ yields intermediates with NO and NO_2, subsequent decomposition must result in NO_X release to the gas phase.

(4) SO_2 + HO_2 → SULFATE

Our experiments indicated that the overall conversion rate for this reaction is considerably less than the literature value of 1.2 $ppm^{-1}min^{-1}$(20). We have suggested that the rate is <0.2 $ppm^{-1}min^{-1}$, but we were not successful in establishing a definite upper limit value.

Graham et al.(21) have recently reported an upper limit rate of $1.5x10^{-3}ppm^{-1}min^{-1}$ for the hydroperoxy reaction with SO_2. The rate was deduced by observing the effect of SO_2 on the equilibrium between HO_2NO_2 and NO_2 + HO_2. In one of their experiments, SO_2 had no measurable effect, while at a higher SO_2 concentration the effect was negative.

Burrows et al.(22), in work we have not reviewed, reported a rate constant $<3\times10^{-2}ppm^{-1}min^{-1}$ for the reaction of HO_2 with SO_2. The measurements were made at low pressure and might, therefore, be subject to upward adjustments if the reaction is actually a three-body reaction.

Additional high-pressure measurements of this reaction are recommended, including the determination of reaction products.

(5) $SO_2 + CH_3O_2 \rightarrow$ SULFATE

From a very limited investigation, we obtained an upper limit estimate of 0.8 $ppm^{-1}min^{-1}$ for the conversion of SO_2 to sulfate via the methylperoxy radical. The mechanism of the conversion was not investigated.

Two independent studies of the same reaction gave kinetic data in good agreement with each other(23,24); the rates being nearly an order of magnitude larger than that obtained in this study. In both studies(23,24), SO_2 oxidation rates were derived by following the absorbance of CH_3O_2 in flash photolysis systems. In one study(24), H_2SO_4 particulate was encountered while in the other study(23), particulates were not observed.

An obvious explanation for the discrepancy between our rate and that obtained in the flash photolysis work is that we measured only the formation of sulfate product while they measured the decay of CH_3O_2 reactant. It is conceivable that reaction products remained in the vapor phase and were interpreted as SO_2 in our system. In that case, the rate we reported is useful for describing SO_2 conversion to sulfate aerosol, but it underestimates the rate of SO_2 oxidation via CH_3O_2 radicals.

(6) $SO_2 + HNO_2 \rightarrow$ Products

It has been suggested by Ross(25) that, in the presence of sulfuric acid aerosols, nitrous acid oxides SO_2 at rapid rates. In our smog chamber experiments with relatively high concentrations of SO_2, HNO_2 and H_2SO_4 aerosols, we found no evidence to indicate that the proposed reaction takes place.

F. SO_2 Oxidation in Simulations of Urban and Rural Atmospheres

A series of smog chamber experiments was conducted to investigate some of the factors affecting SO_2 oxidation under simulated atmospheric conditions and to develop data needed to evaluate photochemical models of SO_2 oxidation in polluted air.

Experiments were conducted using hydrocarbon mixtures selected to represent urban and rural conditions. The urban mixture consisted of: ethane, ethylene, propane*, acetylene*, iso-butane, n-butane, propylene*, trans-2-butane, 2-methyl butane, n-pentane, 2-methyl 2-butene, 2-methyl pentane, benzene, toluene*, m-xylene*, p-ethyl toluene, 1, 2, 4-trimethyl benzene. Hydrocarbons making up the rural mixture are denoted by an asterisk.

For each experiment, the initial NMHC concentration was about 4.5 ppmC, and the initial NO_X concentration was 0.3 ppm. Apart from the control experiments where no SO_2 was introduced, 0.6 ppm SO_2 was injected into the chamber at either 1 or 5 hr. intervals after the irradiation began. Replicate experiments were also conducted in which 0.15 ppm NO was injected, together with 0.6 ppm SO_2. This approach was designed to simulate conditions in which SO_2

is emitted into polluted air from point sources. It was of interest to determine if SO_2 oxidation rates depended substantially on the interval of the photochemical smog period, and to what extent the accompaniment of NO (which is generally emitted along with SO_2) affected the oxidation rates.

Analytical methods for determining SO_2 and sulfate aerosols were identical to those used in the "kinetic experiments". For this experimental series, two Meloy sulfur analyzers were used to monitor SO_2 and particulate sulfate simultaneously.

Rates of SO_2 oxidation were calculated from the formula:

$$\frac{\alpha_1-\alpha_o}{\beta_1-\beta_o} \ln \frac{\beta_o}{\beta_1} = kt$$

where $\alpha = SO_4^{=}/S_T$, $\beta = SO_2/S_T$, and $S_T = SO_4^{=} + SO_2$.
This method accounted for dilution losses of SO_2 and sulfate but not for wall losses of sulfate.

During the period of these experiments, Battelle's large smog chamber was lined with 5-mil FEP Teflon filter. The light intensity corresponding to k_1 was 0.17 min^{-1}. It should be noted that the apparently low rates of SO_2 oxidation observed in the experiments reflect the low light intensity.

(1) Experimental Data

Gas chromatographic analyses for hydrocarbons were obtained initially and at irradiation intervals of 1, 3, 5 and 7 hrs. PAN concentrations were obtained hourly. Results for each experiment are tabulated in Appendix B, Tables B-1 through B-12.

The concentrations of all nonhydrocarbon species measured in each experiment are given as functions of irradiation time in Tables 25-36. Concentrations for toluene, xylene and PAN are also included in these tables. NMHC refers to the total [NMHC] determined by GC rather than by a total hydrocarbon analyzer. ALD_T is the total aldehydes concentration and CH_2O is the formaldehyde concentration. N_T is the total NO_X concentration determined by chemiluminescence, and NO_X loss is the unaccounted NO_X products (HNO_3, HO_2NO_2, RO_2NO_2 and N_2O_5) after correcting for dilution losses of 5%/hr. S_T refers to total sulfur (SO_2 + particulate sulfate). B_{SCAT} is the light scattering coefficient above background ($0.2\ 10^{-4} m^{-1}$) as measured by an integrating nephelometer.

We chose to present these data in tabular rather than graphic form because of the large number of species measured and because of the preference of many people to work directly with numerical data.

A summary of the experimental results and initial reaction conditions is provided in Table 37. Experiments are presented in pairs, i.e., similar experiments except for urban or rural hydrocarbon mixtures. An experiment described in Table 37 as "Urban HC/SO_2-NO at 5 hr." refers to an irradiation with the initial concentrations of 4.5 ppmC of the urban HC mix and 0.3 ppm NO_X, to which 0.6 ppm SO_2 and 0.15 ppm NO were added after 5 hr. Most experiments were conducted for 8 hr., or at least until the maximum rate of SO_2 oxidation and the maximum O_3 level had been reached. Experiments 6 and 12 were continuations of Experiments 5 and 11, respectively, after irradiation periods of about 24 hr. In those cases, SO_2 was added after 24 hrs. of irradiation and NO was added 2 hrs. thereafter.

TABLE 25. RESULTS FOR EXPERIMENT 1.

TIME HR.	NMHC ppbc	TOLUENE ppbc	XYLENE ppbc	*ALD$_T$ ppb	CH$_2$O ppb	NO ppb	NO$_2$ ppb	PAN ppb	N$_T$ ppb	NO$_X$ LOSS ppb	O$_3$ ppb	S$_T$ ppb	SULFATE ppb	B$_{SCAT}$ $10^{-4}m^{-1}$
0	4320	490	600		0	160	143	0	303	0	0	0	0	0
						125	178				5			
					52	59	231		290		23			
				210		18	256				62			
1	4010	490	520			12	237	17	266	22	110	0	0	0
											154			
						5	181				188			
											217			
2						∼0	140	61	201	73	242	0	0	.05
											291			
3	2950	380	250			0	82	102	184	77	322	0	0	.15
											350			
4						0	49	133	182	66	365	0	0	.25
					199									
				375										
5	2430	310	150			0	36	145	181	55	371	0	0	.27
6						0	33	146	179	45	363	0	0	.27
					185									
				375										
7	1800	260	80			0	33	140	173	40	350	0	0	.30
8														

TABLE 26. RESULTS OF EXPERIMENT 7.

TIME HR.	NMHC ppbc	TOLUENE ppbc	XYLENE ppbc	ALD_T ppb	CH_2O ppb	NO ppb	NO_2 ppb	PAN ppb	N_T ppb	NO_X LOSS ppb	O_3 ppb	S_T ppb	SULFATE ppb	B_{SCAT} $10^{-4}m^{-1}$
0	4890	840	940			146	147	0	293	0	0	0	0	0
						129	156		285					
					33	99	181		280		10			
				254										
1	4480	780	810			47	228	0	275	3	33	0	0	0
											85			
2						13	238	16	267	0	157	0	0	.05
											215			
3	3600	650	570			8	218	38	264	12	269	0	0	.05
											316			
4						0	160	72	232	8	351	0	0	.1
					143						390			
				471										
5	2920	530	420			0	115	97	212	16	419	0	0	.1
											447			
6						0	76	115	191	26	468	0	0	.15
					161						468			
				435										
7	2490	450	310			0	46	133	179	27	469	0	0	.15
8														

TABLE 27. RESULTS OF EXPERIMENT 3.

TIME HR.	NMHC ppbc	TOLUENE ppbc	XYLENE ppbc	ALD_T ppb	CH_2O ppb	NO ppb	NO_2 ppb	PAN ppb	N_T ppb	NO_X LOSS ppb	O_3 ppb	S_T ppb	SULFATE ppb	B_{SCAT} $10^{-4}m^{-1}$
0	4860	570	760			164	147	0	311	0	0	0	0	0
						125	181		306		5			
					46	70	229		299		21			
				254		26	257				67			
1	3960	500	520			12	247	22	281	15	125	0	0	0
*												598	0	
						2	193				210			
2						~ 0	152	66	218	63	275	571	10	.4
3	3190	400	280			0	89	105	194	73	373	519	16	1.2
4						0	49	133	162	72	445	464	20	2.0
					184									
				399										
5	2430	320	160			0	33	148	181	61	475	418	21	2.4
6						0	30	151	181	49	480	378	21	2.7
					177									
				362										
7	1960	280	100			0	30	146	176	43	465			2.8
8														

*SO_2 added at 1.25 hr.

TABLE 28. RESULTS OF EXPERIMENT 11

TIME HR.	NMHC ppbc	TOLUENE ppbc	XYLENE ppbc	ALD_T ppb	CH_2O ppb	NO ppb	NO_2 ppb	PAN ppb	N_T ppb	NO_X LOSS ppb	O_3 ppb	S_T ppb	SULFATE ppb	B_{SCAT} $10^{-4}m^{-1}$
0	4960	870	950			153	148	0	301	0	0	0	0	0
				254	22	99	190		289		17			
1	4390	770	770			46	229	4	279	7	51	0	0	0
*												600	0	
						23	231				96			
2						13	214	23	250	22	159	560	5.0	.05
											218			
3	3470	630	510			0	152	51	203	56	276	512	9.0	.5
											319			
4						0	114	78	192	54	362	480	10.9	1.2
				362	125						433			
5	2800	500	360			0	82	103	185	49	468	435	12.7	1.8
											487			
6						0	58	121	179	43	501	400	13.6	2.6
				362	143						494			
7	2280	390	240			0	40	134	174	37	493	350	14.7	3.1
8														

*SO_2 added at 1.25 hr.

TABLE 29. RESULTS FOR EXPERIMENT 2.

TIME HR.	NMHC ppbc	TOLUENE ppbc	XYLENE ppbc	ALD_T ppb	CH_2O ppb	NO ppb	NO_2 ppb	PAN ppb	N_T ppb	NO_x LOSS ppb	O_3 ppb	S_T ppb	SULFATE ppb	B_{SCAT} $10^{-4}m^{-1}$
0	4840	560	720			127	148	0	275	0	0	0	0	0
						104	170		274		9			
					61	49	224		273		19			
				290		12	254		266		65			
1	3770	400	460			0	235	22	257	4	112	0	0	.05
*						33	348	(29)	(410)		46	736	0	
						19	343				63	731	2	
											98			
2						6	310	52	368	22	126	710	5	.2
						3	264							
3	3160	420	310			~0	223	82	305	65	214	657	8	.6
4						0	157	110	267	85	300	602	10	1.3
					164									
5				326		0	107	141	248	87	365	552	12	2.0
6						0	69	164	233	86	405	508	13	2.7
					175									
7				399		0	43	177	220	83	420	461	13	3.4
8														

*SO_2 and NO added at 1.25 hr.

TABLE 37. RESULTS OF EXPERIMENT 8

TIME HR.	NMHC ppbc	TOLUENE ppbc	XYLENE ppbc	ALD_T ppb	CH_2O ppb	NO ppb	NO_2 ppb	PAN ppb	N_T ppb	NO_x LOSS ppb	O_3 ppb	S_T ppb	SULFATE ppb	B_{SCAT} $10^{-4}m^{-1}$
0	4940	830	950			150	142	0	292	0	0	0	0	0
				145	33	108	174		282		10			
1	4510	770	810			56	221	2	279	0	30	0	0	.05
*												603	0	
						94	273	(5)	(372)	0	19			
2						49	297	8	354	0	40	579	5	.15
						30	304				74			
3	3640	640	570			12	297	19	328	9	114	533	9	.30
											156			
4						0	256	36	292	28	203	485	12	.90
				471	125						247			
5	3010	530	400			0	218	58	276	29	295	445	14	1.35
											335			
6						0	173	82	255	35	376	406	15	1.8
				471	136						405			
7	2580	450	320			0	129	104	233	42	430	370	16	2.2
8														

*SO_2 added at 1.25 hr.

TABLE 31. RESULTS OF EXPERIMENT 5.

TIME HR.	NMHC ppbc	TOLUENE ppbc	XYLENE ppbc	ALD_T ppb	CH_2O ppb	NO ppb	NO_2 ppb	PAN ppb	N_T ppb	NO_X LOSS ppb	O_3 ppb	S_T ppb	SULFATE ppb	B_{SCAT} $10^{-4}m^{-1}$
0	4820	560	750			150	148	0	298	0	0	0	0	0
						116	172							
					67	54	228				50			
				326		14	246							
1	3980	500	510			5	221	28	254	29	186	0	0	0
						0	175				279			
2						0	139	80	219	50	350	0	0	0
											412			
3	3020	410	270			0	82	123	205	51	456	0	0	.05
											487			
4						0	49	148	197	47	508	0	0	.07
					203						514			
				544										
5	2590	350	180			0	37	163	200	32	514	0	0	.1
*												608	0	
											505			
6	2370	320	150			0	30	157	187	31	496	568	4	.25
					202						494			
				471										
7						0	25	153	178	20	488	525	8	.55
8														

*SO_2 added at 5.25 hr.

TABLE 32. RESULTS OF EXPERIMENT 13

TIME HR.	NMHC ppbc	TOLUENE ppbc	XYLENE ppbc	ALD_T ppb	CH_2O ppb	NO ppb	NO_2 ppb	PAN ppb	N_T ppb	NO_X LOSS ppb	O_3 ppb	S_T ppb	SULFATE ppb	B_{SCAT} $10^{-4}m^{-1}$
0	4920	860	920			150	150	0	300	0	0	0	0	0
						141	155							
					31	122	168		290		5			
				181		94	190							
1	4500	730	710			66	213		279	6	25	0	0	0
						28	230				55			
2						8	223	10	241	17	95	0	0	0
						0	206				140			
3	3520	650	550			0	178				185	0	0	.05
											230			
4						0	131				275	0	0	.07
				254	97						319			
5	2820	500	380			0	91	49	140	82	360	0	0	.07
*												610	0	
											395			
6						0	56	78	134	77	420	570	3	.3
				399	128						440			
7						0	40	95	135	66	460	520	4.7	.6
8														

*SO_2 added at 5.25 hr.

TABLE 33. RESULTS OF EXPERIMENT 4.

TIME HR.	NMHC ppbc	TOLUENE ppbc	XYLENE ppbc	ALD_T ppb	CH_2O ppb	NO ppb	NO_2 ppb	PAN ppb	N_T ppb	NO_X LOSS ppb	O_3 ppb	S_T ppb	SULFATE ppb	B_{SCAT} $10^{-4}m^{-1}$
0	4740	570	750			150	145	0	295	0	0	0	0	0
						122	170							
					56	56	231				7			
				264		23	254							
1	3920	490	510			14	238	25	277	3	141	0	0	.05
						10	185				239			
2						5	145	75	225	42	309	0	0	.10
											370			
3	2950	400	260			∿ 0	86	118	204	50	412	0	0	.15
											454			
4						0	46	152	198	43	474	0	0	.20
					166						484			
				362										
5	2370	310	140			0	30	168	198	32	488	0	0	.25
*							171	(169)	(340)		334	618	0	
							155				366			
6	2150	280	110			0	125	173	298	54	418	598	6	.6
					203									
				362										
7	1910	250	70			0	84	179	263	82	493	542	12	1.2
8						0	66				535	491	17	1.7

*SO_2 and NO added at 5.25 hr.

TABLE 34. RESULTS OF EXPERIMENT 10

TIME HR.	NMHC ppbc	TOLUENE ppbc	XYLENE ppbc	ALD_T ppb	CH_2O ppb	NO ppb	NO_2 ppb	PAN ppb	N_T ppb	NO_X LOSS ppb	O_3 ppb	S_T ppb	SULFATE ppb	B_{SCAT} $10^{-4}m^{-1}$
0	4950	840	960			159	150	0	309	0	0	0	0	0
					43	106	193				15			
				72										
1	4480	800	810			45	240	6	291	3	50	0	0	0
						21	239				113			
2						11	208	25	244	36	173	0	0	0
											232			
3	3510	630	550			4	158	50	212	54	284	0	0	0
											333			
4						0	112	83	195	58	376	0	0	.05
					120						411			
				395										
5	2860	520	380			0	69	110	179	62	443			.1
*							203	(115)	(318)			580	0	
											312			
6	2600	460	320			0	167	119	286	70	350	550	3.2	.35
					146						388			
				362										
7	2390	420	270			0	129	131	260	79	421	505	7.0	.7
8												465	9.2	1.2

*SO_2 and NO added at 5.25 hr.

TABLE 35. RESULTS OF EXPERIMENT 6

TIME HR.	NMHC ppbc	TOLUENE ppbc	XYLENE ppbc	ALD_T ppb	CH_2O ppb	NO ppb	NO_2 ppb	PAN ppb	N_T ppb	NO_X LOSS ppb	O_3 ppb	S_T ppb	SULFATE ppb	B_{SCAT} $10^{-4}m^{-1}$
23+0	1020	110	10			0	21	77	98	0	424	179	9	2.2
*												768	9	
											420			
1						0	21	62	83	0	414	740	11	2.3
					150						411			
				362										
2	870	100	10			0	21	61	82	0	409	693	14	2.5
**														
						13	162	(61)	(236)		260			
3						11	148	51	210	20	288	644	17	2.7
											311			
4						2	120	-	-	-	328	604	19	2.8
5														
6														
7														
8														

* SO_2 added at 23.25 hr.
** NO added at 25.25 hr.

TABLE 36. RESULTS OF EXPERIMENT 12

TIME HR.	NMHC ppbc	TOLUENE ppbc	XYLENE ppbc	ALD_T ppb	CH_2O ppb	NO ppb	NO_2 ppb	PAN ppb	N_T ppb	NO_X LOSS ppb	O_3 ppb	S_T ppb	SULFATE ppb	B_{SCAT} $10^{-4}m^{-1}$
23+0	880	110	30			0	18	68	86	9	456	85	4.0	3.1
*											453	660	4.0	
1	810	100	20			0	18	68	86	4	449	650	5.0	3.1
					110						446			
				326										
2	750	80	20			0	14	68	82	4	445	610	7.2	3.1
**						2	154	(68)	(224)		239			
3						1	146	59	205	11	271	580	8.6	3.2
											290			
4						0	137	53	190	15	310	520	9.6	3.3
											320			
5	630	210	20			0	129	49	178	17		485	10.2	3.3
6														
7														
8														

* SO_2 added at 23.5 hr.
** NO_2 added at 25.25 hr.

TABLE 37. SUMMARY OF RESULTS OF SO_2 OXIDATION DURING SMOG CHAMBER SIMULATIONS OF URBAN AND RURAL CONDITIONS.

			HYDROCARBON DECAY RATES[a]			SMOG PARAMETERS				
RUN NO.	HC/NO_X	DESCRIPTION OF EXPERIMENT	NMHC %/HR.	XYLENE %/HR.	TOLUENE %/HR.	NO_2-T_{MAX} MIN.	PAN-MAX PPB	NLOSS-MAX[b] PPB	O_3-MAX PPB	R_{SO_2}-MAX %/HR.
1	14.2	Urban HC	11.5	28	9.1	45	146	77	371	--
7	16.7	Rural HC	10.3	16.1	9.2	80	133	27	469	--
3	15.6	Urban HC/SO_2 at 1 hr.	13.8	31	11.5	45	151	73	480	2.40
11	16.5	Rural HC/SO_2 at 1 hr.	11.4	19.4	11.0	70	134	56	501	1.22
2	17.6	Urban HC/SO_2-NO at 1 hr.	12.7	28	9.6	45	177	87	420	0.96
8	16.9	Rural HC/SO_2-NO at 1 hr.	9.9	17.2	8.9	135[c]	104	42	430	1.18
5	16.1	Urban HC/SO_2 at 5 hr.	12.4	29	9.4	41	163	51	514	0.98
13	16.4	Rural HC/SO_2 at 5 hr.	11.1	--	10.8	90	95	82	460	0.73
4	16.1	Urban HC/SO_2-NO at 5 hr.	13.8	33.5	12.1	45	179	82	493	1.37
10	16.0	Rural HC/SO_2-NO at 5 hr.	10.9	18.5	9.0	70	131	79	443	0.85
6A	48	Urban HC/SO_2 at 24 hr.	(d)	(d)	(d)	--	62	--	420	0.56
12A	49	Rural HC/SO_2 at 24 hr.	(d)	(d)	(d)	--	68	--	453	0.43
6B	5.5	Urban HC/NO at 26 hr.	(d)	(d)	(d)	--	51	--	328	0.66
12B	4.6	Rural HC/NO at 26 hr.	(d)	(d)	(d)	--	59	--	320	0.39

(a) Hydrocarbon decay rates are averages over the 1st 5 hrs. and are not corrected for the chamber dilution rate (∿ 5%/hr.).

(b) NLOSS-MAX represents the maximum amount of undetected nitrogen products (N_2O_5, HNO_3 and HO_2NO_2); these products were probably absorbed on chamber surfaces.

(c) Maximum NO_2 concentration had not been reached before more NO was added.

(d) No significant difference from dilution rate.

(2) Discussion

The mixture of 17 hydrocarbons selected as a surrogate for urban hydrocarbon distributions was based on analyses of Los Angeles air by Stephens (26). A similar mixture of hydrocarbon was used in an earlier investigation of the hydrocarbon NO_x precursor effects on SO_2 oxidation(27). The composition of the rural hydrocarbon mix was selected by Dr. Spicer at Battelle upon reviewing GC data collected by Battelle, EPA, and Washington State University at several rural sites in the U.S.

It is interesting that the molar reactivity of the two mixtures, reactivity based on the reaction rates of individual hydrocarbons with HO radicals, is nearly similar. For the urban mixture, the reactivity in terms of an average molar rate with HO is $1.16 \times 10^4 \text{ppm}^{-1}\text{min}^{-1}$. The corresponding reactivity for the rural mixture is $1.08 \times 10^4 \text{ppm}^{-1}\text{min}^{-1}$. The similarity results, in part, because 23 percent of the rural mixture is composed of highly reactive hydrocarbons (propylene and p-xylene) while the urban mixture is composed of only 17 percent of the more reactive species (propylene, p-xylene, 2-butene, 2-methylbutene-2, and 1, 2, 4-trimethylbenzene).

The decay rates of the individual hydrocarbons during the experiments have not been interpreted in any detail. In general, the average rate of disappearance of NMHC was 10-20 percent greater for the urban HC experiments compared to the rural HC experiments.

We also noticed (Table 37) that there was a marked difference in the average rates* of xylene removal depending on the urban or rural mixtures. The average rate was near 30%/hr. for the urban runs and near 18%/hr. for the runs with rural HC mixtures. In contrast, average toluene decay rates were nearly identical for the experimental sets with urban and rural hydrocarbons; the averages being near 10%/hr.

---

*Decay rates were not corrected for the dilution rate (∿5%/hr.)

As shown in Table 37, experiments with the urban HC mixtures were consistently faster in oxidizing NO compared to the runs with the rural HC mixture. For the urban HC runs, the average value for the NO_2-T_{MAX} parameter was about 44 min., while that for the rural HC runs was nearly twice as large.

Experiments with the urban HC mixture consistently produced larger PAN concentrations than did the corresponding experiments with the rural HC.

NO_X losses (presumably products of NO_2 oxidation) were more pronounced for the urban versus rural HC experiments, except for Experiment 5.

The effects of hydrocarbon composition on maximum O_3 levels were mixed. Experiments conducted with the rural HC mixture produced higher peak O_3 concentrations except for the cases where either SO_2 or SO_2 plus NO was added at 5 hr. Then the higher O_3 levels occurred for the runs with urban HC.

With but one exception (NO + SO_2 added at 1 hr.), the maximum rate of SO_2 oxidation was larger for the runs with the urban HC mixture compared to the runs with the rural HC mixture. In general, the differences in the SO_2 oxidation rates were not terribly large. When SO_2 (with or without NO) was added at the 1 hr. mark, the rate of SO_2 oxidation reached a maximum within 2 hrs., and the rate of oxidation gradually diminished thereafter. When SO_2 was added at the 5 hr. point, the rate of SO_2 oxidation proceeded at nearly constant levels for the remainder of the irradiation period (usually 3 hr.).

In the cases (Experiments 6 and 12) where SO_2 was added after 24 hrs. (a transport simulation), the oxidation rates also appeared to be constant but substantially lower than they were during the previous 8 hr. irradiation intervals. For the urban HC experiments, the maximum rate of SO_2 oxidation during the "well aged" period was only one-fourth as large as it was during the early period of aggressive hydrocarbon and NO oxidation.

The effects of added amounts of NO on SO_2 oxidation and on other smog parameters were not very dramatic, perhaps because too little was added relative to the concentrations of O_3 and the overall strength of the smog systems. In the experiments with urban HC, the addition of NO along with SO_2 decreased the rate of SO_2 oxidation when the addition was made early in the irradiation, but it had the opposite effect when added at 5 hr. The addition of NO reduced O_3 and increased PAN in each of the experiments with urban HC. In general, the effects caused by the additions at 5 hrs. were less than those at 1 hr.

For the runs with rural HC, the additional amounts of NO had only marginal (perhaps insignificant) effects on the rates of SO_2 oxidation. NO reduced the peak O_3 levels but had mixed effects on PAN. NO added early in the irradiation reduced PAN, whereas NO added at 5 hrs. increased the PAN concentration.

The effects of additional NO on the rate of SO_2 oxidation after prolonged irradiation periods were virtually insignificant for both urban and rural HC experiments.

The significance of some of these observations and trends will be discussed in the next section in conjunction with kinetic modeling results for these experiments.

(3) Kinetic Model Applied to Smog Chamber Experiments

a. Scope of Model

One objective for this phase of the study was to determine if a relatively simple model of atmospheric chemistry could suffice to represent SO_2 oxidation in polluted air. The smog chamber data previously presented and some field data from the MISTT project provided a basis for applying the model.

Recent reports$^{(28,29)}$ have indicated success in formulating detailed mechanisms for the branching reactions likely to occur during hydrocarbon degradation in smog. The mechanisms have been shown to give reasonably good fits to smog chamber data for simple hydrocarbon systems, e.g. propylene and n-butane. Hov et al.$^{(30)}$ have suggested a scheme to represent the oxidation of aromatic compounds in smog, but data are not available to evaluate such proposals.

In this study, where mixtures of 17 hydrocarbons were involved, the task of incorporating detailed mechanisms for the hydrocarbons was considered too large and beyond the scope of the project. Instead we opted to use a very general mechanism for saturated hydrocarbons, as represented by reactions 41-55 in Table 2. A similar mechanism was found to give good fits to O_3 data for earlier smog chamber experiments conducted with the same mixture of hydrocarbons$^{(31)}$.

b. Hydrocarbon Reactivity

It has been suggested that the rates of reaction of individual hydrocarbons with HO radicals would be a useful basis for indexing the reactivity of hydrocarbons in smog$^{(32)}$. Indeed, Winer et al.$^{(33)}$ have shown that, for several isomeric hydrocarbons, O_3 formation correlated well with the respective rate constants, k_{HC-HO}. Another report found, however, that over a wide range of HC reactivities, the proportionality between k_{HC-HO} and O_3 concentrations (smog chamber data) was nonlinear, and that k_{HC-HO} was a useful index for reactivity only when plugged into a photochemical model of smog$^{(31)}$.

As noted earlier, the average values of k_{HC-HO} for the urban and rural mixtures used in this study turned out to be nearly the same. Accepting considerable scatter that might be due to variations in control variables, the summary data (Table 37) indicate that peak O_3 concentrations for the urban and rural experiments were not too dissimilar; although rural $[O_3]$ was slightly higher in most cases.

There were wider variations, however, in other reactivity parameters for the urban versus rural experiments. Most obvious were the much faster oxidation rates for NO and xylene during the experiments with the urban HC mixture. Aldehyde and PAN formation were also favored in the urban-HC experiments.

These apparent effects of hydrocarbon reactivity posed an immediate problem in applying the kinetic model to the experiments since the only appropriate variable in the model is k_{HC-HO}.

Because the initial rates of NO oxidation and aldehyde (particularly formaldehyde) formation were greater with the urban mixture, we assumed that in spite of the computed averages for k_{HC-HO} certain hydrocarbons in the urban mixture were undergoing more rapid oxidation than in the rural mixture during the initial irradiation period. To adjust for that, higher values for k_{HC-HO}-urban were incorporated initially: for the first 60 min. of irradiation, k_{HC-HO}-urban was set at $7x10^4$ $ppm^{-1}min^{-1}$, while k_{HC-HO}-rural was set at $2x10^4$ $ppm^{-1}min^{-1}$. Thereafter, k_{HC-HO} for both conditions was set at $1x10^4$ $ppm^{-1}min^{-1}$. Thus the concept was to use variable values for k_{HC-HO} to reflect instantaneous rates for the actual mixtures.

c. Model Results

Examples of kinetic modeling results are shown in Tables 38 and 39 for Experiments 3 and 11, respectively. With regard to Experiment 3, the model fit to the NMHC data was fairly good. The model grossly underestimated the formation of aldehyde and PAN. The inadequacies of the model for predicting those species is discussed later. Model predictions for NO_X loss reflect the unsatisfactory distribution of NO_X products as influenced by PAN. The model fit to the O_3 data was acceptable but certainly not perfect. The

TABLE - 38

Experiment and Modeling Results for Experiment 3

Irradiation Time, min.	Specie Concentrations (exp/*model*), ppb					
	NMHC	ALD	PAN	NO_X LOSS	O_3	SULFATE
0	1215 *1215*	0 *0*	0 *0*	0 *0*	0 *0*	0 *0*
60	990 *1000*	254 *126*	22 *2*	15 *23*	125 *142*	0 *0*
180	798 *824*	--- *131*	105 *7*	73 *56*	373 *250*	16 *6.4*
420	490 *558*	362 *96*	146 *26*	43 *154*	465 *501*	21 *16.1*

TABLE - 39

Experiment and Modeling Results for Experiment 11

Irradiation Time, min.	Specie Concentrations (exp/*model*), ppb					
	NMHC	ALD	PAN	NO_X LOSS	O_3	SULFATE
0	1240 *1240*	0 *0*	0 *0*	0 *0*	0 *0*	0 *0*
60	1097 *1100*	254 *70*	4 *1*	7 *13*	51 *47*	0 *0*
180	867 *937*	--- *88*	51 *5*	56 *46*	276 *173*	9.0 *4.8*
420	570 *663*	362 *89*	134 *15*	37 *120*	493 *384*	14.7 *11.3*

model rather severely underestimated SO_2 conversion to sulfate during the first two hours. After that period, the predictions for sulfate formation agreed with the experimental data.

The fit of the model to the data for Experiment 11 (rural HC) was similar to that for Experiment 3 (urban HC). Again, there were reasonably good fits for NMHC decay and O_3 formation, and gross differences for ALD, PAN and NO_X loss (near the end of the run). The initial rate of sulfate formation was only one-half that found experimentally. Thereafter the conversion rates agreed fairly well.

Kinetic simulations were also performed to determine if the observed effects of NO were consistent with the model chemistry. The experimental effects of adding NO together with SO_2 at 1 hour can be observed by comparing the data from Experiments 2 and 3. In this case, excess NO resulted in increases in PAN and NO_X loss, as might be expected. Added NO also reduced the peak O_3 concentration and lowered the conversion of SO_2 to sulfate.

For modeling purposes, the kinetic simulation of Experiment 3 was repeated, but with 150 ppb added to the reaction mixture at 1 hr. The model predicted the same trends as observed experimentally, i.e., NO increased PAN and NO_X loss, while it reduced O_3 and R_{SO_2}.

The effects of adding extra NO during the fifth hour of irradiation were similar to those observed for the addition at 1 hour, with one important difference. When NO was added with SO_2 at 5 hours (compare results of Experiments 4 and 5), the rate of SO_2 conversion to sulfate increased.

Here, too, the modeling results showed identical trends as affected by NO. According to the model, inclusion of NO during the later stages of the smog period "pumped up" the HO concentration, which resulted in increased rates of SO_2 oxidation. It should also be noted that the model predicted that an excess of O_3 would have developed about 4 hours after the NO was added. The experiment, however, was not conducted long enough to verify the prediction.

When NO was added to well-aged smog (Experiments 6B and 12B), the effects on SO_2 oxidation were not significant. These conditions, which appeared to be near steady-state, were not modeled.

d. Limitations of Model

It is apparent that the abbreviated mechanism used to describe the chemistry of the smog chamber experiments with hydrocarbon mixtures is inadequate in many respects. Apart from the adjustments in k_{HC-HO} needed to account for effects of hydrocarbon reactivity, it was necessary to include a source of HO radicals to initiate the chain reactions. Following a practice used by Whitten and Hugo(34), 10 ppb HONO, or about one-third of the equilibrium concentration of HONO, was incorporated for that purpose.

The business of compensating for the inadequate production rate of radicals offered by kinetic models is not uncommon. To fit model results to their smog chamber data, Carter et al.(28) devised a parameter to generate HO radicals from an unknown source. HO generation was used throughout the irradiation periods, and the HO production rate from the unknown was adjusted for each experiment. Justification for such practices are based on mysterious "dirty chamber effects".

The inadequacies of models to reproduce smog chamber data extends beyond the possibilities attributable to contamination. For example, water vapor has been found to have highly significant effects on the overall rates of photochemical smog reactions (rate of NO oxidation to NO_2, NO_2 conversion to products and O_2 formation)(35). Earlier work showed similar results(36,37). The substantial effects of H_2O cannot be explained by any conventional model of smog, and the subject is usually passed over as being another artifact of smog chamber experiments.

In this work, the most glaring inadequacies of the model employed were the estimations for aldehyde and PAN. In large part this was related to the choice of an alkane system to represent the chemistry for the entire hydrocarbon mixture. Without going into the details, it can be shown that the oxidation of olefins and aromatics will generally lead to more organic fragments, including aldehydes, than will alkane oxidation. From the sum of PAN and aldehydes in the experiments compared to NMHC losses, it is clear that the concentration of reactive organics increased during the irradiation period. The reaction scheme used in the model did not provide for the proper degree of fragmentation. In general, the model predicted only 25 percent of the aldehyde formation.

Low aldehyde concentrations were responsible, in part, for the low estimates for PAN by the model. Additional inadequacies regarding PAN must also exist, as the RCO_3 levels appeared to be too low throughout the simulations. Winer et al.(39) point out that the photolysis of methyl ethyl ketone is an important source of acetyl peroxy radicals, and such concepts are missing entirely from the subject model.

Another interesting problem not sufficiently resolved by the model is the experimental variation in NO_X losses (Tables 25-36). NO_X losses in these experiments presumably represent products of NO_2 conversion which were not measured in the catalytic mode of the chemiluminescence analyzer. In these experiments, the unmeasured products were thought to be HO_2NO_2, RO_2NO_2, N_2O_5 and HNO_3. The extent to which these products reached the NO_X detector is unknown. The majority of these products are believed to have undergone irreversible absorption on the chamber surfaces.

In most of the experiments, and particularly those with urban hydrocarbons, the amount of NO_X loss went through a maximum near the middle of the irradiation period. Thus the net increase in NO_X products after such maxima represents a conversion of unmeasured NO_X to measured NO_X (NO, NO_2, HNO_2 or PAN). According to the model, thermal decomposition of HO_2NO_2 and RO_2NO_2 during the latter periods of the experiments would not alone account for the observed trends in NO_X loss. Furthermore, the model predicted ever-increasing concentrations for PAN in contrast to the maxima observed for it. Thus the processes involving the long-lived intermediates of NO_X do not appear to be well represented by the model.

Attempts to better understand and model the NO_X chemistry of these and similar experiments in the Battelle chamber are the objective of another EPA program (Grant R-805812).

e. Analysis of SO_2 Conversion

While it may be somewhat fortuitous, the model's predictions for sulfate formation were reasonably close to the experimental values. For example, in Experiments 3 and 11, SO_2 conversion to sulfate was within 77 percent of the experimental values after 7-hr. irradiation periods. Thus the model seemed to underestimate HO production by some 25 percent overall. However, during the brief periods of most rapid SO_2 oxidation (near the time of peak NO_2 production) the model underestimated the rate of SO_2 oxidation by a factor of about 2. Thus it appears that only one-half of the swarm of radicals was generated by the model during this highly reactive period. That condition, too, is most likely keyed to the proper amount of chain branching within the organic constituency.

Accepting the upper limit rate constants derived in this study for SO_2 conversion to sulfate and the utility of the subject model for approximating the conversion in smog, it is of interest to examine, in theory, the contributions to sulfate formation made by the individual radicals during the smog chamber experiments. Taking the modeling results from Experiment 3 as an example, the relative contributions at the 1 hour period (when R_{SO_2} was a maximum) and the 5 hour period (wnen R_{SO_2} was nearly constant) where:

	Percent Contribution to R_{SO_2}-Total	
	1 Hour	5 Hours
HO	94	75
HO_2	2	6
RO_2	4	19

When the effect of adding NO at 5 hours was modeled, the HO concentration increased about 30 percent, largely at the expense of HO_2, and the total rate of SO_2 oxidation was boosted accordingly.

The conclusion here is that in polluted air HO is overwhelmingly responsible for sulfate production. A similar conclusion regarding the dominant role of HO in SO_2 oxidation was reached for natural tropospheric conditions(7).

(4) Model Applications to Field Data

In spite of the shortcomings of the lumped model, it was of interest to adapt the model to estimate diurnal patterns of SO_2 oxidation in comparison with field data. The effort, under partial sponsorship by EPRI (RP1369-1 and RP860-1) and another EPA contract (68-02-2454), has been described in a paper submitted for publication(39). A summary of the modeling approach and the results, including excerpts from the paper, is given here.

The objective of this exercise was to estimate the rate of SO_2 oxidation for power plant plumes resident in polluted atmospheres, as a function of solar radiation, plume emission periods and plume dispersion rates. Simulations were also performed to investigate ambient HC-NO_x effects, but those results were not included in the referenced paper.

a. Model Equations

The model used for the computer simulations was conceptually similar to that used by Ogren et al.(40). The model treats physical processes affecting the plume (dispersion and transport) in a highly simplified fashion to allow for a more detailed treatment of chemical transformations. The model is formulated in a Lagrangian frame of reference, and its treatment of transport and diffusion is based upon the following two assumptions:

- the wind velocity is spatially uniform; and
- the concentration of a chemical specie in the plume over a cross-section perpendicular to the plume axis may be adequately described by its average concentration over the cross-section.

The formulations used to describe the mixing processes and the concentrations of species in the ambient air and plume cross-section are provided in the paper and are not repeated here.

The chemical mechanism incorporated in the model was essentially the same as the code appearing in Table 2, except the reactions pertaining to azomethane, CH_4 oxidation and chamber effects were not included. In addition, the thermolecular reactions that could form NO_2 and HONO in plumes were added to the code.

Some of the rate constants used in these simulations were different than those appearing in Table 2. The major differences were in the rates of NO oxidation by HO_2, RO_2 and RCO_3. The rates were factors of 3-4 smaller in this case. The effects of using the larger rates for NO oxidation would be to shorten the induction period for oxidation (including SO_2 oxidation) and increase the concentration ratios of HO to HO_2 and RO_2.

Rate constants assigned to the reactions of HO_2 and RO_2 with SO_2 were higher than the values determined finally in this study. The values were $k_{61} = 1.2\ ppm^{-1}min^{-1}$ and $k_{62} = 2.0\ ppm^{-1}min^{-1}$. These higher values were based on our preliminary evaluations of the chamber data. Use of the higher constants had only small effects on the modeling results because SO_2 oxidation was still dominated by HO.

b. Solar Radiation

Our primary intent in these simulations was to investigate the dependence of SO_2 oxidation in plumes on solar radiation. Variable solar radiation was incorporated into the simulations through the use of time varying photodissociation rate constants for NO_2, HNO_2, H_2O_2 and aldehydes. Two solar radiation conditions were used in the simulations, corresponding to clear and partly cloudy skies. Ultraviolet actinic fluxes for mid-July at

40°N latitude were used for the clear sky simulations, approximating the conditions of the Project MISTT Field Study. The diurnal variation of the NO_2 photodissociation rate constant for these conditions was based on data from Peterson$^{(41)}$. For the partly cloudy simulations, photodissociation rate constants were reduced to one-half their clear sky values.

c. Plume Dispersion

Plume dispersion was incorporated into the model through the temporal variation of the plume cross-sectional area, which was a model input. Several different plume dispersion rates were used in the simulations in order to assess the impact of dispersion on SO_2 oxidation. The dispersion rates were chosen as being appropriate to emissions from a tall stack moving over uniform terrain under varying atmospheric conditions.

Plume areas were estimated using Gaussian plume model horizontal and vertical dispersion coefficients, σ_y and σ_z. We somewhat arbitrarily chose

$$A = 16\ \sigma_y \sigma_z$$

since roughly 90% of a Gaussian plume is found within an area of width $4\sigma_y$ and height $4\sigma_z$. Three separate stability regimes were used in the simulations, corresponding to the slightly stable, neutral, and unstable classes of the Pasquill stability classification system$^{(42)}$ For the simulations of neutral and slightly stable conditions, the stability was held constant throughout the diurnal periods. Stability was varied in the simulations of unstable conditions by following the diurnal pattern of boundary layer evolution for a clear summer day. Horizontal dispersion coefficients were taken from Easter et al.$^{(43)}$. For the slightly stable and neutral simulations, vertical dispersion coefficients were obtained from Turner$^{(44)}$. For the unstable condition, σ_z was calculated using a K-theory approach:

$$\frac{d}{dt} (\sigma_z^2) = 2 k_z$$

where K_z is the vertical eddy diffusivity. The eddy diffusivity varied with time but was assumed constant over the vertical extent of the plume. It was calculated using the model and boundary layer data from Gillani(45).

d. Computational Description

A total of 18 simulations was made. The use of two solar radiation conditions (clear and cloudy skies) and three plume dispersion rates (for unstable, neutral, and slightly stable conditions) provided six different sets of atmospheric conditions. For each of these conditions, plume simulations were run with emissions at 6:00 a.m., 11:00 a.m., and 3:00 p.m.

In all the simulations, kinetic calculations for the ambient species began at 5:00 a.m. This allowed at least an hour for quasi-equilibrium to be reached before the plume emissions were entered. The following initial concentrations of ambient species were used: NO - 0.020 ppm; NO_2 - 0.005 ppm; SO_2 - 0.015 ppm; non-methane hydrocarbons - 0.16 ppm C; aldehydes - 0.002 ppm; CO - 0.5 ppm; H_2O - 1.7%. Under clear sky conditions, these pollutants yielded a peak ambient O_3 concentration of 108 ppb; a peak concentration of 68 ppb was obtained for ambient air under cloudy conditions.

Emission rates were chosen to approximate those for the Labadie power plant. A SO_2 emission rate of 4.7×10^6 ppm m^3/sec (or 6 kg sulfur/sec) and a NO emission rate of 1.8×10^6 ppm m^3/sec were used. In order to reduce computational time, kinetic calculations for the plume species were begun after the power plant emissions had dispersed for 5 minutes.

A constant wind speed of 5 m/sec was assumed and the boundary layer expansion factor was held constant at 0.03 $hr.^{-1}$.

e. Simulation Results

The model predictions of SO_2 oxidation rates are presented in Figure 5. Each plot in Figure 5 shows the SO_2 oxidation rate in ambient air and in plumes emitted at 6:00 a.m., 11:00 a.m., and 3:00 p.m., for a particular set of solar intensity and plume dispersion conditions. The plume oxidation rates were calculated using "net-plume" SO_2 and sulfate concentrations (i.e., average plume concentrations minus ambient concentrations), in the same manner that quasi-first-order transformation rates are typically calculated from field experiment data for plumes.

The dependence of the predicted SO_2 oxidation rates on solar radiation intensity is pronounced. The diurnal variations of ambient SO_2 oxidation rates paralleled the variation of solar intensity, although they were somewhat skewed. A 50 percent reduction in solar intensity, as simulated for the clear- and cloudy-sky conditions, resulted in a somewhat greater decrease in the ambient SO_2 oxidation rates. According to modeling estimates, the primary contribution to SO_2 oxidation comes from the SO_2-HO reaction. The HO concentration, while being dependent on solar intensity, is also affected by the concentration of other species which are depleted as the irradiation period approaches the end of the day.

For the particular set of ambient conditions chosen, the plume SO_2 oxidation rates are bound by the ambient rates. As shown later, certain HC-NO_x conditions for the ambient air can, in theory, reverse that trend. Plume SO_2 oxidation rates show a distinct dependence on solar intensity; the rates are lowest near dawn and dusk, and they are significantly lower in the simulations of cloud-sky versus clear-sky conditions.

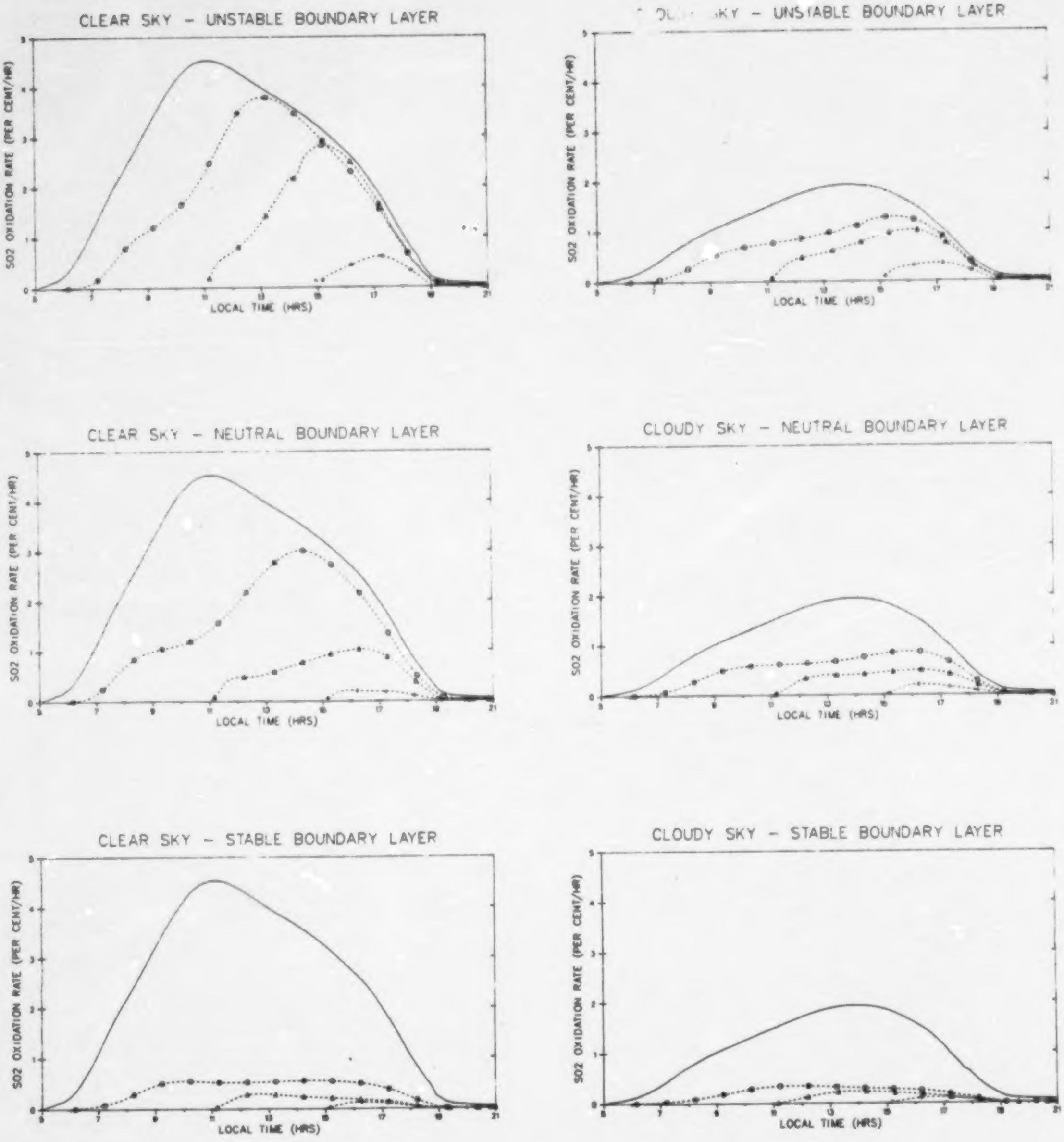

Figure 5. SO_2 Oxidation Rates Simulated by Kinetic Modeling. The solid curve in each plot is the SO_2 oxidation rate in ambient air. The dashed curves are the net SO_2 oxidation rates predicted for power plant plumes emitted at 6:00 a.m., 11:00 a.m., and 3:00 p.m.

The plume SO_2 oxidation rates are also predicted to be sensitive to the plume dispersion rate. Several hours are usually required after emission before the oxidation rate in the plume reaches the ambient rate, and this induction period is lengthened by slower plume dispersion. Free radical concentrations in the plume are depressed below ambient levels during this initial period, until plume NO concentrations are eventually reduced by dispersion and by reaction with ambient ozone. The induction period is also lengthened by lower solar radiation because of the resulting lower ambient ozone levels.

The relative importance of solar intensity versus dispersion rate to SO_2 oxidation rates is difficult to assess. For example, in comparing the simulations for unstable and neutral conditions, the relative reduction in SO_2 oxidation rates depends both on emission times and radiation conditions. The oxidation rates for the stable conditions are much lower than for the other cases; however, the stable plume dispersion rates are unrealistically slow.

Overall, the simulations suggest that maximum SO_2 oxidation rates in plumes should be reached near noon, but that plumes must also have dispersed several hours before high oxidation rates can be attained.

f. Comparison of Model Predictions with Project MISTT Field Data

A primary objective of this work was to provide a theoretical basis for interpretation of the plume transformation data from EPA's Project MISTT (Midwest Interstate Sulfur Transformation and Transport). As part of that project, extensive measurements were made in the plume of the coal-fired Labadie power plant during summer months and under non-stagnant, non-precipitating conditions. Analyses of plume SO_2 transformation data from the project have been presented by Gillani et al.(45) and Husar et al.(46). A summary of the project's SO_2 transformation results appears here as Figure 6, reproduced from Husar et al. A main conclusion of the Project MISTT investigators was that SO_2 conversion rates in the Labadie plume depended primarily on the time of day; high conversion rates ($>0.5\%\ hr^{-1}$) occurred only during daylight hours and low conversion rates ($<0.5\%\ hr^{-1}$) were limited to nighttime periods. And, as indicated in Figure 6, highest SO_2 oxidation rates were observed during the period of 11:00 - 15:00 hours.

The simulations presented here were tailored to the MISTT data. As indicated before, plume emission rates approximated those from the Labadie plant, and solar intensity and ambient pollutant levels appropriate for the St. Louis area in summer were used. The simulation results for the clear sky, unstable cases are most appropriate for comparison purposes, and as noted earlier, boundary layer stability was varied diurnally in the unstable cases.

Comparisons of these results (Figure 5, upper left panel) with the data in Figure 6 of Husar et al., suggests good qualitative and even quantitative agreement. In both cases, significant SO_2 oxidation is limited to daylight hours and the highest oxidation rates occur near midday. It should be noted that the SO_2 oxidation rates predicted in our simulations are instantaneous rates, while the MISTT results are presented in terms of average SO_2 conversion rates from emission time to sampling time. If our simulation results were averaged in a similar fashion, the diurnal variations remain, but the simulated rates would be lower in magnitude than the MISTT results. Considering the uncertainties in the kinetic mechanism this is not distressing; the qualitative agreement is the main consideration.

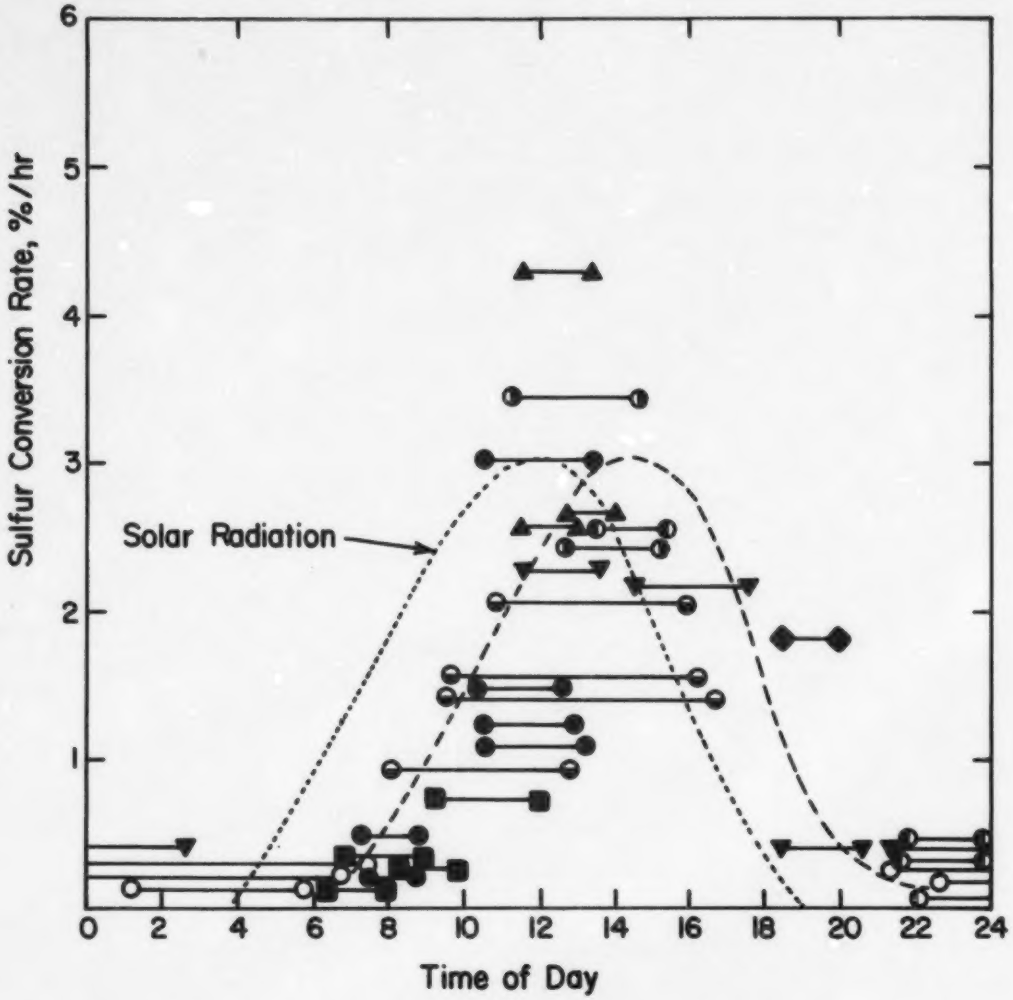

Figure 6. SO_2 Oxidation Rates Composited from 9 Sampling Missions of the Labadie Power Plant in St. Louis Project MISTT, Husar et al.(47). This figure was reproduced with permission from the authors. Horizontal bars represent the plume sampling periods.

g. Hydrocarbon and Nitrogen Oxides Effects

In the simulations described above, a HC/NO_X ratio (ppbC/ppbV) of 6.4 was chosen to represent ambient conditions for St. Louis. Under those conditions, the model predicted that plume O_3 levels did not exceed ambient O_3 concentrations and the rate of SO_2 oxidation in the plume did not exceed that for the ambient air. The MISTT investigators showed, however, that excess O_3 was frequently observed in the Labidie plume(48).

A previous report on this subject suggested that the HC/NO_X ratio in ambient air is key to the development of excess ozone in power plant plumes(49). Therefore, it is very likely that the HC-NO_X conditions chosen for the previous simulations were not entirely appropriate for St. Louis and that higher HC/NO_X ratios may have prevailed. To investigate this possibility, additional plume simulations with this model were conducted with various concentrations of HC and NO_X having HC/NO_X ratios > 8/1.

The theoretical effects of the hydrocarbon and NO_X conditions on SO_2 oxidation rates and O_3 concentrations for ambient air and power plant plumes are summarized in Table 40.

Simulation No. zero represents the HC-NO_X conditions used in the previous simulations of St. Louis air when other set conditions were: full sun, unstable boundary layer and 11:00 a.m. release of emissions. The remaining simulations in Table 40 represent different HC-NO_X conditions for ambient air. In each case, the model predicts the development of excess O_3 in the plumes.

In general, the higher HC/NO_X ratios resulted in higher estimates for the rates of oxidation in ambient air and in the plume. These higher rates appear to be similar to the rates observed in the MISTT study. The higher HC/NO_X ratios also caused the SO_2 oxidation rates in the plume to reach maximum values sooner (2-3 hrs.). That also improves on the model's agreement with the field data.

In some cases (simulation nos. 3-6, Table 40), the SO_2 oxidation rate in the plume was predicted to exceed that in ambient air. A similar trend was found in an analyses of plume data in the Lake Michigan area(49).

TABLE 40. EFFECTS OF AMBIENT HC AND NO_x ON PLUME TRANSFORMATIONS TO YIELD O_3 AND SULFATE

Simulation No.	Ambient NMHC* (ppbC)	Ambient NMHC/NO_x (ppbC/ppbv)	Ambient O_3-Max (ppb)	Plume O_3-Max (ppb)	Plume O_3-Excess (ppb)	Ambient R_{SO_2}-Max (%/hr)	Plume R_{SO_2}-Max (%/hr)
0	160	6.4	108	108	0	4.5	2.7
1	640	25.6	234	246	12	7.4	6.9
2	640	12.8	188	210	22	6.7	6.1
3	320	25.6	154	140	14	5.3	5.8
4	320	51.2	112	128	16	5.1	6.1
5	160	25.6	90	82	8	4.0	5.2
6	160	51.2	77	66	11	3.7	5.7

---

*For modeling purposes, the average relationship of 4 carbon atoms per NMHC molecule was assumed.

REFERENCES

(1) Pierson, W.R., W.W. Brachaczek, T.J. Truex, J.W. Butler and T.J. Kornishi. Ambient Sulfate Meausrements on Allegheny Mountain and the Question of Atmospheric Sulfate in the Northeastern United States. Accepted for publication, Annals of the N.Y. Academy of Sciences, 1979.

(2) Friedlander, S.K. A Review of the Dynamics of Sulfate Containing Aerosols. Atmospheric Environ., 12, 187, 1978.

(3) Middleton, P. and C.S. Kiang. Experimental and Theoretical Examination of the Formation and Sulfuric Acid Particles. Atmospheric Environ., 12, 179, 1978.

(4) Kiang, C.S. and P. Middleton. Formation of Secondary Sulfuric Acid Aerosols in Urban Atmosphere. Geophy. Res. Letters, 4, 17, 1977.

(5) Bufalini, M. Oxidation of Sulfur Dioxide in Polluted Atmosphere - A Review. Environ. Sci., Technol., 5, 685, 1971.

(6) Sander, S.P. and J.H. Seinfeld. Chemical Kinetics of Homogeneous Atmospheric Oxidation of Sulfur Dioxide. Environ. Sci. Technol.,10, 1114, 1976.

(7) Calvert, J.G., F. Su, J.W. Bottenheim and O.P. Strausz. Mechanism of the Homogeneous Oxidation of Sulfur Dioxide in the Troposphere. Atmospheric Environ., 12, 197, 1978.

(8) Eggleton, A.E.J. and R.A. Cox. Homogeneous Oxidation of Sulfur Compounds in the Atmosphere. Atmospheric Environ., 12, 227, 1978.

(9) Kok, G.L., T.P. Holler, M.B. Lopez, H.A. Nachtrieb and M. Yuan. Chemiluminescent Method for Determination of Hydrogen Peroxide in the Ambient Atmosphere. Environ. Sci. Technol., 12, 1072, 1978.

(10) Chan, W.C., R.J. Nordstrom, J.G. Calvert and J.H. Shaw. Kinetic Study of HONO Formation and Decay Reactions in Gaseous Mixtures of HONO, NO, NO_2, H_2O and N_2. Environ. Sci. Technol., 10, 674, 1976.

(11) Durham, J.L., W.E. Wilson and B.E. Bailey. Application of an SO_2-denuder for Continuous Measurement of Sulfur in Submicrometric Aerosols. Atmospheric Environ., 12, 883, 1978.

(12a) Hampson, R.F. and D. Garvin. Reaction Rate and Photochemical Data for Atmospheric Chemistry - 1977. NBS Special Publication 513, National Bureau of Standards, Washington, DC, 1978.

(12b) Workshop on Chemical Kinetic Data Needs for Modeling the Lower Troposphere, Environmental Protection Agency and National Bureau of Standards, Reston, VA, 1978.

(13) Cox, R.A., R.G. Derwent and P.M. Holt. Relative Rate Constants for the Reactions of OH Radicals with H_2, CH_4, CO, NO, and HONO at Atmospheric Pressure and 296 K. J. Chem. Soc., Faraday Trans. I, 72: 2044, 1976.

(14) Cox, R.A., R.G. Derwent and M.R. Williams. Atmospheric Photooxidation Reactions. Rates, Reactivity, and Mechanisms for Reaction of Organic Compounds with Hydroxyl Radicals. Environ. Sci. Technol., 14: 47, 1980.

(15) Castleman, A.W., H.R. Munkelwitz and B. Manowitz. Isotopic Studies of the Sulfur Component of the Stratospheric Sulfur Layer. Tellus, 26: 222, 1974.

(16) Schroeder, W.H. and P. Urone. Isolation and Identification of Nitrosonium Hydrogen Sulfate ($NOHSO_4$) as a Photochemical Reaction Produce in Air Containing Sulfur Dioxide and Nitrogen Dioxide. Environ. Sci. Technol., 12: 545, 1978.

(17) Cox, R.A. The Photolysis of Nitrous Acid in the Presence of Carbon Monoxide and Sulfur Dioxide. J. Photochem., 3: 291, 1974.

(18) Morris, E.D. and H. Niki. The Reaction of Dinitrogen Pentoxide with Water. J. Phys. Chem., 77: 1929, 1973.

(19) Connel, P. and H.S. Johnston. The Thermal Decomposition of N_2O_5 in N_2. Geophys. Res. Lett., 6: 553, 1979.

(20) Payne, W.A., L.J. Stief and D.D. Davis. A Kinetics Study of the Reaction of HO_2 with SO_2 and NO. J. Am. Chem. Soc., 95: 7614, 1973.

(21) Graham, R.A., A.M. Winer, R. Atkinson and J.N. Pitts. Rate Constants for the Reaction of HO_2 with HO_2, SO_2, CO, N_2O, trans-2-Butene and 2,3-Dimethyl-2-butene at 300 K. J. Phys. Chem., 83: 1563, 1979.

(22) Burrows, J.P., D.I. Cliff, G.W. Harris, B.A. Thrush and J.P.T. Wilkinson. Paper presented at the W.M.O. Symposium on the Geophysical Aspects and Consequences of Changes in the Composition of the Stratosphere, Toronto, 1978. See Reference (23).

(23) Sanhueza, E., R. Simonaitis and J. Heiklen. The Reaction of CH_3O_2 with SO_2. Int. J. Chem. Kinet., 11: 907, 1979.

(24) Kan, C.S., R.D. McQuigg, M.R. Whitbeck and J.G. Calvert. Kinetic Flash Spectroscopic Study of the CH_3O_2-CH_3O_2 and CH_3O_2-SO_2 Reactions. Int. J. Chem. Kinet., 11: 921, 1979.

(25) Ross, D.S. Correspondence: Nitrate Formation in Atmospheric Aerosols. Environ. Sci. Technol., 12: 726, 1978.

(26) Stephens, E.R. Hydrocarbons in Polluted Air, Summary Report to the Coordinating Research Council (Project CAPA-5-68), Statewide Air Pollution Research Center at Riverside, CA, 1973.

(27) Miller, D.F. Precursor Effects on SO_2 Oxidation. Atmospheric Environ., 12: 273, 1978.

(28) Carter, W.P.C., A.C. Lloyd, J.L. Sprung and J.N. Pitts. Computer Modeling of Smog Chamber Data: Progress in Validation of a Detailed Mechanism for the Photooxidation of Propene and n-Butane in Photochemical Smog. Int. J. Chem. Kinet., 11: 45, 1979.

(29) Falls, A.H. and J.H. Seinfeld. Continued Development of a Kinetic Mechanism for Photochemical Smog. Environ. Sci. Technol., 12: 1398, 1978.

(30) Hov, O., I.S.A. Isaksen and E. Hesstvedt. Diurnal Variations of Ozone and Other Pollutants in an Urban Area. Atmospheric Environ., 12: 2469, 1978.

(31) Miller, D.F., G.M. Sverdrup and K. Jones. Factors Affecting the Design of Oxidant Control Strategies. Battelle Report to the U.S. Council on Environmental Quality, 1977.

(32) Darnall, K.R., A.C. Lloyd, A.M. Winer, J.N. Pitts. Reactivity Scale for Atmospheric Hydrocarbons Based on Reaction with Hydroxyl Radicals. Environ. Sci. Technol., 10: 692, 1976.

(33) Winer, A.M., K.R. Darnall, R. Atkinson and J.N. Pitts. Smog Chamber Study of the Correlation of Hydroxyl Radical Rate Constants with Ozone Formation. Environ. Sci. Technol., 13: 822, 1979.

(34) Whitten, G.Z. and H. Hogo. Mathematical Modeling of Simulated Photochemical Smog. EPA-600/3-77-011, U.S. Environmental Protection Agency, Research Triangle Park, NC, 1977.

(35) Battelle Quarterly (III) Technical Progress Report to the Electric Power Research Institute, Contract RP 1369-1, Palo Alto, CA, 1979.

(36) Miller, D.F. and A. Levy. Aerosol Formation in Photochemical Smog: The Effects of Humidity and Small Particles. Proceedings of the Third International Clean Air Congress, Düsseldorf, 1973.

(37) Ripperton, L.A. and D. Lillian. The Effect of Water Vapor on Ozone Synthesis in the Photooxidation of α-Pinene. J. Air Poll. Control Assoc., 21: 629, 1971.

(38) Winer, A.M., G.M. Breuer, W.P.L. Carter, K.R. Darnall and J.N. Pitts. Effects of Ultraviolet Spectral Distribution on the Photochemistry of Simulated Polluted Atmospheres. Atmospheric Environ., 13: 989, 1979.

(39) Easter, R.C., D.F. Miller and W.E. Wilson. Kinetic Simulation of the Diurnal Rates of SO_2 Oxidation in a Polluted Atmosphere. Submitted to Atmospheric Environ., 1979.

(40) Ogren, J.A., D.L. Blumenthal, W.H. White, T.W. Tesche, M.A. Yocke, and M.K. Liu. Determination of the Feasibility of Ozone Formation in Power Plant Plumes. Electric Power Research Institute, Report EA-307, Vol. II, by Systems Applications, Inc., and Meteorology Research, Inc., 1976.

(41) Peterson, J.T. Dependence of the NO_2 Photodissociation Rate Constant on Altitude. Atmos. Environ., 11: 689, 1977.

(42) Pasquill, F. The Estimation of Dispersion of Windborne Material. Meteorol. Magazine, 90: 33, 1961.

(43) Easter, R.C., K.M. Business, J.M. Hales, R.N. Lee, D.A. Arbuthnot, D.F. Miller, G.M. Sverdrup, C.W. Spicer, and J.E. Howes, Jr. Plume Conversion Rates in the SURE Region, Electric Power Research Institute, Report, in Review, by Battelle, Pacific Northwest Laboratories, 1979.

(44) Turner, D.B. Workbook of Atmospheric Dispersion Estimates, Office of Air Programs, Publication No. AP-26, 1969.

(45) Gillani, N.V. Project MISTT: Mesoscale Plume Modeling of the Dispersion, Transformation and Ground Removal of SO_2. Atmospheric Environ., 12: 569 1978

(46) Gillani, N.V., R.B. Husar, J.D. Husar, D.E. Patterson, and W.E. Wilson, Jr. Project MISTT: Kinetics of Particulate Sulfur Formation in a Power Plant Plume Out to 300 km. Atmospheric Environ., 12: 589, 1978.

(47) Husar, R.B., D.E. Patterson, J.D. Husar, N.V. Gillani and W.E. Wilson, Jr. Sulfur Budget of a Power Plant Plume. Atmospheric Environ., 12: 549, 1978.

(48) Gillani, N.V. and W.E. Wilson, Jr. Formation and Transport of Ozone and Aerosols in Power Plant Plumes. Accepted for publication, Annals of the N.Y Academy of Sciences, 1979.

(49) Miller, D.F. and A.J. Alkezweeny. Aerosol Formation in Urban Plumes over Lake Michigan. Accepted for publication, Annals of the N.Y. Academy of Sciences, 1979.

APPENDIX A

SMOG PROFILES OF EXPERIMENTS CONDUCTED WITH INORGANIC SMOG SYSTEM

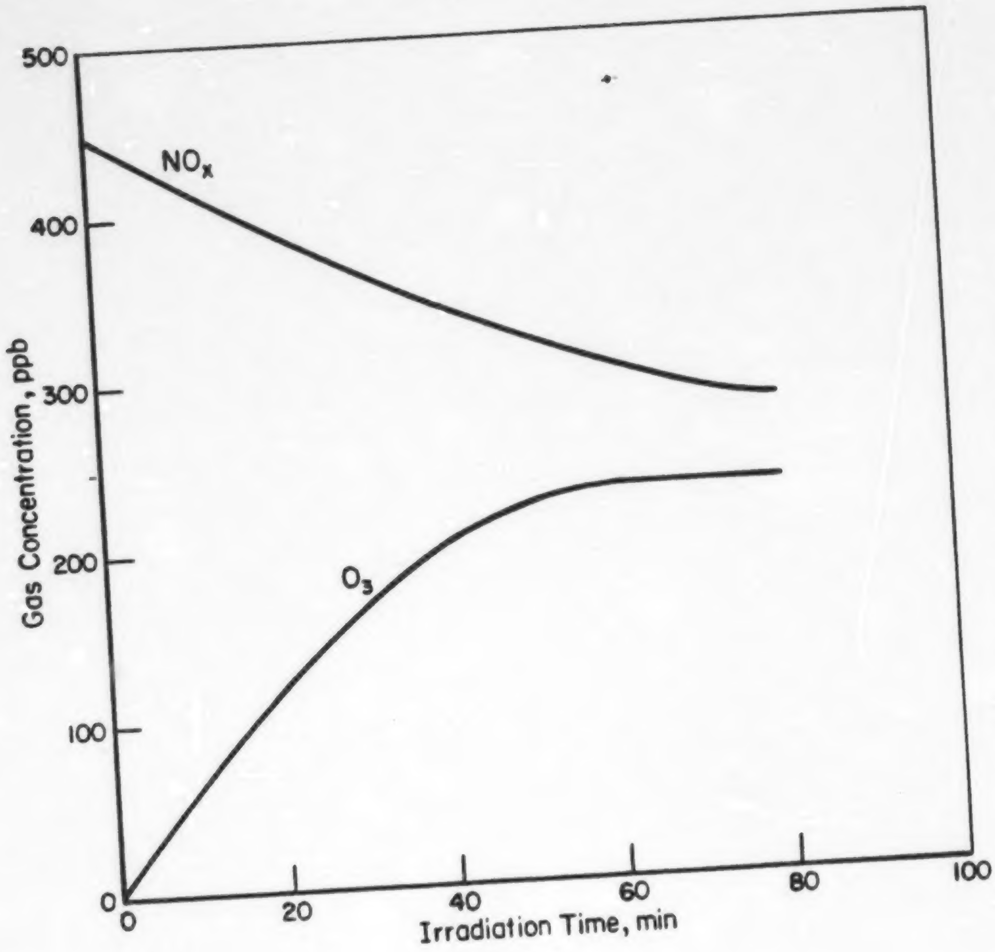

Figure A-1. Experiment 11-7-77

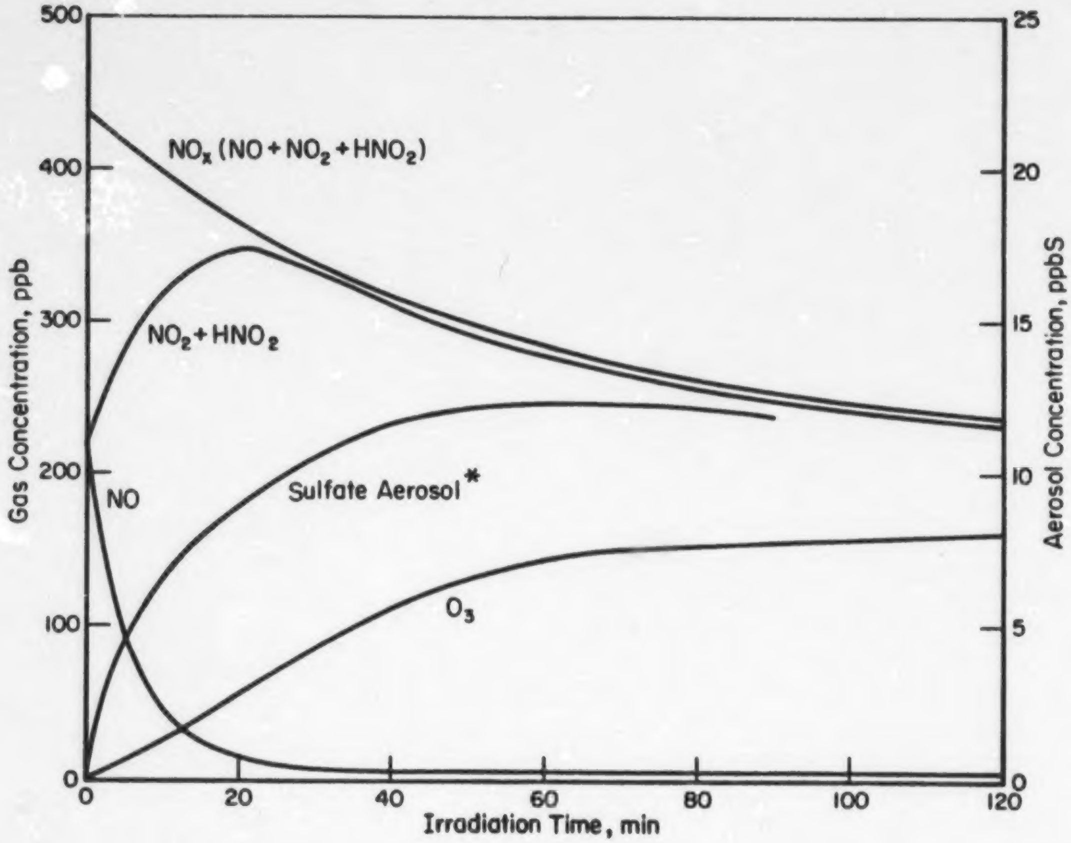

Figure A-2. Experiment 11-9-77.
(*) Sulfate Inferred from EAA.

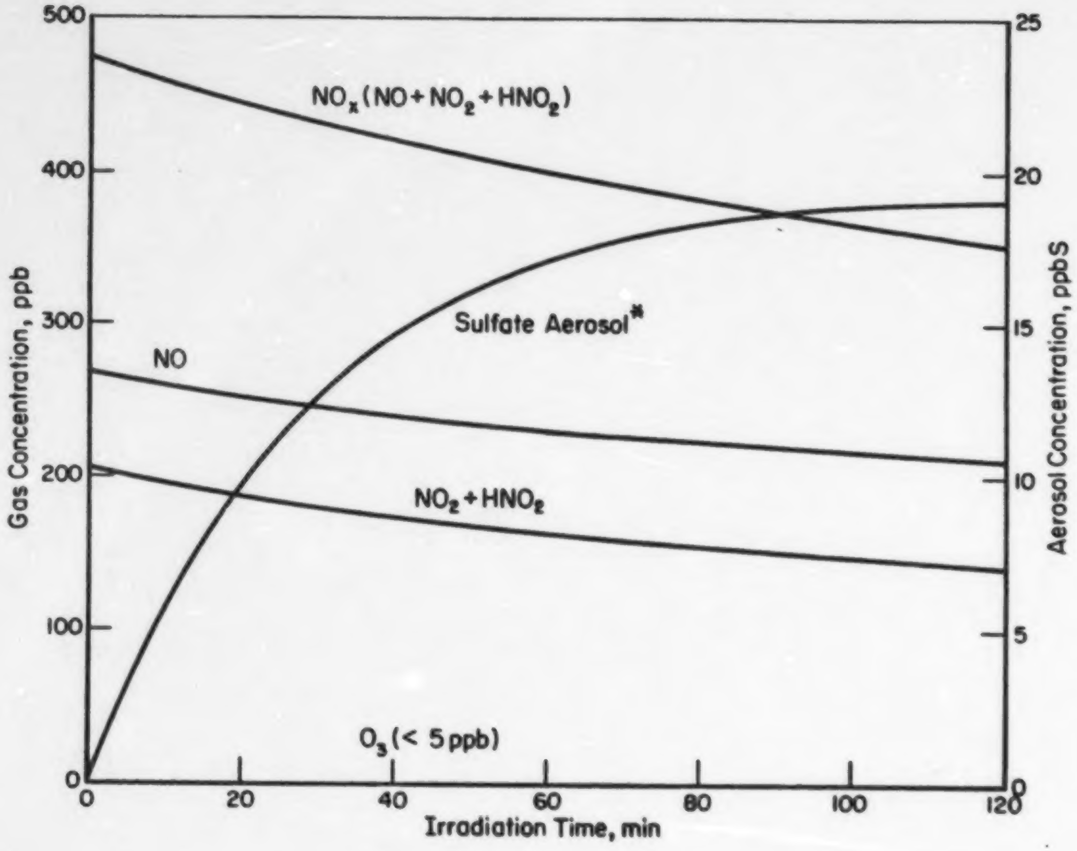

Figure A-3. Experiment 11-10-77.
(*) Sulfate Inferred from EAA.

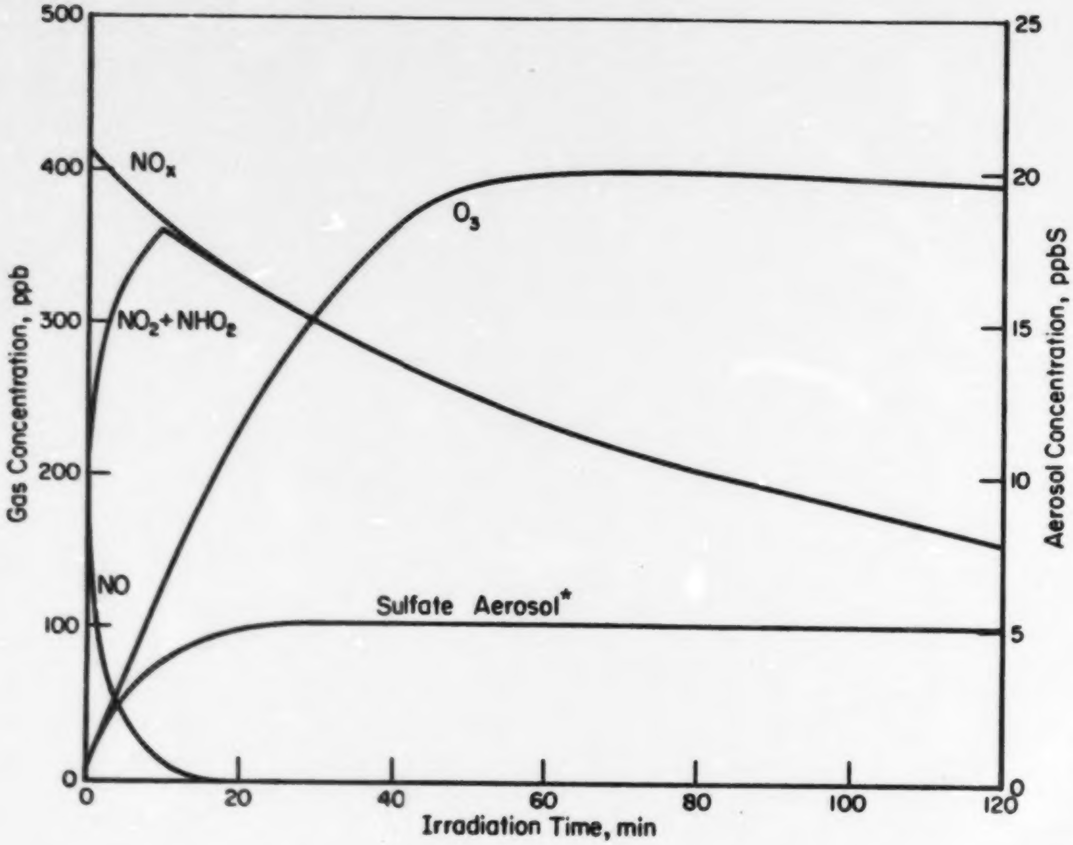

Figure A-4. Experiment 11-11-77.
(*) Sulfate Inferred from EAA.

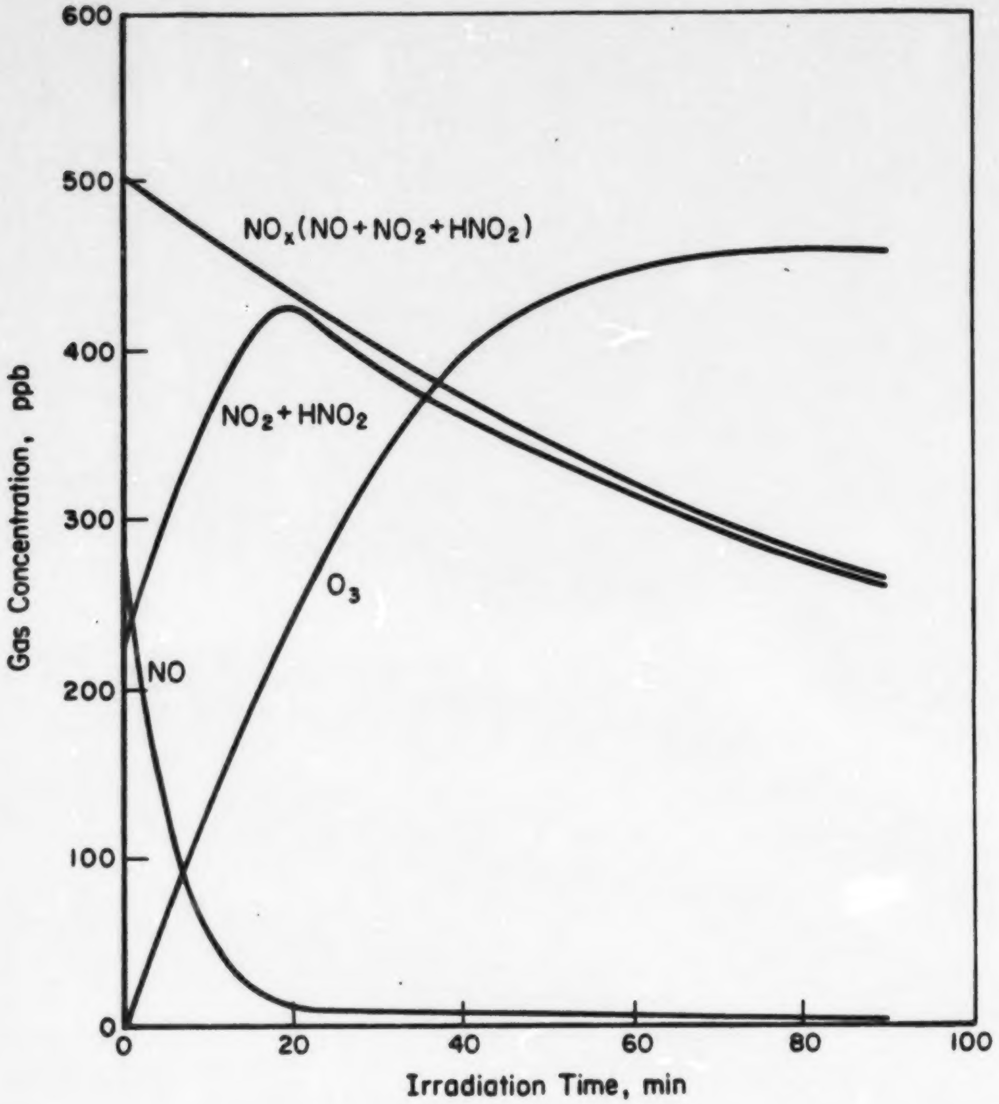

Figure A-5. Experiment 12-13-77

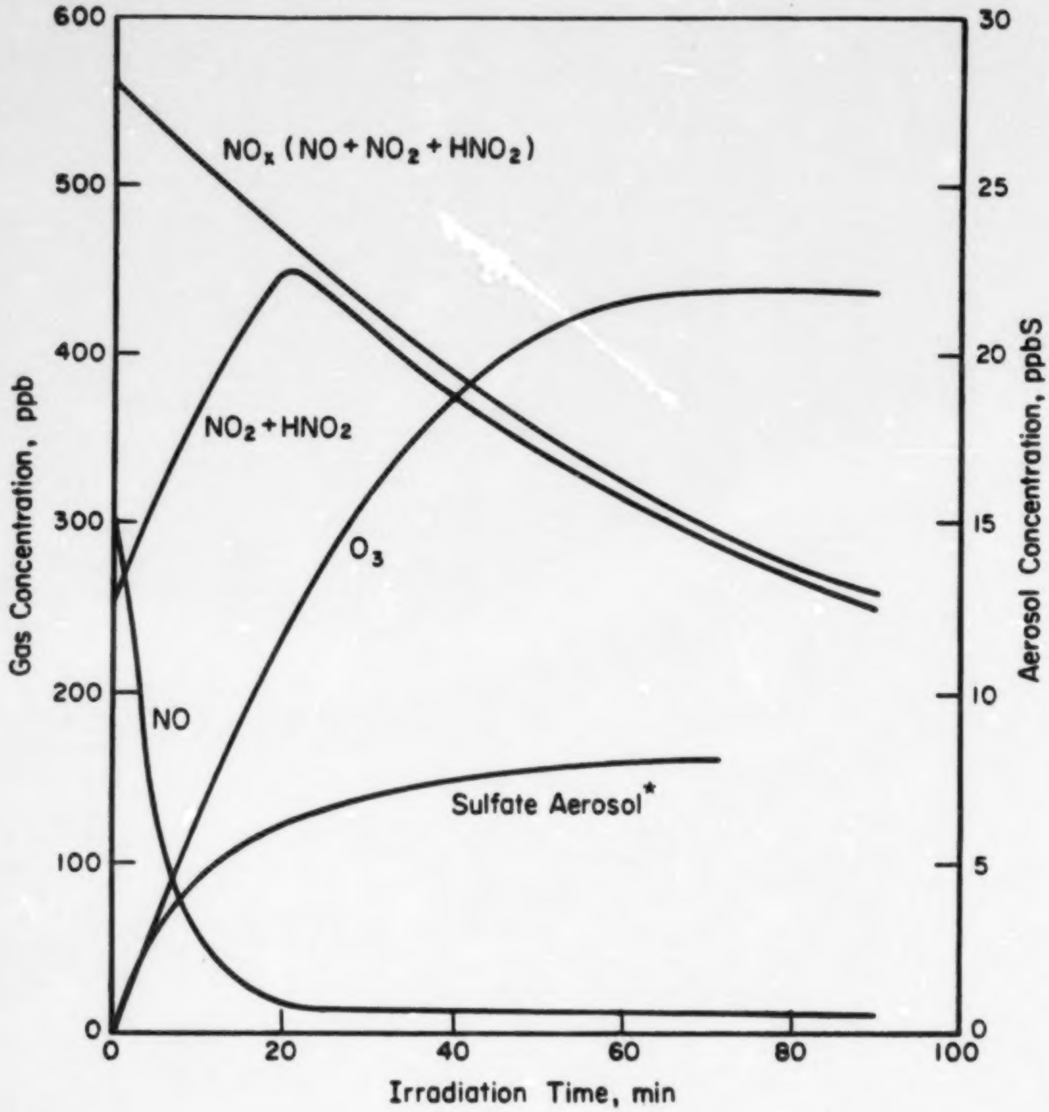

Figure A-6. Experiment 12-14-77.
(*) Sulfate Inferred from EAA.

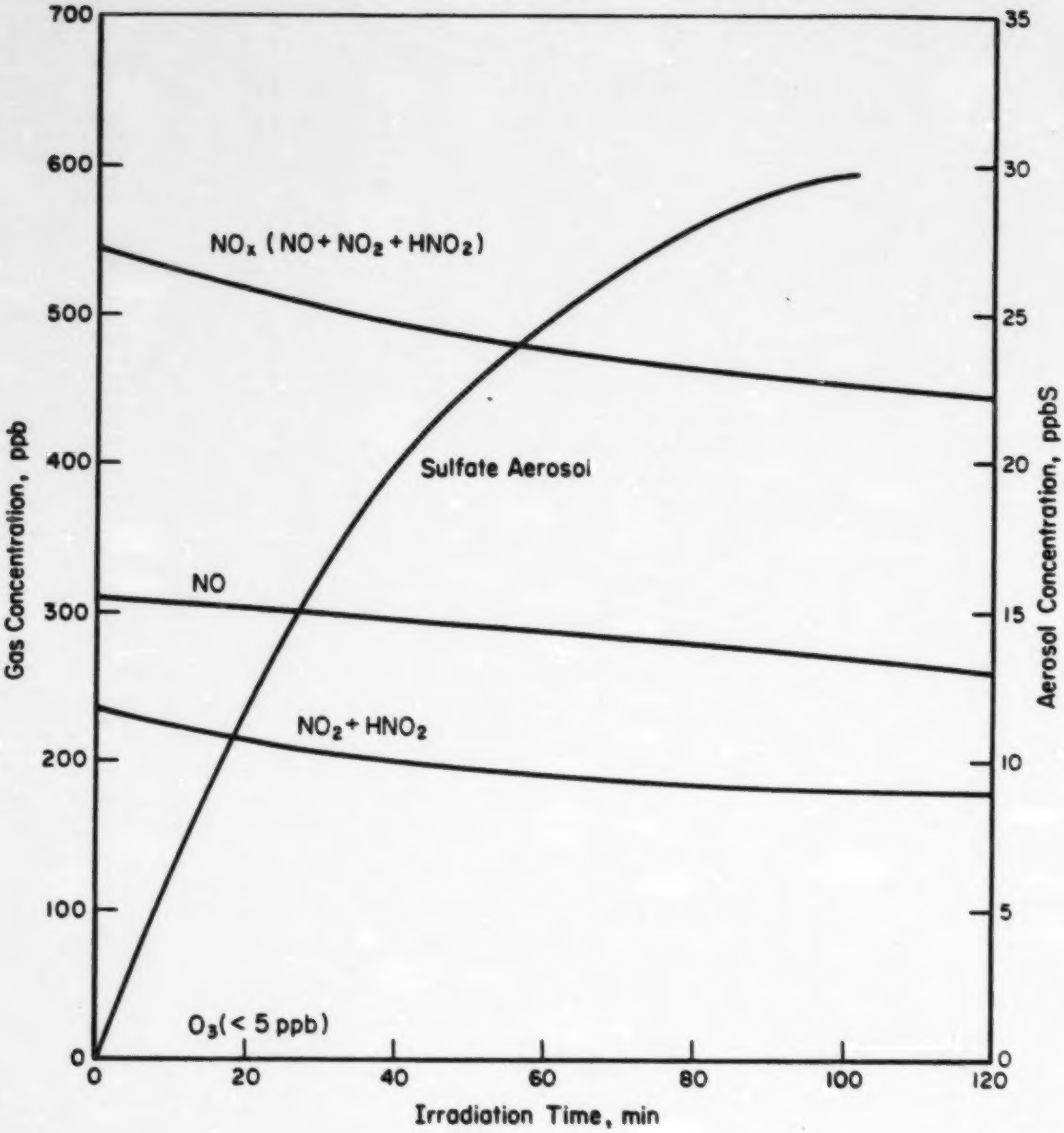

Figure A-7. Experiment 1-9-78.

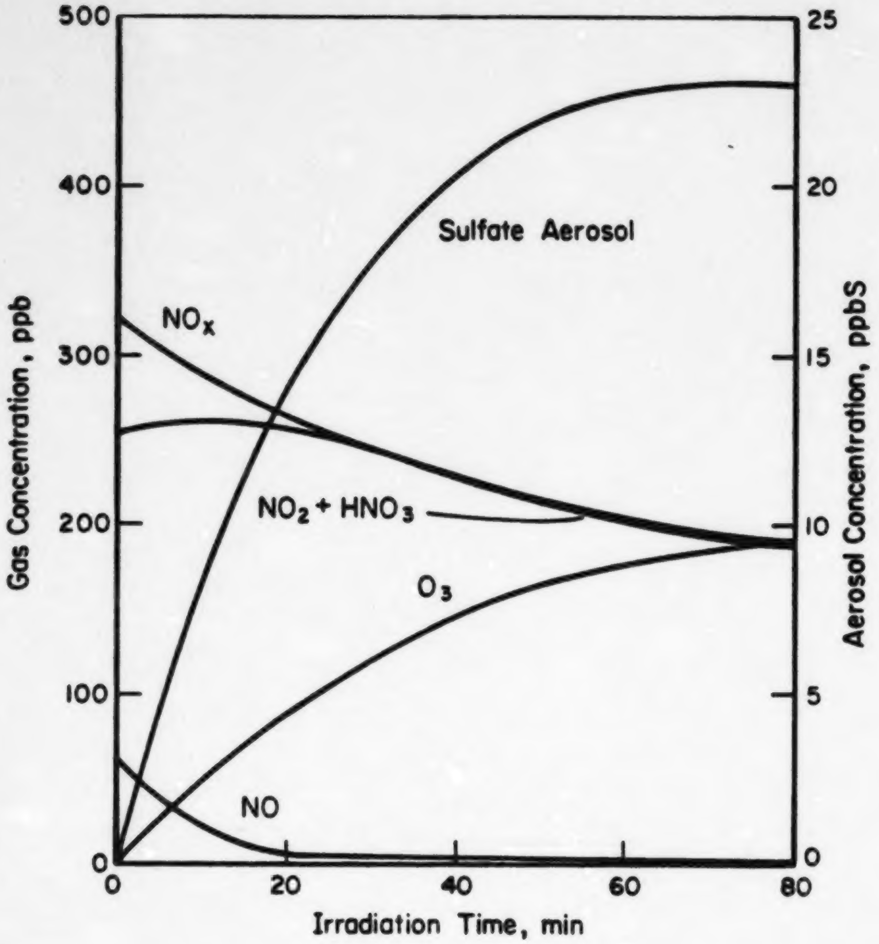

Figure A-8. Experiment 1-10-78.

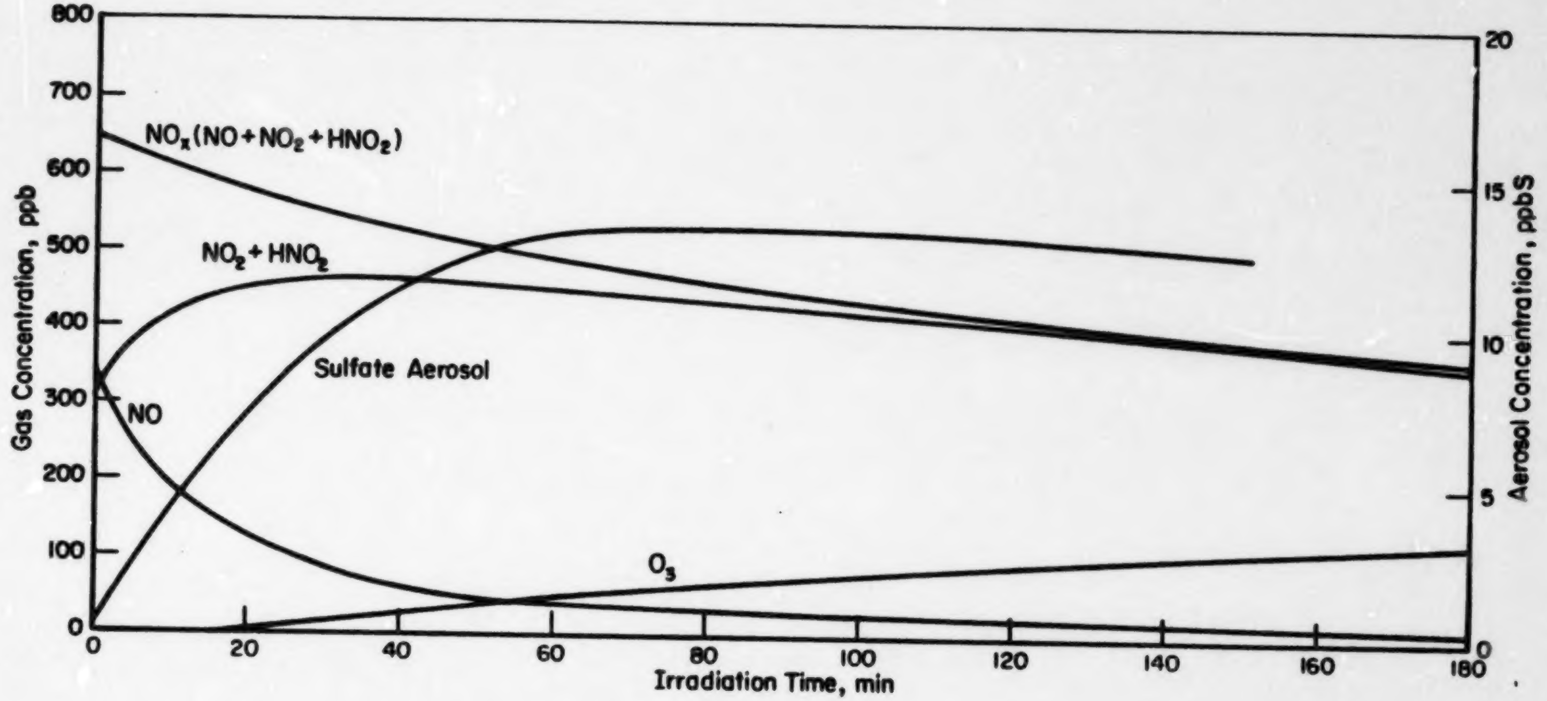

Figure A-9. Experiment 1-11-78

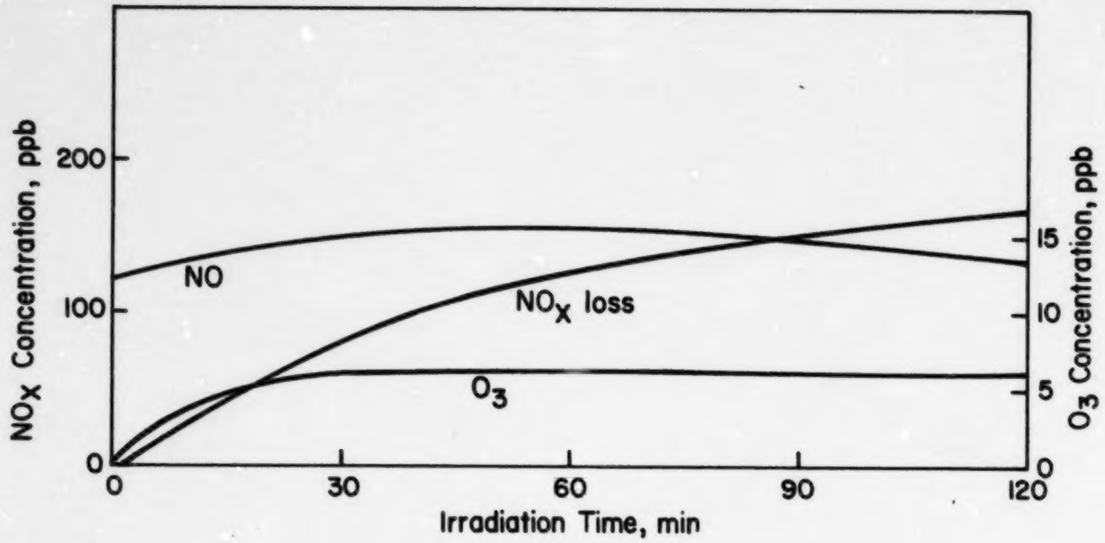

Figure A-10. Experiment 6-5-78.

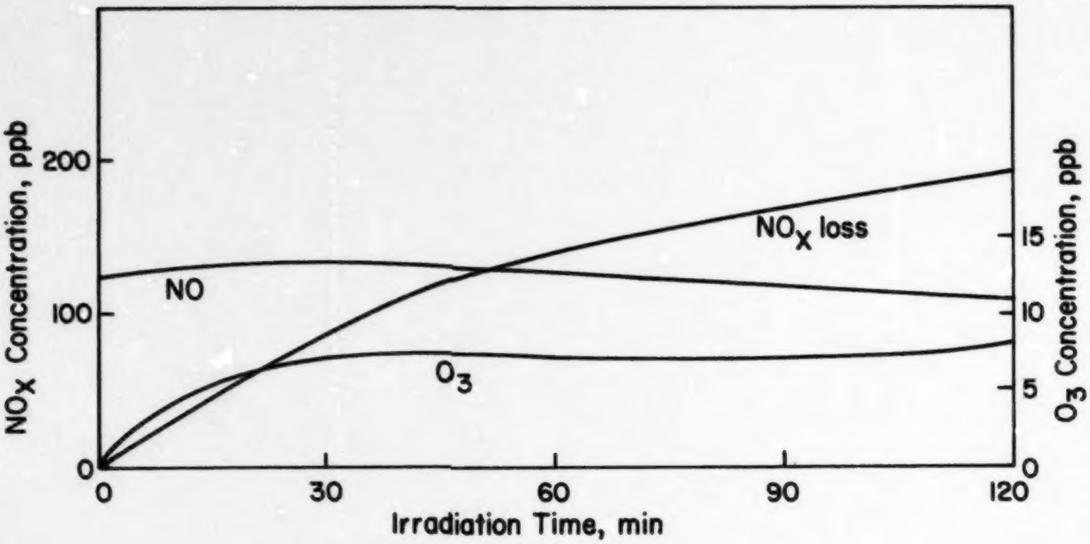

Figure A-11. Experiment 6-6-78.

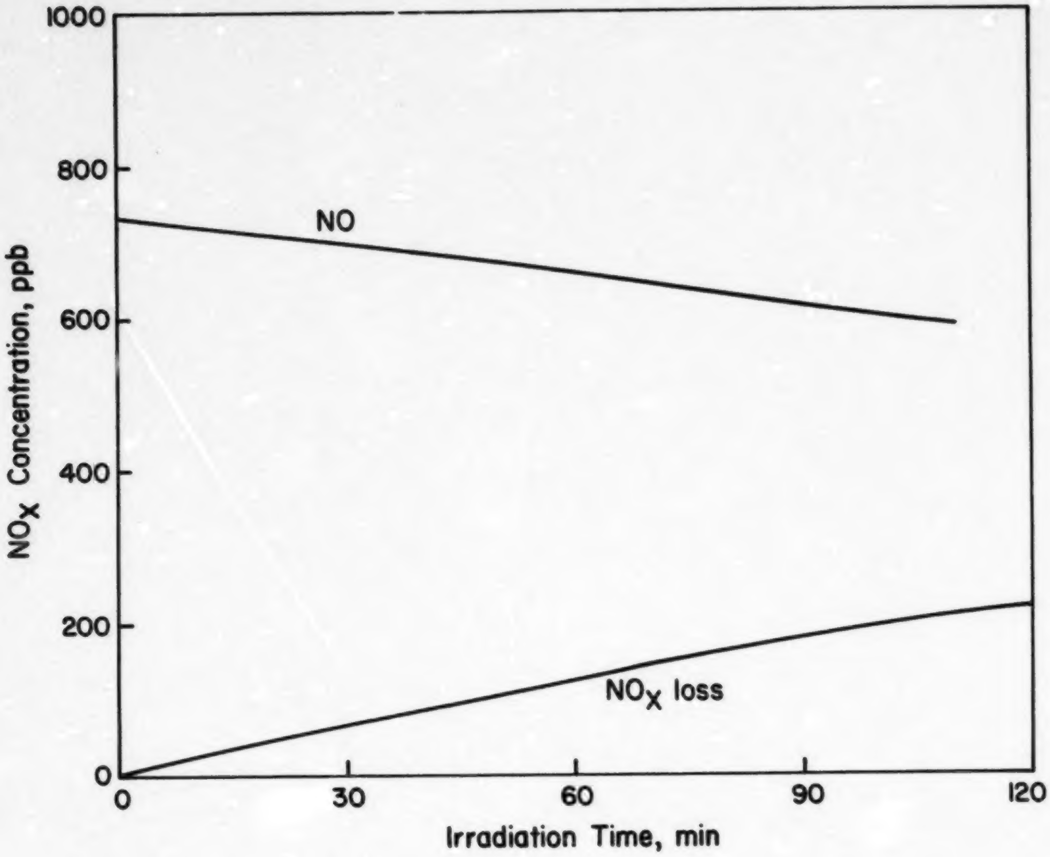

Figure A-12. Experiment 6-8-78.

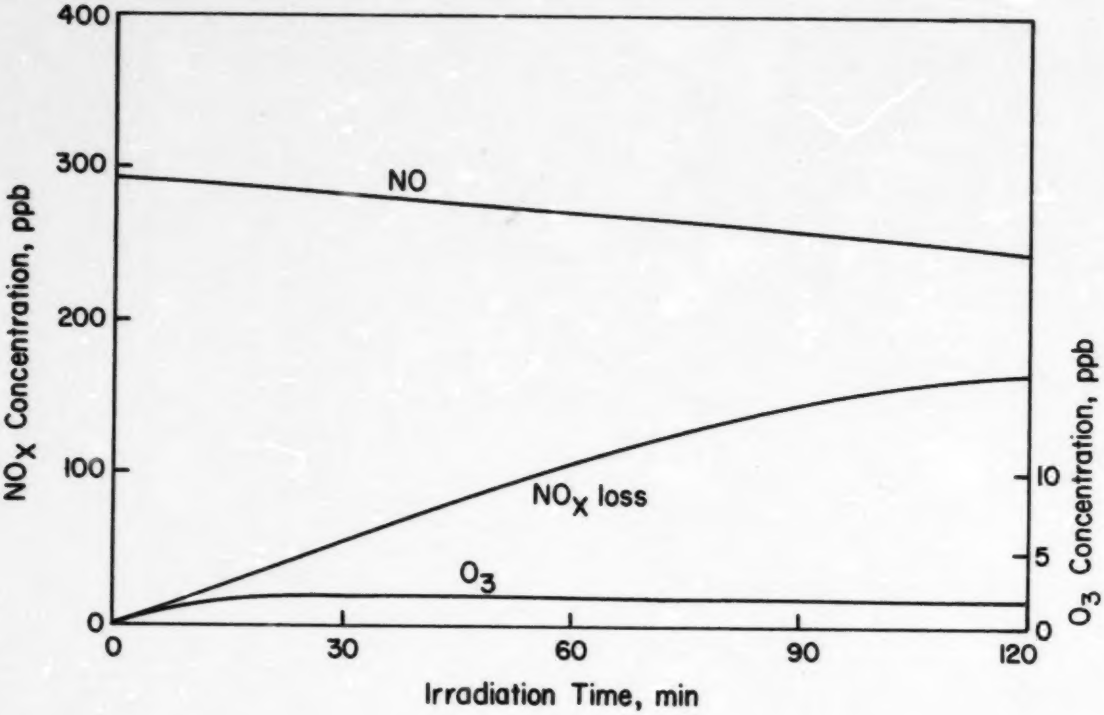

Figure A-13. Experiment 6-14-78

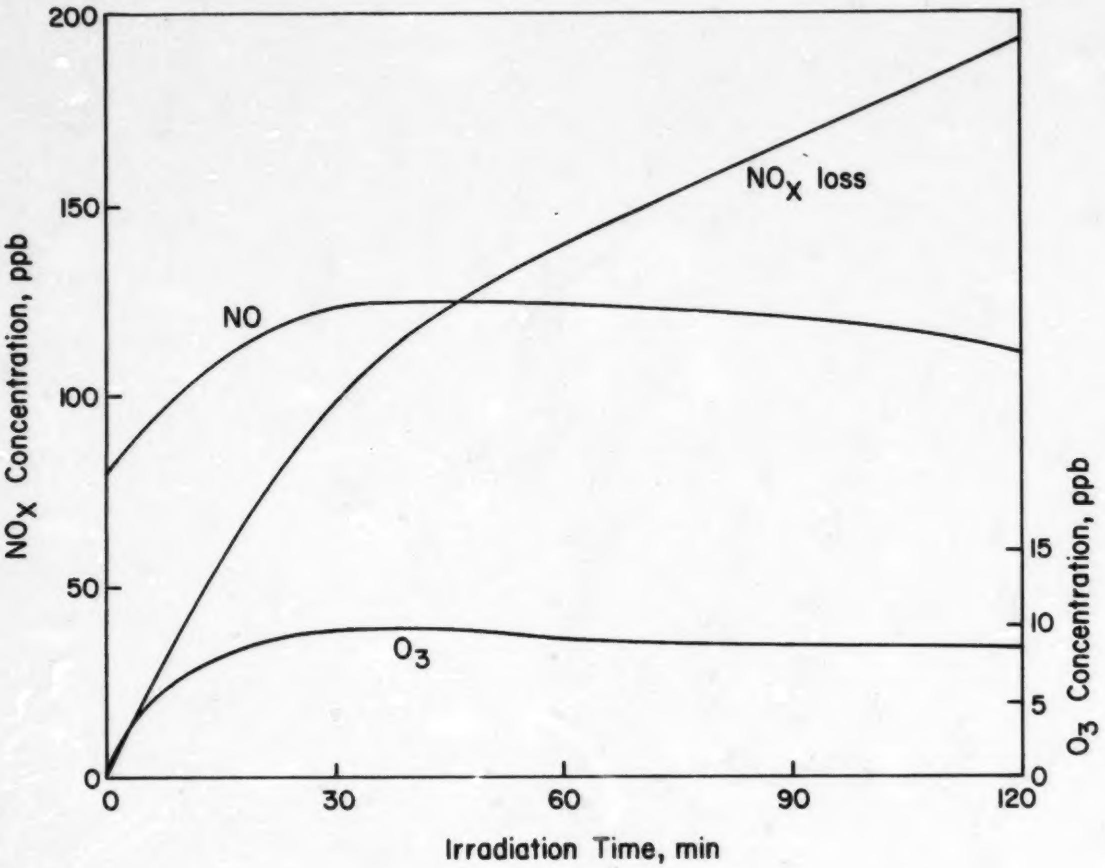

Figure A-14. Experiment 6-15-78

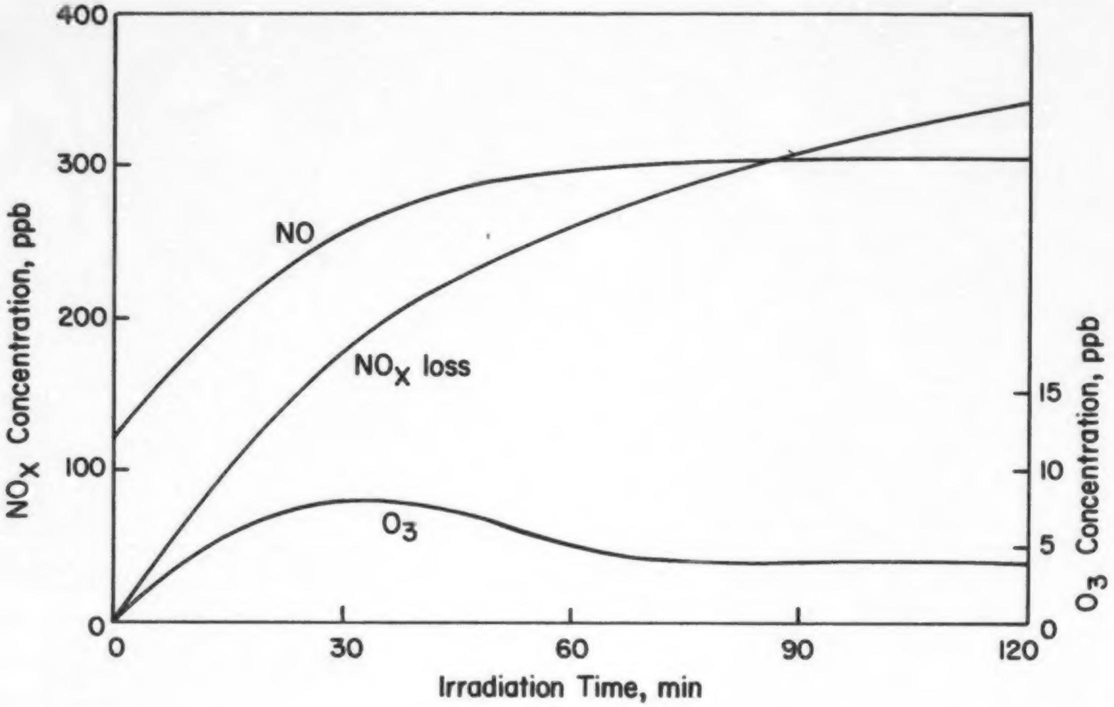

Figure A-15. Experiment 6-16-78.

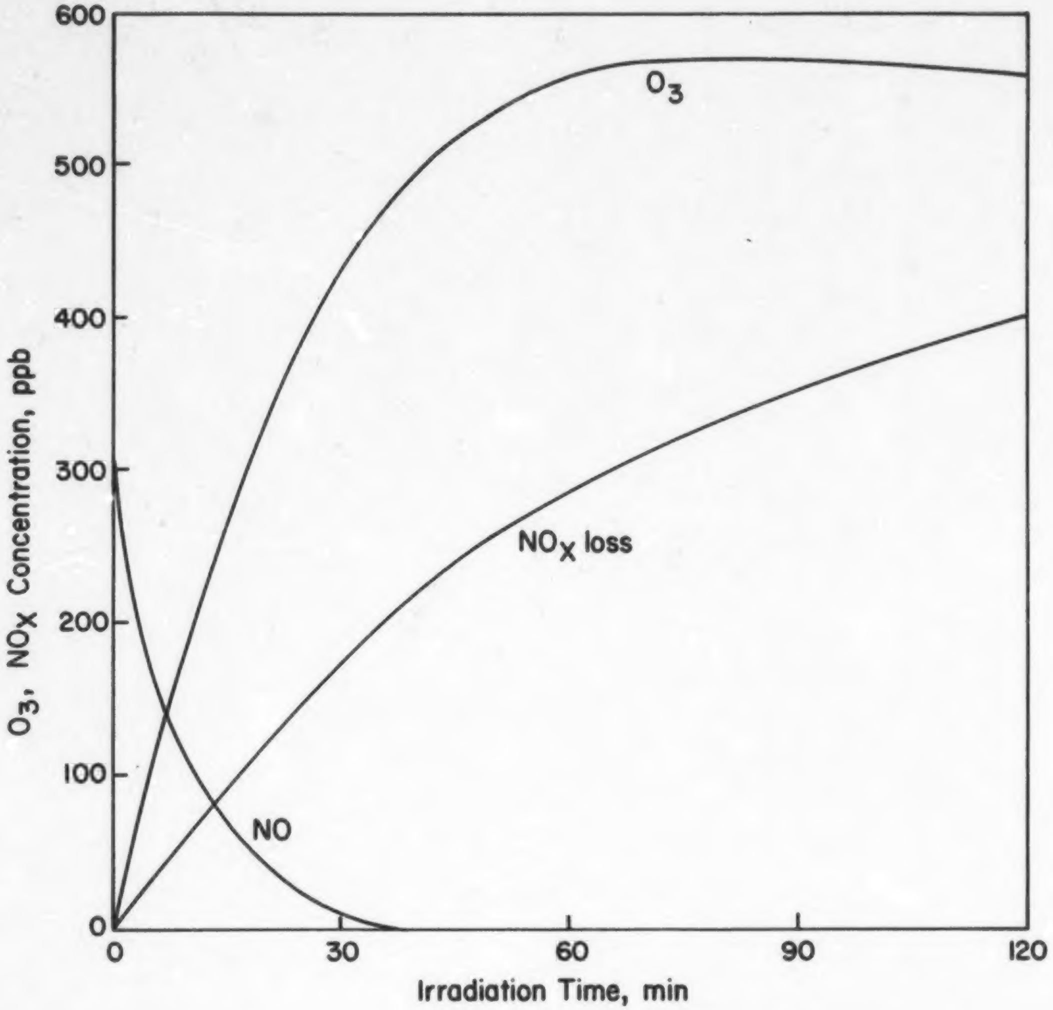

Figure A-16. Experiment 6-23-78.

APPENDIX B
HYDROCARBON AND PAN DATA

TABLE - B-1

Hydrocarbon and PAN Data for Experiment 1

HYDROCARBON, ppmC	Irradiation Time, min.							
	0	60	120	180	240	300	360	420
Ethane	.19	.19		.17		.16		.14
Ethylene	.37	.31		.21		.14		.10
Propane	.16	.15		.13		.12		.11
Acetylene	.29	.28		.25		.22		.20
Iso-Butane	.12	.11		.10		.08		.08
N-Butane	.50	.47		.39		.35		.31
Propylene	.11	.07		0		0		0
Trans-2-Butene	.10	0		0		0		0
2-Methyl Butane	.40	.40		.33		.29		.22
N-Penetane	.20	.20		.16		.14		.11
2-Methyl 2-Butene	.05	0		0		0		0
2-Methyl Pentane	.31	.31		.24		.20		.05
Benzene	.17	.21		.19		.18		.14
Toluene	.49	.49		.38		.31		.26
m-Xylene	.60	.52		.25		.15		.08
P-Ethyl Toluene	.19	.21		.12		.08		.04
1,2,4 - Trimethyl Benzene	.09	.09		.03		.01		0
PAN (ppb v/v)	0	17	61	102	133	146	147	140
Hydrocarbons - Total	4.32	4.01		2.95		2.43		1.80

TABLE - B-2
Hydrocarbon and PAN Data for Experiment 2

HYDROCARBON, ppmC	Irradiation Time, min.							
	0	60	120	180	240	300	360	420
Ethane	.21	.20		.18				
Ethylene	.38	.31		.03				
Propane	.16	.15		.14				
Acetylene	.29	.27		.25		.22		.20
Iso-Butane	.11	.10		.09		.08		.07
N-Butane	.49	.46		.39		.34		.30
Propylene	.11	.07		0		0		0
Trans-2-Butene	.13	0		0		0		
2-Methyl Butane	.44	.36		.33		.22		
N-Penetane	.22	.18		.17		.11		
2-Methyl 2-Butene	.07	0		0		0		
2-Methyl Pentane	.36	.29		.26		.16		
Benzene	.22	.19		.20		.17		
Toluene	.56	.48		.42		.25		
m-Xylene	.72	.46		.31		.13		
P-Ethyl Toluene	.25	.18		.15		.07		
1,2,4 - Trimethyl Benzene	.12	.07		.04		.01		
PAN (ppb v/v)	0	22.2	52.1	82	110.4	141.2	163.9	177.4
Hydrocarbons - Total	4.84	3.77		3.16		2.19		

TABLE - B-3
Hydrocarbon and PAN Data for Experiment 3

HYDROCARBON, ppmC	Irradiation Time, min.							
	0	60	120	180	240	300	360	420
Ethane	.22	.21		.19		.17		.16
Ethylene	.37	.32		.21		.15		.10
Propane	.16	.15		.13		.12		.11
Acetylene	.29	.27		.24		.22		.20
Iso-Butane	.11	.10		.10		.08		.08
N-Butane	.47	.45		.38		.33		.29
Propylene	.10	.07		0		0		0
Trans-2-Butene	.11	0		0		0		0
2-Methyl Butane	.42	.37		.31		.27		.20
N-Penetane	.21	.19		.15		.13		.12
2-Methyl 2-Butene	.06	0		0		0		0
2-Methyl Pentane	.35	.31		.25		.21		.09
Benzene	.23	.20		.20		.17		.16
Toluene	.57	.50		.40		.32		.28
m-Xylene	.76	.52		.28		.16		.10
P-Ethyl Toluene	.29	.22		.13		.09		.06
1,2,4 - Trimethyl Benzene	.14	.08		.03		.01		.01
PAN (ppb v/v)	0	22.4	66.3	104.6	133.4	148.4	150.7	146.4
Hydrocarbons - Total	4.86	3.96		3.19		2.43		1.96

TABLE - B-4

Hydrocarbon and PAN Data for Experiment 4

HYDROCARBON, ppmC	Irradiation Time, min.							
	0	60	120	180	240	300	360	420
Ethane	.20	.20		.18		.17	.16	.15
Ethylene	.37	.31		.21		.14	.12	.9
Propane	.15	.15		.13		.12	.11	.10
Acetylene	.28	.27		.24		.22	.22	.20
Iso-Butane	.11	.11		.10		.08	.08	.07
N-Butane	.46	.43		.38		.33	.30	.28
Propylene	.10	.07		0		0	0	0
Trans-2-Butene	.11	0		0		0	0	0
2-Methyl Butane	.41	.37		.31		.27	.24	.22
N-Penetane	.20	.17		.15		.12	.11	.10
2-Methyl 2-Butene	.05	0		0		0	0	0
2-Methyl Pentane	.34	.31		.24		.21	.19	.17
Benzene	.22	.21		.19		.17	.16	.16
Toluene	.57	.49		.40		.31	.28	.25
m-Xylene	.75	.51		.26		.14	.11	.07
P-Ethyl Toluene	.28	.23		.13		.08	.07	.05
1,2,4 - Trimethyl Benzene	.14	.09		.03		.01	0	0
PAN (ppb v/v)	0	24.6	75.3	117.9	152.6	167.8	173.1	178.9
Hydrocarbons - Total	4.74	3.92		2.95		2.37	2.15	1.91

TABLE - B-5
Hydrocarbon and PAN Data for Experiment 5

HYDROCARBON, ppmC	Irradiation Time, min.							
	0	60	120	180	240	300	360	420
Ethane	.22	.22		.20		.18	.18	
Ethylene	.37	.32		.22		.15	.13	
Propane	.17	.15		.14		.13	.12	
Acetylene	.29	.28		.25		.23	.22	
Iso-Butane	.11	.10		.09		.09	.08	
N-Butane	.47	.43		.38		.34	.32	
Propylene	.10	.06		0		0	0	
Trans-2-Butene	.11	0		0		0	0	
2-Methyl Butane	.41	.37		.31		.28	.26	
N-Penetane	.21	.18		.15		.14	.12	
2-Methyl 2-Butene	.06	0		0		0	0	
2-Methyl Pentane	.35	.31		.25		.22	.21	
Benzene	.22	.25		.19		.18	.17	
Toluene	.56	.50		.41		.35	.32	
m-Xylene	.75	.51		.27		.18	.15	
P-Ethyl Toluene	.28	.22		.13		.10	.09	
1,2,4 - Trimethyl Benzene	.14	.08		.03		.02	.01	
PAN (ppb v/v)	0	28.3	80.1	122.8	148.6	163.5	157.4	152.7
Hydrocarbons - Total	4.82	3.98		3.02		2.59	2.37	

TABLE - B-6
Hydrocarbon and PAN Data for Experiment 6

HYDROCARBON, ppmC	Irradiation Time, min.							
	0	60	120	180	240	300	360	420
Ethane	.12		.11					
Ethylene	.02		.01					
Propane	.08		.07					
Acetylene	.13		.11					
Iso-Butane	.05		.03					
N-Butane	.16		.14					
Propylene	0		0					
Trans-2-Butene	0		0					
2-Methyl Butane	.11		.10					
N-Penetane	.06		.04					
2-Methyl 2-Butene	0		0					
2-Methyl Pentane	.07		.06					
Benzene	.10		.09					
Toluene	.11		.10					
m-Xylene	.01		.01					
P-Ethyl Toluene	0		0					
1,2,4 - Trimethyl Benzene	0		0					
PAN (ppb v/v)	77.2	62.1	61.0	51.4				
Hydrocarbons - Total	1.02		.82					

TABLE - B-7

Hydrocarbon and PAN Data for Experiment 7

HYDROCARBON, ppmC	Irradiation Time, min.							
	0	60	120	180	240	300	360	420
Ethane								
Ethylene								
Propane	1.06	1.02		.91		.81		.73
Acetylene	.16	.16		.14		.13		.12
Iso-Butane								
N-Butane								
Propylene	.37	.29		.12		0		0
Trans-2-Butene								
2-Methyl Butane	1.52	1.42		1.21		1.03		.88
N-Penetane								
2-Methyl 2-Butene								
2-Methyl Pentane								
Benzene								
Toluene	.84	.78		.65		.53		.45
m-Xylene	.94	.81		.57		.42		.31
P-Ethyl Toluene								
1,2,4 - Trimethyl Benzene								
PAN (ppb v/v)	0	.03	15.8	37.8	71.2	97.1	115.5	133.3
Hydrocarbons - Total	4.89	4.48		3.60		2.92		2.49

TABLE - B-8
Hydrocarbon and PAN Data for Experiment 8

HYDROCARBON, ppmC	Irradiation Time, min.							
	0	60	120	180	240	300	360	420
Ethane								
Ethylene								
Propane	1.11	1.06		.94		.85		.78
Acetylene	.18	.18		.16		.14		.13
Iso-Butane								
N-Butane								
Propylene	.39	.30		.15		.05		0
Trans-2-Butene								
2-Methyl Butane	1.48	1.39		1.18		1.04		.90
N-Penetane								
2-Methyl 2-Butene								
2-Methyl Pentane								
Benzene								
Toluene	.83	.77		.64		.53		.45
m-Xylene	.95	.81		.57		.40		.32
P-Ethyl Toluene								
1,2,4 - Trimethyl Benzene								
PAN (ppb v/v)	0	2.04	7.51	19.12	36.4	58.1	81.6	103.9
Hydrocarbons - Total	4.94	4.51		3.64		3.01		2.58

TABLE - B-9
Hydrocarbon and PAN Data for Experiment 10

HYDROCARBON, ppmC	Irradiation Time, min.							
	0	60	120	180	240	300	360	420
Ethane								
Ethylene								
Propane	1.07	1.01		.90		.81	.76	.72
Acetylene	.18	.17		.15		.14	.13	.12
Iso-Butane								
N-Butane								
Propylene	.38	.27		.10		0	0	0
Trans-2-Butene								
2-Methyl Butane	1.52	1.42		1.18		1.01	.93	.86
N-Penetane								
2-Methyl 2-Butene								
2-Methyl Pentane								
Benzene								
Toluene	.84	.80		.63		.52	.46	.42
m-Xylene	.96	.81		.55		.38	.32	.27
P-Ethyl Toluene								
1,2,4 - Trimethyl Benzene								
PAN (ppb v/v)	0	6.19	25.3	50.7	83.4	110.7	119.6	131.8
Hydrocarbons - Total	4.95	4.48		3.51		2.86	2.60	2.39

TABLE - B-10

Hydrocarbon and PAN Data for Experiment 11

HYDROCARBON, ppmC	Irradiation Time, min.							
	0	60	120	180	240	300	360	420
Ethane								
Ethylene								
Propane	1.08	.103		.91		.82		.72
Acetylene	.15	.15		.14		.13		.11
Iso-Butane								
N-Butane								
Propylene	.37	.27		.09		0		0
Trans-2-Butene								
2-Methyl Butane	1.54	1.40		1.19		.99		.82
N-Penetane								
2-Methyl 2-Butene								
2-Methyl Pentane								
Benzene								
Toluene	.87	.77		.63		.50		.39
m-Xylene	.95	.77		.51		.36		.24
P-Ethyl Toluene								
1,2,4 - Trimethyl Benzene								
PAN (ppb v/v)	0	4.0	23.1	51.0	78.0	103.2	121.2	134.6
Hydrocarbons - Total	4.96	4.39		3.47		2.80		2.28

TABLE - B-11
Hydrocarbon and PAN Data for Experiment 12

HYDROCARBON, ppmC	Irradiation Time, min.							
	0	60	120	180	240	300	360	420
Ethane								
Ethylene								
Propane	.38	.35	.34			.28	.27	
Acetylene	.06	.06	.06			.05	.05	
Iso-Butane								
N-Butane								
Propylene	0	0	0			0	0	
Trans-2-Butene								
2-Methyl Butane	.30	.28	.26			.21	.21	
N-Penetane								
2-Methyl 2-Butene								
2-Methyl Pentane								
Benzene								
Toluene	.11	.10	.08			.07	.06	
m-Xylene	.03	.02	.02			.02	.01	
P-Ethyl Toluene								
1,2,4 - Trimethyl Benzene								
PAN (ppb v/v)	68.1	68.2	68.3	59.3	53.3	49.4	47.7	46.7
Hydrocarbons - Total	.88	.81	.75			.63	.60	

TABLE - B-12
Hydrocarbon and PAN Data for Experiment 13

HYDROCARBON, ppmC	Irradiation Time, min.							
	0	60	120	180	240	300	360	420
Ethane								
Ethylene								
Propane	1.09	1.02		.88		.80		
Acetylene	.17	.16		.15		.13		
Iso-Butane								
N-Butane								
Propylene	.37	.23		.14		.02		
Trans-2-Butene								
2-Methyl Butane	1.51	1.35		1.15		.99		
N-Penetane								
2-Methyl 2-Butene								
2-Methyl Pentane								
Benzene								
Toluene	.86	.73		.65		.50		
m-Xylene	.92	.71		.55		.38		
P-Ethyl Toluene								
1,2,4 - Trimethyl Benzene								
PAN (ppb v/v)			10.4			48.7	78.6	
Hydrocarbons - Total	4.92	4.50		3.52		2.82		